Contract No:

This document was prepared in conjunction with work accomplished under Contract No. DE-AC09-08SR22470 with the U.S. Department of Energy (DOE) Office of Environmental Management (EM).

Disclaimer:

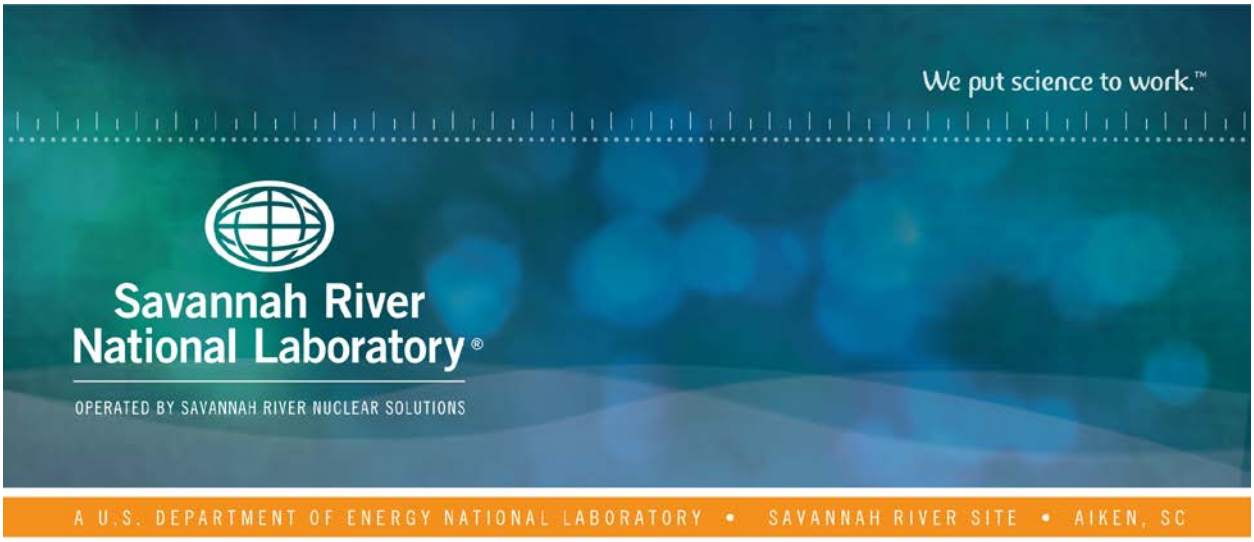

Evaluation of Thermolytic Production of Hydrogen from Glycolate and Common Tank Farm Organics in Simulated Waste

W. H. Woodham

C. J. Martino

April 2020

SRNL-STI-2019-00605, Revision 1

DISCLAIMER

Printed in the United States of America

Prepared for
U.S. Department of Energy

SRNL-STI-2019-00605
Revision 1

Keywords: *Hydrogen*

Retention: *Permanent*

Evaluation of Thermolytic Production of Hydrogen from Glycolate and Common Tank Farm Organics in Simulated Waste

W. H. Woodham
C. J. Martino

April 2020

Prepared for the U.S. Department of Energy under contract number DE-AC09-08SR22470.

Savannah River National Laboratory®
OPERATED BY SAVANNAH RIVER NUCLEAR SOLUTIONS

REVIEWS AND APPROVALS

AUTHORS:

W. H. Woodham, Chemical Flowsheet Development Date

C. J. Martino, Chemical Flowsheet Development Date

TECHNICAL REVIEW:

C. L. Crawford, Separation Sciences & Engineering, Reviewed per E7 2.60 Date

T. B. Edwards, Applied Materials Research, Reviewed per E7 2.60 Date

APPROVAL:

F. M. Pennebaker, Chemical Processing Sciences Date

S. D. Fink, Manager Date
Chemical Processing Sciences

T. H. Huff, Manager Date
SSR, DWPF/SS Facility Engineering

J. E. Occhipinti, Manager Date
SRR, Waste Removal and Tank Closure

R. E. Edwards, Jr., Manager Date
SRR, Nuclear Safety & Engineering Integration

ACKNOWLEDGEMENTS

The authors wish to acknowledge the efforts of all of those involved in the planning, design, performance, analysis, and documentation of this research. David Newell was instrumental in the design and testing of the experimental apparatus used throughout this study. Meagan Kinard and Kandace Miles expertly performed the experiments described herein, working day and night. Whitney Riley, Kim Wyszynski, Tom White, Amy Ekechukwu, and many more were involved in the process of analyzing the countless samples generated as a result of this testing. John Pareizs and Matt Williams served invaluably as the process experts for the gas chromatography columns and infrared spectrometers employed during these tests. Holly Hall served as the facility coordinator, ensuring that the increasing demand for resources could always be supplied. Amy Blunt managed the samples and materials generated in the course of this research.

To those listed here, and to the countless others unlisted, we say “thank you.”

EXECUTIVE SUMMARY

The Savannah River National Laboratory (SRNL) has performed testing to investigate the thermolytic production of hydrogen gas from organic species present in the Savannah River Site (SRS) Concentration, Storage, and Transfer Facilities (CSTF). SRNL designed an experimental apparatus to measure the time-dependent concentration of hydrogen in the headspace over a reacting mixture of simulated caustic waste media and organic compounds as well as a methodology to calculate a steady-state hydrogen generation rate (HGR) from this data. Special focus was given to glycolate, which is not currently present in CSTF waste but will be contained in the recycle stream from the Defense Waste Processing Facility (DWPF) under the upcoming alternate reductant flowsheet.

Conclusions drawn from this research are given below.

- An experimental apparatus has been developed to study the time-dependent generation rate of hydrogen from liquids. A methodology to determine steady-state generation rates greater than 4.0×10^{-8} ft^3 h^{-1} gal^{-1} has been described.
- Screening tests using Tank 38 simulant material have been performed to identify the most reactive organic compounds introduced to the SRS tank farm. The following designations were assigned to each species.
    - Glycolate (not currently in CSTF waste), propanal, Xiameter AFE-1010 (formerly marketed as Dow Corning antifoam H-10), and some resin digestion products (such as those expected from Reillex HPQ) were identified as being significantly reactive toward the generation of hydrogen gas in caustic waste media.
    - Polyethylene oxide (a suspected degradation product of Antifoam 747) was identified as being marginally reactive, with HGRs similar to or just above those observed at baseline conditions without added organic material.
    - Sodium formate, Caustic Side Solvent Extraction (CSSX) solvent, dibutylphosphate, butanol, and trimethylsilanol were identified as not being significantly reactive compared to baseline conditions.
    - Marginal HGR was observed when oxalate was tested in the presence of formate and CSSX solvent. However, it is believed that this observation is due to the combination of multiple organic species and hydrogen observations near the limits of detection and should not be interpreted as propensity of oxalate to produce thermolytic hydrogen (oxalate has no hydrogen atoms available to form hydrogen gas).
    - Methane generation was identified from trimethylsilanol.
- Thermolytic HGR from glycolate was shown to be independent of glycolate source (e.g., processing history of glycolate has no appreciable impact on generation rates).
- Testing performed with propanal suggests that while propanal exhibits a relatively high reactivity to produce hydrogen, its volatility and high reaction rate limits its ability to endure for longer than approximately 3 hours and is not expected to be present in measurable concentrations in tank farm waste at elevated temperatures.
- Statistically-designed matrices of test conditions were generated to evaluate the reactivity of glycolate, Xiameter AFE-1010, IONAC A-641 resin digestion products, and Reillex HPQ resin digestion products across the range of composition and temperature conditions expected in the SRS CSTF. The results from these statistically-designed test matrices were used to regress models to predict the thermolytic HGR at standard conditions of 25 °C and 1 atm from glycolate, Xiameter, IONAC, and Reillex-containing samples. The resulting models are given by the following expressions. Note that these expressions calculate the mean expected HGR and do not account for the uncertainty of the models' fit to the data.

$$HGR_{Glycolate} = 6.262\times10^{5}\left[Na\right]^{1.520}\left[NO_3\right]^{0.282}\left[OH\right]^{1.441}\left[C_{GLY}\right]e^{-82{,}300/RT}$$

$$HGR_{Xiameter} = 3.238\times10^{5}\left[OH\right]^{1.141}\left[C_{XIA}\right]e^{-62{,}300/RT}$$

$$HGR_{IONAC} = 1.361\times10^{6}\left[NO_3\right]^{0.542}\left[OH\right]^{1.065}\left[C_{IAC}\right]e^{-76{,}100/RT}$$

$$HGR_{Reillex} = 8.134\times\left[OH\right]^{0.891}\left[C_{RLX}\right]e^{-27{,}900/RT}$$

- The difference in thermolytic HGR observed from glycolate in the presence of additional Lewis acids (i.e., silicon and boron) versus that observed in the absence of additional Lewis acids was not statistically significant.
- The thermolytic HGR from glycolate was shown to be independent of the presence of select noble metals (i.e., silver, palladium, rhodium, and ruthenium).
- The thermolytic HGR from glycolate was shown to be somewhat dependent on the presence of sludge solids. It is believed that this dependence was observed due to the ability of sludge solids (notably MnO_2 solids) to oxidize glycolate and reduce the available concentration of hydrogen-producing reagent.
- The thermolytic HGR from glycolate was shown to be strongly dependent on the presence of added $Hg(NO_3)_2$, with near complete disappearance of all HGR in the presence of added $Hg(NO_3)_2$. Due to the apparent formation of an HgO phase, insolubility of the Hg used during this testing, and the introduction of suspended Hg-containing solids in the supernatant phase, it is not believed that this species is representative of conditions in radioactive SRS supernatant waste and is therefore not recommended as a credit to be used to decrease the amount of hydrogen expected during thermolysis.
- Testing at extreme conditions (of high aluminum, high temperature) in Tank 30 simulant has been performed with glycolate. These results fall within the 95% confidence limit predicted by the glycolate thermolytic model.
- The HGR profiles yielded from testing with glycolate suggest the presence of a hydrogen-producing reactive intermediate, implying that the measured HGRs may be slower than the unmeasured destruction rates of glycolate in caustic waste media.
- Testing performed with IONAC A-641 digestion products revealed that HGRs from resin digestion products are not impacted by the presence of solids, suggesting that its thermolysis should be considered a supernatant phenomenon.
- Propanal thermolysis was shown to be dependent primarily on hydroxide concentrations and temperatures, which is consistent with the Cannizzaro-type reaction mechanism put forward by Ashby for the generation of hydrogen from aldehydes in caustic waste media.
- Testing with combined additions of glycolate, Xiameter, IONAC, and Reillex digestion products suggests that there is little to no risk of synergistic interactions between organic molecules. Further, test results suggest that antagonistic effects may be present, possibly due to the interaction of organic molecules with MnO_2 added with resin digestion products. This antagonistic effect is not universal, is believed to be scale- and process-dependent, and would not be expected in a settled tank's supernatant phase; therefore, it is not recommended as a credit to decrease expected HGRs from organic compounds.

- A global, source-independent model for organic thermolytic HGR at standard conditions of 25 °C and 1 atm in SRS waste media has been developed, taking the following form. Note that this model is not applicable to HGRs from glycolate.

$$HGR_{real} = 2.45 \times 10^{6} \left[OH\right]^{0.925} \left[TOC\right] e^{-82{,}900/RT}$$

- From comparison with thermolytic HGR data from waste tank samples, the global model is expected to be applicable to all SRS waste tanks except Tanks 48 and 50, which should be managed under separate flammability evaluations. Data for Tank 50 has been previously generated by Duignan using a sealed HGR system.

The following recommendations are made for the optimal application of the information described in this report.

- Additional investigations should be made into the generation rates of methane from organic molecules in the CSTF. The organic compounds of most importance are methylsilanes (such as those employed as antifoam agents throughout SRS processing) and methylmercury (a known toxin in the high-level waste (HLW) flowsheet at SRS).
- Previous work predicting the impact of glycolate thermolysis on the composition of hydrogen in bubbles of trapped gas in SRS waste should be revised to account for the improved rate prediction models generated in this report.
- Further investigation should be made in the composition of total gas evolutions from organic thermolysis to develop a better model for hydrogen retention in trapped gas bubbles.
- Further investigation should be made into the mechanism of mercury impact on glycolate and non-glycolate HGR to assess creditability in the CSTF.
- Further testing is recommended to validate the models proposed herein at extremes in hydroxide concentration and temperature ([OH] > 12.2 M and T > 134 °C for glycolate; [OH] > 12.5 M, T < 70 °C, and T > 130 °C for non-glycolate TOC).

TABLE OF CONTENTS

LIST OF TABLES xi
LIST OF FIGURES xii
LIST OF ABBREVIATIONS xv
1.0 Introduction 1
2.0 Experimental 3
2.1 Experimental Apparatus 3
2.2 Simulant Preparation 5
2.3 Experimental Procedure 5
2.4 Experimental Design 6
2.5 Liquid Analyses 7
2.6 Offgas Analyses 7
2.7 Quality Assurance 8
3.0 Results and Discussion 8
3.1 Common CSTF Organics Initial Screening Tests 8
3.2 Organic-Free Hydrogen Measurements 20
3.3 Glycolate 24
3.3.1 Model Generation Experiments 24
3.3.2 Model Validation Experiments 30
3.3.3 High Boiling Point (Tank 30) Simulant Experiments 33
3.3.4 Interactions with Other Components in Waste Tanks 40
3.3.4.1 Testing with Sludge Solids 40
3.3.4.2 Testing with Hg 41
3.3.4.3 Testing with Other Lewis Acids (Si and B) 42
3.3.4.4 Testing with Noble Metals (Ag, Pd, Rh, and Ru) 43
3.3.4.5 Comparison to Glycolate HGR Measurements in Radioactive Waste 44
3.3.4.6 Extrapolation of Temperature-Modified Glycolate Model to Lower Temperatures 47
3.4 Xiameter AFE-1010 47
3.4.1 Model Generation Experiments 47
3.4.2 Model Validation Experiments 51
3.5 IONAC A-641 Ion Exchange Resin 54
3.5.1 Model Generation Experiments 54
3.5.2 Model Validation Experiments 57
3.5.2.1 Impact of Solids on Resin Digestion Material Thermolysis 57

3.5.2.2 Testing to Improve Thermolytic Model Equation 61
3.6 Reillex HPQ Ion Exchange Resin 64
3.6.1 Model Generation Experiments 64
3.6.2 Model Validation Experiments 68
3.7 Propanal 71
3.8 Synergistic Interactions of Organic Molecules 77
3.9 Generation of a Global TOC HGR Model 81
3.10 Extrapolation of the Global TOC HGR Model to Lower Temperatures 91
3.11 Applicable Ranges of Salt Species Concentrations and Temperature 91
4.0 Conclusions 93
5.0 Recommendations 95
6.0 References 95
Appendix A . Previous (August 2017) High Boiling Point (HBP) HGR Test with 10 g/L Glycolate A-1
Appendix B . Use of JMP 11.2.0 Statistical Mathematics Software Package to Evaluate HGR Data and Generate Empirical Reaction Rate Expressions. B-1
Appendix C . Use of Global TOC and Glycolate HGR Models in CSTF Waste Tank Flammability Calculations C-1

LIST OF TABLES

Table 2-1. Proposed Design Space for Simulant HGR Experiments. 6

Table 3-1. Composition of Tank 38 Simulant Used During Initial Organics Screening. 9

Table 3-2. Test List for Common CSTF Organic Screening Experiments 10

Table 3-3. Observed HGRs from Preliminary Screening Experiments. 18

Table 3-4. Calculated Hu Reactivity Factors for Each Organic Compound Tested in Initial Screening Experiments. 20

Table 3-5. Concentrations, Temperatures, and Results from Salt-Only HGR Testing. 21

Table 3-6. HGR Test Conditions for Glycolate Model Generation. 25

Table 3-7. HGR Test Results for Glycolate Model Generation. 26

Table 3-8. HGR Test Conditions for Glycolate Model Validation and Improvement. 31

Table 3-9. HGR Test Results for Glycolate Model Validation and Improvement. 31

Table 3-10. Composition of Tank 30 Simulant. 34

Table 3-11. Observed HGRs With and Without Glycolate and Glycolate-Attributable HGR from Tank 30 Simulant Testing. 36

Table 3-12. Conditions and Results from Glycolate HGR Testing with Radioactive Waste. 45

Table 3-13. Conditions and Results from Glycolate HGR Testing in Previous Studies. 45

Table 3-14. HGR Test Conditions for Xiameter Model Generation. 49

Table 3-15. HGR Test Results for Xiameter Model Generation. 49

Table 3-16. HGR Test Conditions for Xiameter Model Validation and Improvement. 52

Table 3-17. HGR Test Results for Xiameter Model Validation and Improvement. 52

Table 3-18. HGR Test Conditions for IONAC A-641 Model Generation. 55

Table 3-19. HGR Test Results for IONAC A-641 Model Generation. 55

Table 3-20. HGR Test Conditions for IONAC Model Validation and Improvement. 62

Table 3-21. HGR Test Results for IONAC Model Validation and Improvement. 62

Table 3-22. HGR Test Conditions for Reillex HPQ Model Generation. 66

Table 3-23. HGR Test Results for Reillex HPQ Model Generation. 66

Table 3-24. HGR Test Conditions for Reillex Model Validation and Improvement. 69

Table 3-25. HGR Test Results for Reillex Model Validation and Improvement. 69

Table 3-26. Concentrations and Conditions from Test PRO-1. 72

Table 3-27. Concentrations and Conditions from Tests PRO-2 Through PRO-10. 73

Table 3-28. Changes in Propanal Concentration During Propanal Testing. 77

Table 3-29. Kinetic Parameters for Xiameter, IONAC, and Reillex Obtained During Global Model Regression..... 85

Table 3-30. Summary of HGR Experiments Performed Using SRS HLW Tank Samples..... 87

Table 3-31. Parameter Ranges for Experimental Design and Performance of Glycolate HGR Measurements. 91

Table 3-32. Parameter Ranges for Experimental Design and Performance of Non-Glycolate HGR Measurements. 92

Table 3-33. Recommended Parameter Applicability Ranges for HGR Models..... 92

LIST OF FIGURES

Figure 1-1. Flowchart of Organic-Bearing Waste Streams at SRS. 2

Figure 2-1. Process Schematic of HGR Measurement Experimental Apparatus. 4

Figure 2-2. Photograph of HGR Reaction Vessel Used in Experiments. 5

Figure 3-1. HGR Profiles of P1S1-Test 1 (Stainless Steel) and P1S1-Test 2 (PTFE)..... 11

Figure 3-2. HGR Profiles of P1S1-Test 2B (Baseline 1), P1S1-Test 2C (Baseline 2), P1S1-Test 3A (Sodium Glycolate 1), P1S1-Test 3B (Sodium Glycolate 2), and P1S1-Test 4 (SME Product Glycolate). 12

Figure 3-3. HGR Profiles of P1S1-Test 5 (Formate), P1S1-Test 13 (CSSX Solvent), and P1S1-Test 17 (Formate + Oxalate + CSSX Solvent). 13

Figure 3-4. HGR Profiles of P1S1-Test 8 (Trimethylsilanol) and P1S1-Test 9 (PEO). 14

Figure 3-5. IR Spectra of Offgas from P1S1-Test 8. The black line is the IR spectrum sampled from the vapor space of the reaction. The blue line is a library spectrum of methane. Note that evidence of methane and HMDSO can be seen in the IR spectrum..... 15

Figure 3-6. HGR Profiles of P1S1-Test 7 (Xiameter AFE-1010) and P1S1-Test 10 (Propanal)..... 16

Figure 3-7. HGR Profiles of P1S1-Test 11 (Butanol) and P1S1-Test 12 (Dibutylphosphate)..... 17

Figure 3-8. HGR Profiles of P1S1-Test 14 (Terephthalic Acid), P1S1-Test 15 (Methylcarboxypyridinium), and P1S1-Test 16 (Sulfobenzoic Acid). 18

Figure 3-9. Illustration of a Lower, One-Sided 95% Confidence Interval Around a Normal Distribution. The normal distribution is situated around the mean HGR (μ) and distributed symmetrically such that the one-sided 95% confidence limit is equal to the corresponding two-sided 90% confidence limit. 23

Figure 3-10. Measured HGR from Organic-Free Testing vs. HGR Predicted from the Blank HGR Model Given in Equation [8]. 24

Figure 3-11. Scatterplot of HGR Measurements vs. Values Predicted from Equation [12]. 29

Figure 3-12. Plot of Measured HGRs from Model Generation (Yellow) and Validation (Green) Tests for Glycolate vs. Predicted HGRs According to Interim Model Shown in Equation [12]. 32

Figure 3-13. Plot of Measured HGRs from Model Generation (Yellow) and Validation (Green) Tests for Glycolate vs. Predicted HGRs According to Final Model Shown in Equation [14]. 33

Figure 3-14. HGR (blue, in $ft^3\ h^{-1}\ gal^{-1}$) and Temperature (orange, in °C) as a Function of Time During the Glycolate-Free Tank 30 Simulant Experiment..... 35

Figure 3-15. HGR (blue, in $ft^3\ h^{-1}\ gal^{-1}$) and Temperature (orange, in °C) as a Function of Time During the Glycolate-Added Tank 30 Simulant Experiment. 36

Figure 3-16. Arrhenius Plot of Glycolate-Attributable HGR. 37

Figure 3-17. Evaluation of Tank 30 Simulant Test Results Against the Empirical Glycolate HGR Model Shown in Equation [14]. 38

Figure 3-18. Plot of Measured HGRs from Model Generation (Yellow), Validation (Green), and Tank 30 Simulant (Blue) Tests for Glycolate vs. Predicted HGRs According to the Temperature-Modified Glycolate Model Shown in Equation [16]. 39

Figure 3-19. HGR from 1,000 mg/L Glycolate as a Function of Time in the Presence (Red) and Absence (Blue) of SB9 Sludge Solids (1 wt%). 40

Figure 3-20. HGR from 1,000 mg/L Glycolate as a Function of Time in the Presence (Red) and Absence (Blue) of Mercury (430 mg Hg/L, added as $Hg(NO_3)_2 \cdot H_2O$). 41

Figure 3-21. Mechanism of Aluminum-Catalyzed Thermolytic Production of Hydrogen from Glycolate Theorized by Ashby *et al.*[10] 42

Figure 3-22. HGR from 1,000 mg/L Glycolate as a Function of Time in the Presence (Red) and Absence (Blue) of Boron and Silicon (190 and 130 mg/L, respectively). 43

Figure 3-23. HGR from 1,000 mg/L Glycolate as a Function of Time in the Presence (Red) and Absence (Blue) of Silver, Palladium, Rhodium, and Ruthenium (0.4, 0.2, 0.2, and 1 mg/L, respectively). 44

Figure 3-24. Plot of Measured HGRs from Simulant Experiments (Diamonds) and Radioactive Waste Samples (Circles) for Glycolate vs. Predicted HGRs According to the Temperature-Modified Glycolate Model Shown in Equation [17]. For comparison, results from previously-performed simulant experiments (squares) and literature-reported values (triangles) are also given. 46

Figure 3-25. Modified Arrhenius Plot of Glycolate HGRs Measured in Radioactive Waste Vs. Temperature-Modified Glycolate HGR Model Predictions..... 47

Figure 3-26. Plot of Measured HGRs from Model Generation Tests for Xiameter vs. Predicted HGRs According to Interim Model Shown in Equation [20]. 50

Figure 3-27. Plot of Measured HGRs from Model Generation (Yellow) and Validation (Green) Tests for Xiameter vs. Predicted HGRs According to Interim Model Shown in Equation [20]..... 53

Figure 3-28. Plot of Measured HGRs from Model Generation (Yellow) and Validation (Green) Tests for Xiameter vs. Predicted HGRs According to Final Model Shown in Equation [22]. 54

Figure 3-29. Plot of Measured HGRs from Model Generation Tests for IONAC vs. Predicted HGRs According to Interim Model Shown in Equation [24]. 56

Figure 3-30. HGR Results from Condition D with Added IONAC Digestion Product Material. 58

Figure 3-31. HGR Results from Condition E with Added IONAC Digestion Product Material. 59

Figure 3-32. HGR Results from Condition F with Added IONAC Digestion Product Material. 60

Figure 3-33. Plot of Measured HGRs from Model Generation (Yellow) and Validation (Green) Tests for IONAC vs. Predicted HGRs According to Interim Model Shown in Equation [24]. 63

Figure 3-34. Plot of Measured HGRs from Model Generation (Yellow) and Validation (Green) Tests for IONAC vs. Predicted HGRs According to Final Model Shown in Equation [26]. 64

Figure 3-35. Plot of Measured HGRs from Model Generation Tests for Reillex vs. Predicted HGRs According to Interim Model Shown in Equation [28]. 67

Figure 3-36. Plot of Measured HGRs from Model Generation (Yellow) and Validation (Green) Tests for Reillex vs. Predicted HGRs According to Interim Model Shown in Equation [28]. 70

Figure 3-37. Plot of Measured HGRs from Model Generation (Yellow) and Validation (Green) Tests for Reillex vs. Predicted HGRs According to Final Model Shown in Equation [30]. 71

Figure 3-38. HGR and Propanal Offgas Results from PRO-1. 72

Figure 3-39. Impacts of Salt Species Concentrations on Propanal HGR. 74

Figure 3-40. Impacts of Organic Carbon Concentration on Propanal HGR. 75

Figure 3-41. Impacts of Temperature on Propanal HGR. 76

Figure 3-42. Results from Individual and Combined Organics Testing at Condition C. 78

Figure 3-43. Results from Individual and Combined Organics Testing at Condition D. 79

Figure 3-44. Results from Individual and Combined Organics Testing at Condition E. 80

Figure 3-45. Results from Individual and Combined Organics Testing at Condition F. 81

Figure 3-46. Linear Regression of Simulant HGR Data to Determine Global Salt Species Dependence. 84

Figure 3-47. Plot of Measured HGRs from All Simulant Experiments vs. Predicted HGRs According to Global Model Regression Results Described in Equation [40] and Table 3-29. 85

Figure 3-48. Modified Arrhenius Plot of Real Waste HGR Measurements Designated as Thermolytic Hydrogen Generation. 88

Figure 3-49. Modified Arrhenius Plot of Real Waste HGR Measurements Designated as Thermolytic Hydrogen Generation from Tanks Other Than Tank 50. 90

LIST OF ABBREVIATIONS

ACTL	Aiken County Technology Laboratory
AD	Analytical Development
BDL	Below Detection Limit
BIC	Bayesian Information Criterion
CL	Confidence Level
CPC	Chemical Processing Cell
CSSX	Caustic Side Solvent Extraction
CSTF	Concentration, Storage and Transfer Facilities
DAC	Data Acquisition and Control
DBP	dibutylphosphate
DI	deionized
DWPF	Defense Waste Processing Facility
ELN	Electronic Laboratory Notebook
FT-IR	Fourier-transform infrared
GC	Gas Chromatograph(y)
GPE	General Purpose Evaporator
HBP	High Boiling Point
HEDTA	(N-hydroxyethyl)ethylenediaminetriacetate
HGR	hydrogen generation rate
HLW	High-Level Waste
HMDSO	hexamethyldisiloxane
IC	Ion Chromatography
ICP-ES	Inductively Coupled Plasma - Emission Spectrometer
LWO	Liquid Waste Operator
M&TE	Measuring and Test Equipment
MCU	Modular CSSX Unit
MS&E	Measurement Systems and Equipment
PEO	poly(ethyleneoxide)
PISA	Potential Inadequacy in the Safety Analysis
PSAL	Process Science Analytical Laboratory
PTFE	polytetrafluoroethylene
PUREX	Plutonium Uranium Redox Extraction
RSD	Residual Standard Deviation
SB	Sludge Batch

SME	Slurry Mix Evaporator
SRAT	Sludge Receipt and Adjustment Tank
SRNL	Savannah River National Laboratory
SRR	Savannah River Remediation
SRS	Savannah River Site
SWPF	Salt Waste Processing Facility
TBP	tri-n-butylphosphate
TCD	thermal conductivity detector
TIC	Total Inorganic Carbon
TMS	trimethylsilanol
TOC	Total Organic Carbon
VOA	Volatile Organic Analysis
VOC	Volatile Organic Compounds

1.0 Introduction

Since the construction of the Savannah River Site (SRS) in the 1950s, several reprocessing, treatment, and remediation campaigns have been carried out involving radioactive materials, almost always resulting in the generation of hazardous, radioactive waste. Many of these campaigns resulted in the introduction of minor or limited amounts of organic material to radioactive, caustic waste media stored in the 43 active High Level Waste (HLW) tanks maintained at the SRS Concentration, Storage, and Transfer Facilities (CSTF) today.[1] The majority of these organic compounds were incidental to SRS operation and are therefore only expected at minor levels in SRS waste.

In 2017, the SRS Liquid Waste Operator (LWO), Savannah River Remediation (SRR), announced three Potential Inadequacies in the Safety Analyses (PISAs) in which it was revealed that no allowance had been made for the impacts of these trace organic compounds on the generation of flammable gases in the CSTF.[2-4] SRR requested that the Savannah River National Laboratory (SRNL) study the hydrogen generation rates (HGRs) due to the presence of organic compounds in waste media.[5-6]

The history of organic compound use at SRS is as diverse as it is complicated. Several compounds have previously been identified from a number of sampling campaigns conducted at SRS.[1] The majority of these compounds are reported to be present at near-detection limit values and are not of concern to this study due simply to the effects of dilution. Of greater concern are the concerted programs that either previously have added or currently are adding incidental organic carbon to the CSTF. These processes have been previously identified and are listed below.

- Vitrification of radioactive waste in the Defense Waste Processing Facility (DWPF) – The process of HLW vitrification at DWPF involves the use of formic acid to reduce mercury. While most of this formic acid is retained with the HLW and destroyed in the melter, some is inadvertently lost to volatilization and through sludge carryovers. These low levels of formate are then transferred to the CSTF via condensate recycle streams.
- Acidic cleaning of emptied tanks in the CSTF – The process of cleaning empty tanks in the CSTF utilizes oxalic acid. Residual amounts of oxalate may be lost to recycle streams.
- Material reprocessing at F- and H-Canyons – SRS canyon operations have historically used organic solvents to extract valuable isotopes from spent nuclear fuel. These solvents include tributylphosphate (TBP) as a complexing agent. Following contact with aqueous waste streams, some TBP (and corresponding degradation products) is expected in the HLW system. Furthermore, the SRS canyons have employed organic resins to separate radionuclides from waste. While the largest fraction of this organic resin was oxidatively digested before introduction to the CSTF, some organic carbon remaining from the digestion process and from undigested resin is unavoidable.
- Foam control throughout the site facilities (including the DWPF and CSTF evaporators) – Historically, the HLW evaporators in the CSTF have used antifoaming agents to mitigate foaming while HLW is evaporated. While the use of these agents has been suspended, it is expected that residual degradation products from antifoam addition in the CSTF persist in the HLW system. Similar antifoaming agents are currently employed in the DWPF and are subject to loss to condensate recycle streams.
- Use of organic solvents to remove cesium from aqueous waste streams – Salt waste processing flowsheets at SRS such as those employed at the Modular Caustic Side Solvent Extraction (CSSX) Unit (MCU) and the Salt Waste Processing Facility (SWPF) involve the use of an organic solvent extraction process. While this extraction process is designed to minimize organic solubility in the aqueous waste phase, trace organic material is inherently entrained in the aqueous streams output from the process.

Figure 1-1 is a simplified chart showing the facilities of greatest concern as identified by Walker[1] and organic compounds resulting from these processes.

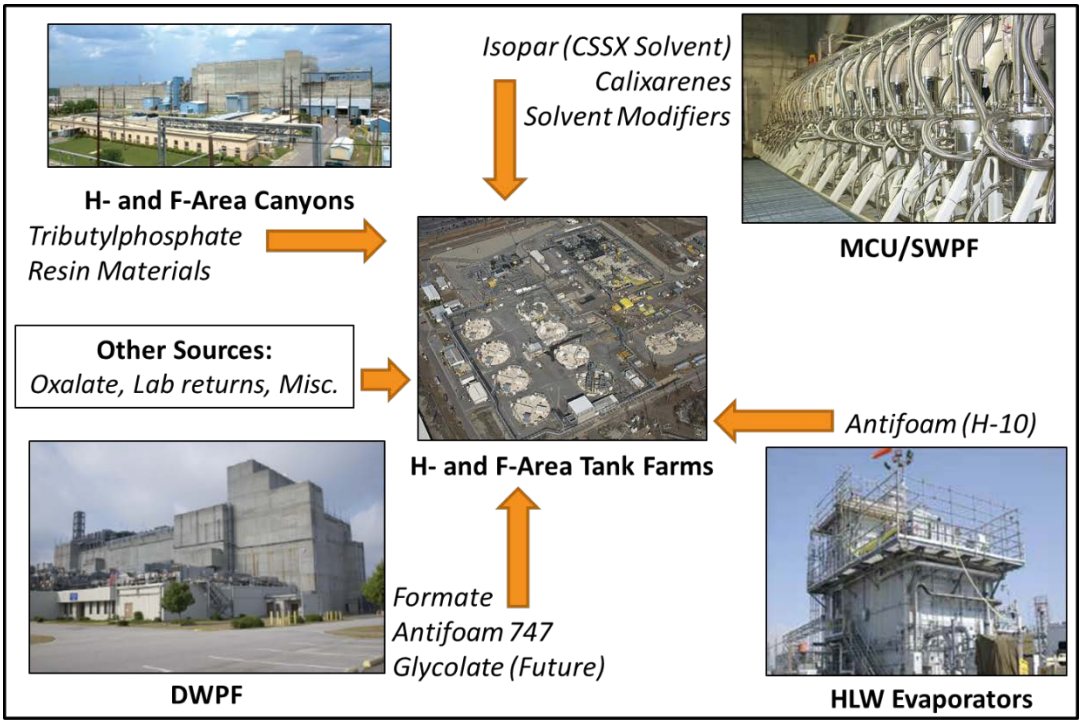

Figure 1-1. Flowchart of Organic-Bearing Waste Streams at SRS.

Summaries of the processes and organics identified as prominent in Figure 1-1 are given below.

- H- and F-Area Canyon Facilities
  - Tri-n-butylphosphate (TBP) – This compound is used as a solvent during the Plutonium Uranium Redox Extraction (PUREX) separation process and is introduced into aqueous streams by its measurable (albeit diminished) solubility in aqueous solutions. TBP has degradation products in the CSTF of dibutylphosphate (DBP), butylphosphate and butanol.
  - Resins and resin-related materials – Resins have been employed for several decades at SRS as methods to separate radionuclides. These resins are often digested with potassium permanganate before direct addition to HLW tanks to reduce the amount of organic material transferred to the CSTF. A sizeable fraction of the discarded resin transferred without digestion.
- MCU/SWPF Processes
  - CSSX solvents – These complex organic mixtures are used to remove cesium from salt solutions and are introduced to aqueous waste streams by their diminished solubility in aqueous phases or by entrainment from incomplete separation. Note that kerosene-like compounds (similar to the Isopar-L component in CSSX solvents) have also been used previously in H- and F-Canyon operations.
- DWPF
  - Antifoam 747 – This siloxane-containing mixture is added to the Chemical Processing Cell (CPC) to mitigate foam overs and is introduced to the aqueous waste by both its solubility in carryover materials and its generation of soluble degradation products (such as

trimethylsilanol (TMS) and hexamethyldisiloxane (HMDSO)). Propanal concentrations in the DWPF have also been linked to the presence of Antifoam 747.
    - Formate – Formic acid is added as a reducing agent to the CPC for the reduction of mercury and other oxidized metals and is introduced to aqueous waste streams by carryover.
    - Glycolate – Glycolic acid has not been added to any facility at SRS to date but will be added under the upcoming alternate reductant flowsheet. It is expected to be introduced to the aqueous waste streams by the process of carryovers in the CPC. It should be noted that current operating plans for DWPF include the implementation of a permanganate oxidation step to minimize the transfer of glycolate to the CSTF.
- CSTF
    - H-10/Xiameter AFE-1010 - CSTF 2-H and 3-H Evaporators historically employed antifoam H-10 (modern brand is Xiameter AFE-1010) to control foaming while evaporating waste. This compound was directly added to waste. While it is no longer employed in the 2-H and 3-H Evaporators, it is currently employed in the H-Canyon General Purpose Evaporator (GPE).
    - Oxalate – Oxalic acid has historically been used as a precipitating agent and is currently used as a cleaning agent in tank operations and is expected to have marginal solubility in high-salt wastes.

The presence of organic compounds is expected to have an impact on HGR in radioactive waste due primarily to two generation mechanisms: radiolysis and thermolysis. Organic radiolysis is expected to occur by either 1) direct exposure of organic material to radiation, leading to the formation of hydrogen, or 2) action of radiation on water molecules to produce hydrogen radicals that may then abstract a proton from organic compounds. The first process (direct radiolysis) is not expected to be a significant contributor to HGR in SRS wastes due to the relatively low content of organic in the waste matrix (i.e., Total Organic Carbon, TOC, less than 1 wt %). The second process (indirect radiolysis) has been previously explored by Bibler[7] and quantified for formate and glycolate by King and Crawford,[8] and is not discussed here.

Organic thermolysis (herein defined as production of hydrogen gas by non-radiative chemical reaction) is less understood in the context of SRS waste. The phenomena of organic thermolysis has been previously studied for the Hanford site,[9] with particular focus given to hydroxyethylethylenediaminetriacetate (HEDTA) and glycolate.[10] The study of organic thermolysis in SRS waste streams is the subject of this report and is discussed herein.

The first revision of this report was issued to address the applicable range of salt concentrations and temperatures for the thermolytic models described herein as well as the impacts of extrapolating the model for glycolate thermolysis to temperatures below 60 °C. The discussion of glycolate model extrapolation to lower temperatures is presented in Section 3.3.4.6, and the discussion of applicable HGR parameter ranges is initiated in Section 2.4 and refined in Section 3.11. Furthermore, an edit was made to the minimum specified temperature range of the Global TOC HGR model, shifting it from 60 °C to 70 °C. Additional discussion on the extrapolation of the Global TOC model to temperatures below 70 °C is given in Section 3.10.

2.0 Experimental

2.1 Experimental Apparatus

The work described herein was performed using a custom-designed reaction apparatus at the SRNL facilities within the Aiken County Technology Laboratory (ACTL). The apparatus consisted of a 1.2 L polytetrafluoroethylene (PTFE) kettle sealed with a PTFE lid. PTFE was identified as the preferred material of construction due to the observation in previous testing[11] that glass vessels tend to react with higher

hydroxide loadings to form sodium aluminosilicates. The center of the lid was fit with a magnetic drive from Parr Instrument Company. Stainless-steel fittings were installed in a circle around the magnetic drive. The ports were used to 1) install two Incoloy® 800 heating rods for temperature control within the apparatus, 2) install an Inconel® 600 thermocouple to monitor liquid temperature within the vessel, 3) provide a purge gas to continuously sweep the headspace of the vessel, 4) connect the headspace of the vessel to a glass condenser, 5) provide a reflux route for condensed liquid, and 6) add materials.

Upstream from the reaction vessel, two MKS mass flow controllers were used to supply 1) CO_2-free compressed air, or 2) 0.5 vol % Kr and 20 vol % O_2 in N_2 cylinder gas. Downstream from the reaction vessel, a glass condenser was employed to remove condensables from the gas phase before proceeding to vapor phase analysis. After passing through the condenser, the gas phase was sampled and quantified for hydrogen content by an Inficon Micro 3000 GC-TCD (gas chromatograph – thermal conductivity detector) before being vented to a chemical hood. An in-line, gas-phase Fourier-transform infrared (FT-IR) spectrophotometer was occasionally used in cases where volatile organic compounds (VOCs) were expected. A process schematic is given in Figure 2-1. A photograph of the reaction vessel is given in Figure 2-2.

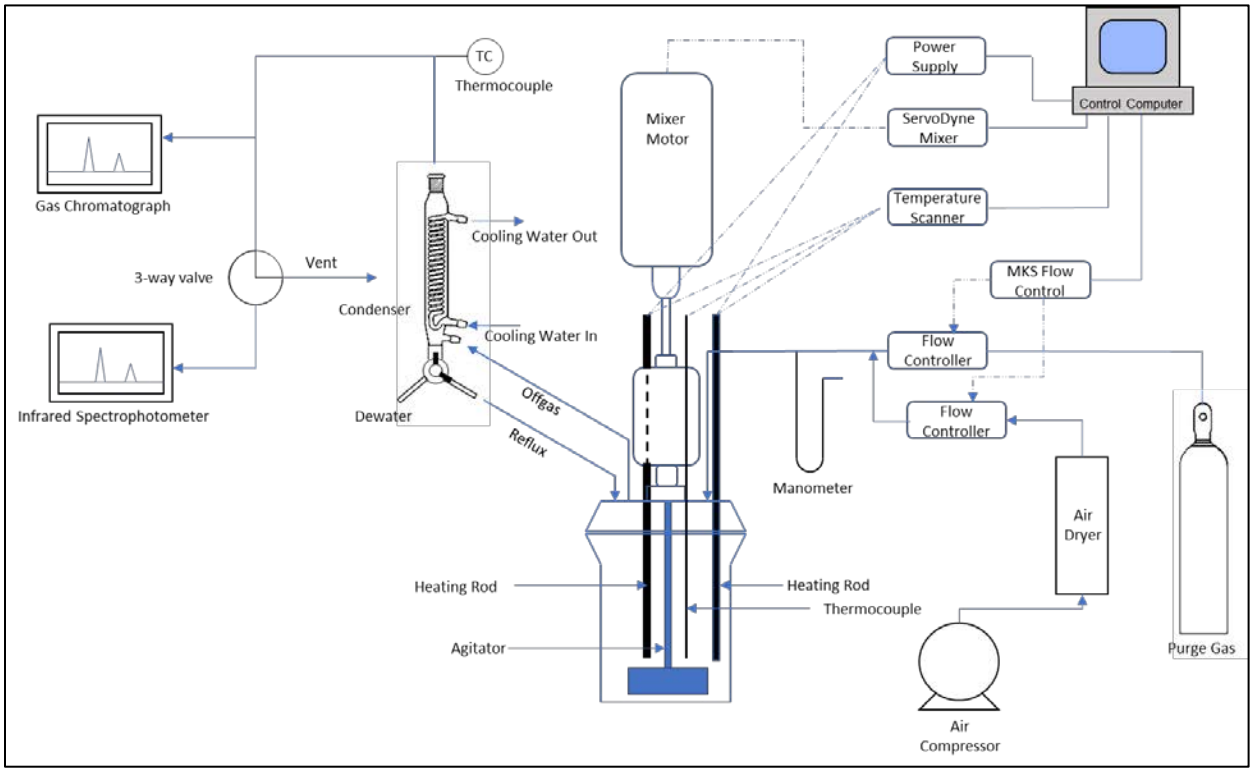

Figure 2-1. Process Schematic of HGR Measurement Experimental Apparatus.

Figure 2-2. Photograph of HGR Reaction Vessel Used in Experiments.

2.2 Simulant Preparation

Reagent grade sodium nitrate, sodium nitrite, sodium sulfate, sodium carbonate, 50 wt % sodium hydroxide solution, and aluminum trinitrate nonahydrate were purchased from Alfa Aesar and used as received. In cases where target nitrate-to-aluminum ratios would not permit the use of aluminum trinitrate, sodium aluminate was used as the source of aluminum. Simulants were prepared by first mixing the specified amount of 50 wt % sodium hydroxide solution with a minimal amount of deionized (DI) H_2O. This highly-caustic mixture was then used to dissolve the targeted amount of aluminum trinitrate nonahydrate. Following the addition of aluminum salt, the remaining species (sodium nitrate, sodium sulfate, sodium nitrite, and sodium carbonate) were added to the specified levels. The mixture was then diluted with DI H_2O until the requisite volume was reached to ensure that the desired concentrations of each species was met.

Some of the simulants prepared in this work exhibited a solid phase at room temperature. When problematic (i.e., not easily transferred to the reaction vessel), these simulants were filtered using a 0.5 L, 0.25-micron nylon vacuum filter cup. Note that filtration of solids results in a decrease in total material and a shift in the expected concentrations. The concentrations of salt species in each test was determined by measurement of the tested material, so filtration of solids is not expected to have a significant impact on reported concentrations.

2.3 Experimental Procedure

For every experiment described in this work, approximately 1 L of the specified simulant was added to the kettle via an addition port installed in the top of the apparatus. When appropriate, additional simulant aliquots were used to assist in the transfer and dissolution of the chemical additive under investigation. Liquid samples were drawn as needed to confirm final simulant composition after addition of chemical additives. After addition of all chemicals and subsequent sampling, the kettle was resealed and checked for leaks by mass balance of air flow through the process headspace. Once leak-free conditions had been

confirmed, stirring was initiated and a purge flow of dried air was applied to the process to sweep residual CO_2 out of the vessel. The system controls were then set to apply heat via two electric heating rods such that the difference between the process (fluid) temperature and that of the heating rod interior could not exceed 20 °C. Once the process fluid reached the desired temperature, the purge gas was switched from the higher-purge air stream to the generally lower-purge process gas stream (0.5 vol % Kr, 20 vol % O_2 in N_2). This point is designated as the start of the experiment.

The experiment continued while monitoring for hydrogen concentration via GC. At a minimum, the experiment duration was planned such that the kettle headspace could undergo approximately three vapor space volume turn-overs (achieving 99.7% of pseudo steady-state, assuming continuously-stirred reactor dynamics; note that this time is volume- and purge rate-dependent). Once this time was reached and hydrogen measurements by GC stabilized or began to decrease, heating rod power was turned off and the experiment was stopped. The high-purge air was then reapplied to the vessel to sweep out residual hydrogen. The simulant mixture was then removed from the vessel and subsampled as needed for product analyses.

2.4 Experimental Design

The experiments described in this report were designed according to one of two methodologies: 1) variation of conditions around a single centroid, or 2) selection of minimum optimized experiments within a specified range of conditions. Centroid variation closely mimics traditional techniques for determining reaction kinetics. In this approach, a single experiment is performed at a standard condition (including species concentrations and temperature). Afterward, a second experiment is performed in which only a single parameter (temperature, the concentration of a single species, etc.) is changed (e.g., increased by 3X). By comparing the impact of a single parameter on the observed reaction rate, the functional dependency of that parameter within a rate expression may be calculated (e.g., an increase of hydroxide by 2X that results in a 4X increase in observed reaction rate may indicate a second-order impact of hydroxide on the reaction).

The range optimization approach was also employed in this work, due to the wide range of conditions expected during processing at SRS. Table 2-1 lists the maximum and minimum concentrations and temperatures used to generate a subset of optimized experiments.

Table 2-1. Proposed Design Space for Simulant HGR Experiments.

Parameter	Minimum	Maximum	Units
$[Al]$	1.29E-03	1.98E+00	M
$[NO_2]$	2.21E-01	2.58E+00	M
$[NO_3]$	6.75E-02	5.58E+00	M
$[OH]$	1.58E-01	1.18E+01	M
$[SO_4]$	4.94E-04	2.05E-01	M
$[CO_3]$	8.14E-03	5.79E-01	M
T	70	130	°C

The experimental design employed in this work used D-optimality within the parameter ranges described in Table 2-1 as a criterion for experiment selection. In this approach, ten-thousand possible conditions were randomly generated to completely cover the ranges described in Table 2-1. Afterwards, between 7 and 14 of these ten-thousand possible testing conditions were selected D-optimally, according to the following model assumption (Equation [1]):

$$\ln HGR = a\ln[Al] + b\ln[NO_2] + c\ln[NO_3] + d\ln[OH] + \ldots$$
$$\ldots + e\ln[SO_4] + f\ln[CO_3] + g\ln[Na] - \frac{h}{T + 273.15} \quad [1]$$

where $[Na]$ is expressed as the linear combination of the products of concentration and valency of the expected counteranions, according to Equation [2] (the full loading of aluminum is expected to be present as sodium aluminate).

$$[Na] = [Al] + [NO_2] + [NO_3] + [OH] + 2\times[SO_4] + 2\times[CO_3] \quad [2]$$

The selection of a subset of experimental conditions according to D-optimality does not reduce the applicability of resulting model expressions to only those conditions or ranges of conditions evaluated during testing. Rather, the use of D-optimal selection of experimental conditions is intended to minimize the variance of the model coefficient estimates over the design space (i.e., the ranges expressed in Table 2-1). Therefore, the models generated in this report are applicable over the planned design space as well as any additional conditions tested.

2.5 Liquid Analyses

Liquid samples were submitted to SRNL's Analytical Development (AD) and Process Science Analytical Laboratory (PSAL) groups for analysis. AD determined the concentrations of Total Inorganic Carbon (TIC), TOC, and free hydroxide, while PSAL determined the concentrations of metals and anions, as well as measured the density of the sample.

Free hydroxide was determined in a titration method in which the concentration of hydroxide is assumed to equal the concentration of acid necessary to decrease the sample pH to 7, accounting for the presence of other caustic species (e.g., CO_3^{2-}). TIC was determined by charging an aqueous sample with phosphoric acid and measuring the amount of CO_2 released upon addition. TOC was determined by treating the acidified aqueous sample with an aliquot of persulfate to digest any organic species present and measuring the amount of CO_2 evolved from the sample.

Density was determined using an Anton-Parr Densitometer. Concentrations of dissolved metals were determined using an Inductively Coupled Plasma - Emission Spectrometer (ICP-ES). Concentrations of anions were determined using an Ion Chromatography (IC) column.

2.6 Offgas Analyses

An Inficon MicroGC was used to analyze offgas content for all experiments. The GC was equipped with two analysis channels, one using a Molsieve 5A column for H_2, O_2, N_2, and Kr analysis and a second using a PoraPLOT Q column for N_2O and CO_2 analysis. Each column employed a thermal conductivity detector which measured against the background of pure argon (also used as a carrier gas). The GC calibration was verified before every experiment using a calibration gas with a composition of 50 ppm_v H_2, 100 ppm_v CH_4, 0.5 vol % Kr, 1 vol % N_2O, 1 vol % CO_2, and 20 vol % O_2 in N_2. The GC was also used to qualitatively track the concentrations of He and H_2O.

When necessary, an FT-IR was also used to screen for the presence of other species (such as VOCs). This unit was plumbed in line after the GC and was exclusively used as a qualitative tool.

When presented, HGR is reported in units of standard cubic feet per hour per gallon of simulant mixture ($ft^3\ hr^{-1}\ gal^{-1}$). The purge rates employed during this testing were supplied at standard conditions of 21.11 °C and 1 atm. The HGRs presented herein have been corrected to a standard temperature and pressure of 25 °C and 1 atm.

2.7 Quality Assurance

The customer-identified functional classification for the HGR measurement tasks Safety Class.[5-6] Requirements for performing reviews of technical reports and the extent of review are established in Manual E7, Procedure 2.60.[12] SRNL documents the extent and type of review using the SRNL Technical Report Design Checklist contained in WSRC-IM-2002-00011, Rev. 2.[13] The data described in this report is recorded for permanent retention in the Electronic Laboratory Notebook (ELN) within notebook L7748-00246. Similarly, the use of any Measuring and Test Equipment (M&TE) or Measurement Systems and Equipment (MS&E) is recorded in this notebook. Measurements, calculations, documentation, and technical review comply with the customer required quality assurance level to support Safety Class use of information contained in this report.

The Data Acquisition and Control (DAC) software employed in this testing was used to control mass flow controllers, overhead mixers, and liquid addition pumps, as well as record data taken from thermocouples and GC-TCD stations. This software is classified as level D. The DAC software does not perform calculations that are used in this report. The logged data that contributes to HGR calculations are the purge gas flows and the reaction temperature. The purge gas flow instruments, thermocouples, and temperature scanner are in the M&TE program. Each of these instruments has an alternative reading outside of the DAC software. Data is periodically recorded manually (e.g., every 30 minutes) to supplement the files generated by the DAC software.

Additionally, the statistical software package JMP 11.2.0 was used for the regression of linear models developed in this report. The results generated from JMP 11.2.0 were checked using JMP Pro 11.2.1, which has undergone verification and validation[14] and is classified as level D software.

3.0 Results and Discussion

3.1 Common CSTF Organics Initial Screening Tests

Initial screening tests were performed to evaluate the potential of common CSTF organics to form hydrogen in processing conditions.[15] These tests were conducted by adding predetermined organic species to ~1 L of Tank 38 simulant, heating the vessel to 100 °C, and monitoring the headspace for hydrogen formation by GC. The measured composition for the Tank 38 simulant is given in Table 3-1, as are the residual standard deviations (RSD) for each measurement.

Table 3-1. Composition of Tank 38 Simulant Used During Initial Organics Screening.

Component	Unit	Concentration	%RSD
TIC	M	7.45E-01	15.6
TOC	mg/L	1.15E+02	17.9
OH	M	2.84E+00	2.7
Cl	M	<2.82E-03	N/A
NO_2	M	2.53E+00	6.4
NO_3	M	1.23E+00	4.7
SO_4	M	7.06E-02	9.9
Al	M	8.30E-02	8.8
Fe	M	1.29E-05	9.8
K	M	2.36E-04	7.2
Na	M	7.04E+00	14.0

Table 3-2 gives the test list of each experiment performed to initially assess the ability of common CSTF organics to produce hydrogen. Note that the test names are derived from the run plan specifying the conditions for each test and are not an indicator of the total number of experiments performed or the order in which tests were conducted. The TOC values shown are calculated from the empirical formula of each organic additive.

Table 3-2. Test List for Common CSTF Organic Screening Experiments

Test ID	Additive	Additive Concentration† (mg/L)	Added TOC (mg/L)	Description
P1S1-Test 1	None	N/A	N/A	Screening of Stainless-Steel Vessel at 95 °C
P1S1-Test 2	None	N/A	N/A	Screening of PTFE Vessel at 95 °C
P1S1-Test 2B	None	N/A	N/A	Measurement of Baseline HGR at 100 °C
P1S1-Test 2C	None	N/A	N/A	Repeat of Test 2B
P1S1-Test 3A	Sodium Glycolate	1351	331	HGR measurement of Glycolate at 100 °C
P1S1-Test 3B	Sodium Glycolate	1351	331	Repeat of Test 3A
P1S1-Test 4	Slurry Mix Evaporator (SME) Supernatant	31,550††	407	HGR measurement of glycolate from SME products
P1S1-Test 5	Sodium Formate	4650	821	HGR measurement of formate
P1S1-Test 7	Xiameter AFE-1010	1029	10	HGR measurement of tank farm antifoam
P1S1-Test 8	TMS	256	102	HGR measurement of DWPF Antifoam Decomposition Products
P1S1-Test 9	(Poly)ethyleneoxide (PEO)	670	363	
P1S1-Test 10	Propanal	101	63	
P1S1-Test 11	Butanol	205	133	HGR measurement of TBP Decomposition Products
P1S1-Test 12	DBP	820	375	
P1S1-Test 13	CSSX Blended Solvent	80	63	HGR measurement of CSSX solvent
P1S1-Test 14	Terephthalic Acid	520	372	HGR measurement of resin surrogates
P1S1-Test 15	Methylcarboxypyridinium	390	187	
P1S1-Test 16	Sulfobenzoic Acid	615	215	
P1S1-Test 17	Formate+Oxalate+CSSX Solvent	N/R	912	HGR measurement of formate, oxalate, and CSSX solvent

N/R = "Not Reported"; multiple additives were used.
†The basis for the targeted concentrations of additives was developed in SRNL-L3300-2018-00004.[15]
††Glycolate in the SME supernatant was diluted, so ~30 grams of supernatant phase were added to charge glycolate at a concentration of 1000 mg/L.

Experiments P1S1-Test 1 and P1S1-Test 2 were performed to evaluate differences in observed baseline HGR (no added organics) due to the material of construction used in the reaction vessel. P1S1-Test 1 was performed with a stainless-steel vessel, PTFE lid, and stainless-steel agitator shaft. P1S1-Test 2 was performed with a PTFE vessel, PTFE lid, and a PTFE-coated agitator shaft. Both tests were performed at 95 °C. The HGR results from these tests are shown in Figure 3-1.

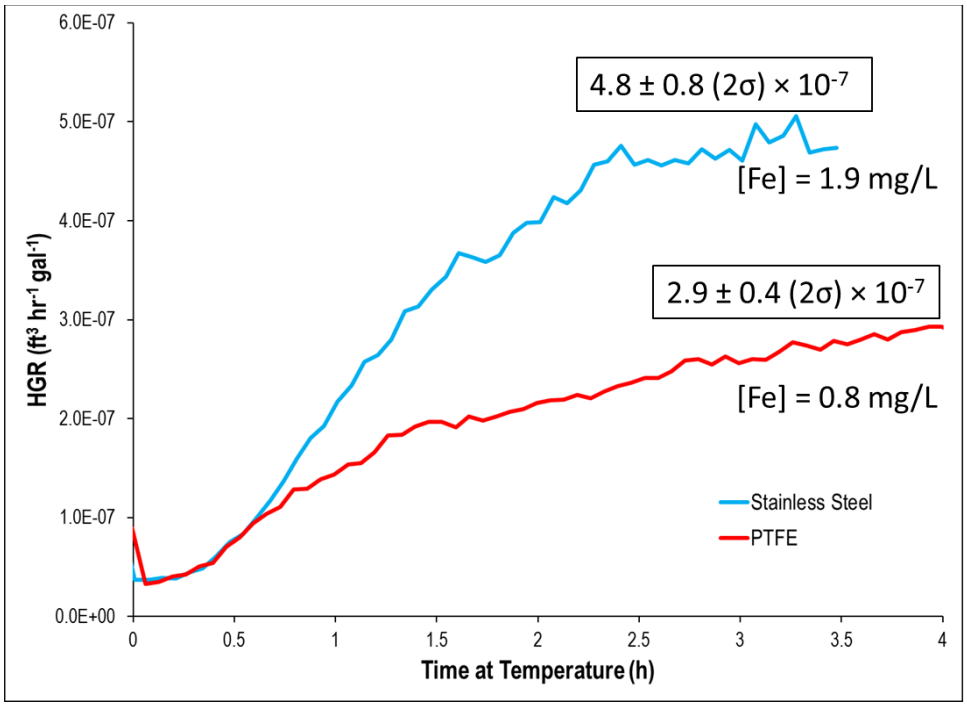

Figure 3-1. HGR Profiles of P1S1-Test 1 (Stainless Steel) and P1S1-Test 2 (PTFE).

Initial HGR results shown in Figure 3-1 suggested that more baseline hydrogen is evolved in the presence of stainless-steel ($4.8 \pm 0.8 \times 10^{-7}$ ft^3 h^{-1} gal^{-1}) than in the presence of PTFE ($2.9 \pm 0.4 \times 10^{-7}$ ft^3 h^{-1} gal^{-1}). Note that it is not certain if this increase in HGR is due to formation of a passivation layer on the stainless steel, caustic corrosion of the steel, or enhanced reactivity of the organic impurities in the simulant. It was also observed that the concentration of dissolved iron in the product of the stainless-steel test (1.9 mg/L) was measurably higher than that seen in PTFE (0.8 mg/L). It was therefore determined, following discussion with the customer, to use a PTFE vessel for all HGR experiments in subsequent testing to limit the interference of changing metal content. The wall thickness of the PTFE vessel was selected such that hydrogen diffusion through the vessel wall was minimal. This was confirmed by measuring 1) the lack of hydrogen in a sample of hydrogen-free purge gas charged to the vessel at the lowest employed flowrate of 3 sccm and 2) the balance of hydrogen added to the vessel using a purge gas containing 50 ppm_v hydrogen.

After these initial tests, glycolate thermolysis was briefly investigated to answer questions of glycolate source dependence before designing an experimental test matrix to specifically elucidate glycolate kinetics. Experiment P1S1-Test 3A was performed by charging ~1000 mg/L of glycolate (in the form of sodium glycolate salt) to the Tank 38 simulant, while P1S1-Test 4 was performed by charging ~1000 mg/L of glycolate (in the form of basified SME supernatant). The sources of glycolate in these tests were varied to determine if differences could be observed in thermolysis of glycolate that had undergone CPC Sludge Receipt and Adjustment Tank (SRAT) and SME processing. P1S1-Test 3A yielded an HGR value of $5.4 \pm 0.8 \times 10^{-6}$ ft^3 h^{-1} gal^{-1}, while P1S1-Test 4 yielded an HGR of $5.0 \pm 0.8 \times 10^{-6}$ ft^3 h^{-1} gal^{-1}.

While HGR results from P1S1-Test 3A exhibited a regular behavior (increasing hydrogen concentration until achieving steady-state behavior), results from P1S1-Test 4 were irregular, rapidly evolving a larger amount of hydrogen before decreasing to a consistent HGR. Currently, it is uncertain if this temporarily higher rate of hydrogen formation was due to the presence of other organic molecules in the SME supernatant phase or a disturbance due to the addition of the relatively large SME supernatant aliquot (~30 mL). Nevertheless, the observation that steady-state HGR is apparently independent of glycolate source

within the sensitivity of this equipment suggests that either source may be used. Furthermore, the complications just described suggest that use of sodium glycolate salt may introduce less uncertainty to HGR measurement. It was therefore decided, after review with the customer, to use sodium glycolate as a glycolate source for all future simulant experiments with glycolate. A repeat of the glycolate thermolysis experiment was performed (P1S1-Test 3B) to better understand the uncertainty of the glycolate HGR measurement, yielding a comparable HGR of $4.8 \pm 0.7 \times 10^{-6}$ ft^3 h^{-1} gal^{-1}. Two "blank" tests (P1S1-Test 2B and P1S1-Test 2C) were performed at 100 °C to better define the baseline HGR expected from tests with no added organics. The results of these five experiments (P1S1-Tests 2B, 2C, 3A, 3B, and 4) are shown in Figure 3-2. Note that the maximum HGR reported in the Figure (~7.5×10^{-6} ft^3 h^{-1} gal^{-1}) corresponds to a glycolate degradation rate of less than 0.2 mg/L per hour, suggesting that the decrease in starting material due to HGR is negligible during the experiment.

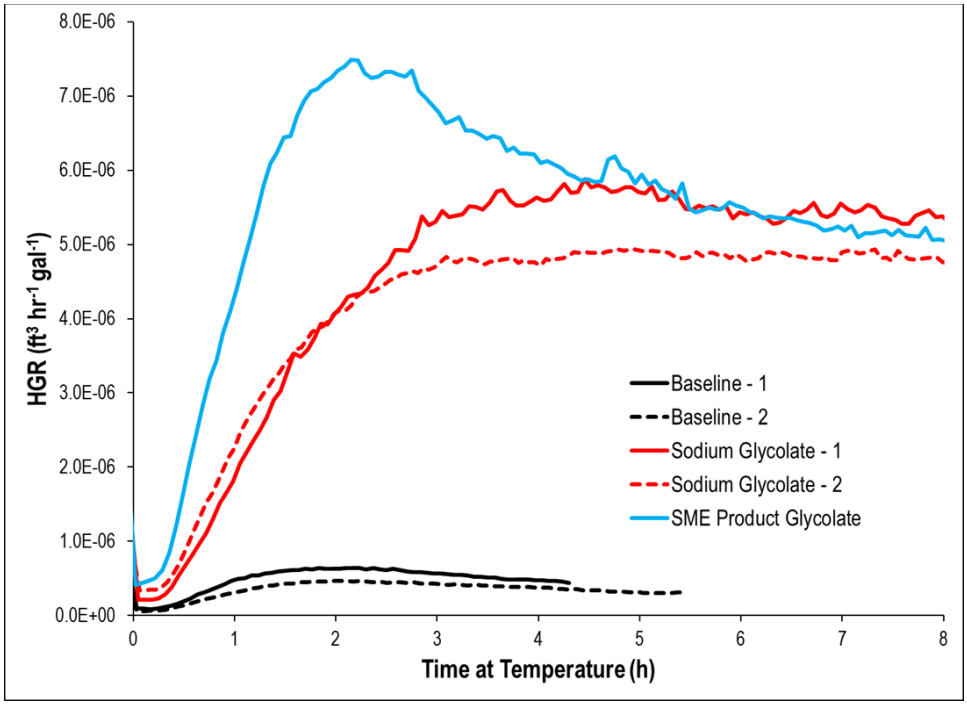

Figure 3-2. HGR Profiles of P1S1-Test 2B (Baseline 1), P1S1-Test 2C (Baseline 2), P1S1-Test 3A (Sodium Glycolate 1), P1S1-Test 3B (Sodium Glycolate 2), and P1S1-Test 4 (SME Product Glycolate).

Following initial glycolate tests, experiments were performed to determine the HGR evolved from organic molecules currently found in CSTF waste. Prior to testing, it was hypothesized that sodium formate, sodium oxalate, and CSSX solvent would be low hydrogen producers. These three organic additives were therefore tested simultaneously at first in P1S1-Test 17. This experiment yielded an HGR of $5.9 \pm 0.9 \times 10^{-7}$ ft^3 h^{-1} gal^{-1}, which was considered comparable to the HGR observed with no added organics ($4.1 \pm 1.4 \times 10^{-7}$ ft^3 h^{-1} gal^{-1}). Confirmatory tests were performed for sodium formate (P1S1-Test 5) and CSSX solvent (P1S1-Test 13), yielding HGR values of $3.3 \pm 0.6 \times 10^{-7}$ ft^3 h^{-1} gal^{-1} and $3.8 \pm 0.6 \times 10^{-7}$ ft^3 h^{-1} gal^{-1}, respectively. The results of these tests are shown in Figure 3-3.

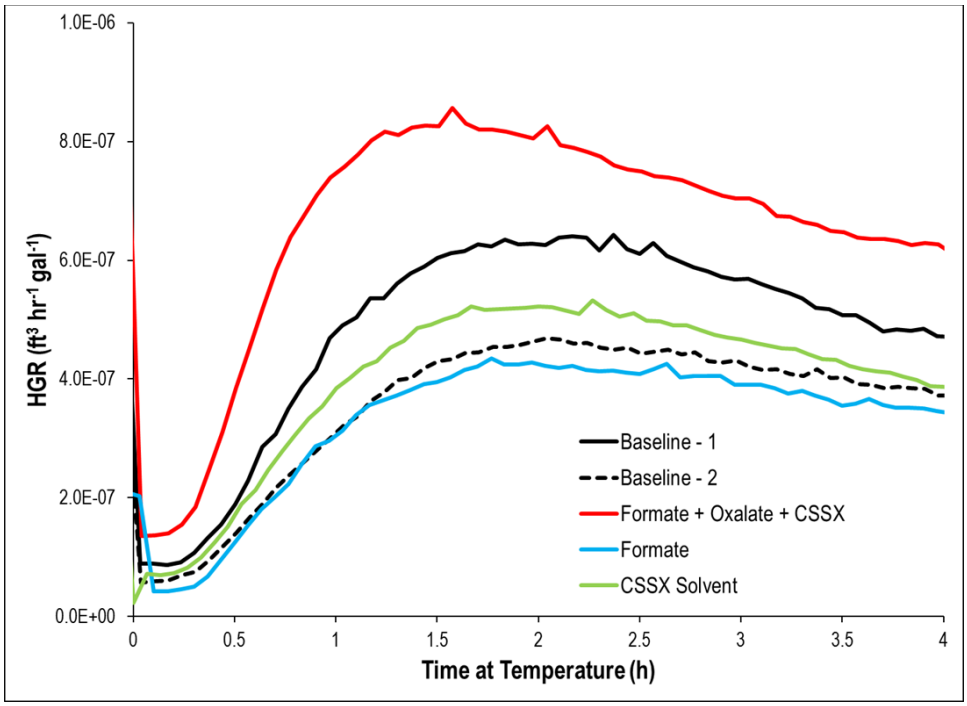

Figure 3-3. HGR Profiles of P1S1-Test 5 (Formate), P1S1-Test 13 (CSSX Solvent), and P1S1-Test 17 (Formate + Oxalate + CSSX Solvent).

Further HGR experiments were performed with TMS and PEO, both of which are known degradation products from hydrolysis of Antifoam 747.[16] P1S1-Test 8 was conducted at approximately 250 mg TMS per L of simulant and yielded an HGR of $4.0 \pm 0.6 \times 10^{-7}$ ft^3 h^{-1} gal^{-1}, similar to the baseline values observed without added organics. Similar results were seen when testing at approximately 650 mg PEO per L of simulant (P1S1-Test 9), with HGRs remaining as low as $5.9 \pm 0.9 \times 10^{-7}$ ft^3 h^{-1} gal^{-1}. Results of these experiments are depicted in Figure 3-4.

It is important to note that TMS is a known volatile compound, exhibiting a boiling point slightly lower than that of water (99 °C). During testing, an appreciable amount of TMS was lost to evaporation and to formation of HMDSO. The vapor phase concentration of these compounds became so concentrated that the purge gas flow rate had to be increased to prevent formation of a flammable headspace. This purge rate modification is the reason for a data gap in the P1S1-Test 8 profile shown in Figure 3-4.

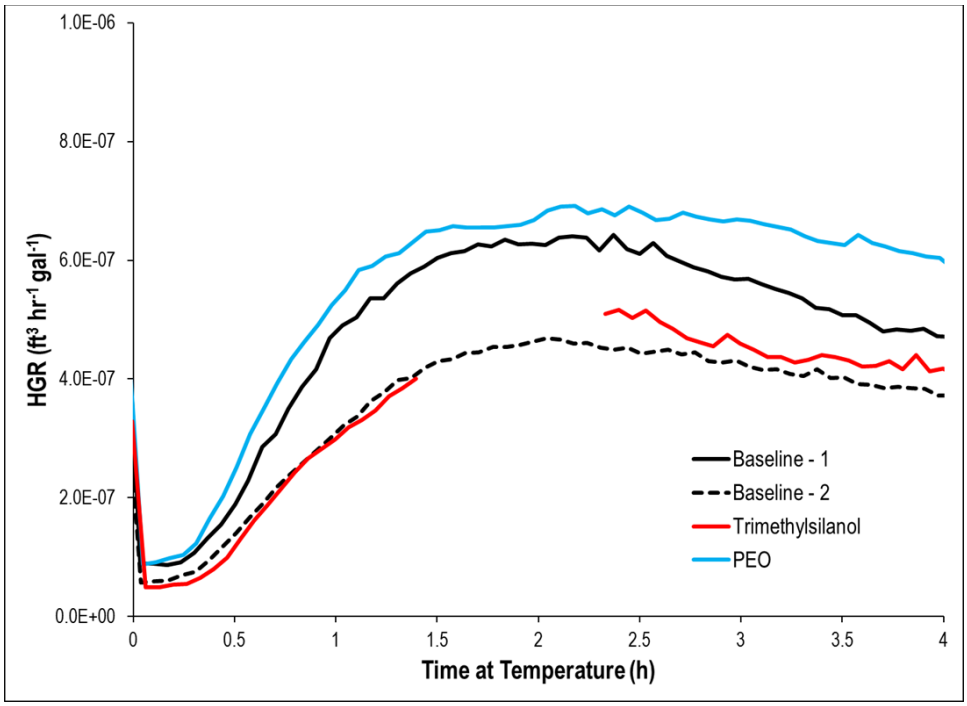

Figure 3-4. HGR Profiles of P1S1-Test 8 (Trimethylsilanol) and P1S1-Test 9 (PEO).

It should be noted that hydrogen was not the only flammable gas observed during testing with TMS. Methane (CH_4) was also observed during testing with TMS, suggesting hydrolysis of the Si-CH_3 bonds present. While this finding is significant from a flammability prevention stance, it is difficult to accurately quantify the generation rate of CH_4, given that the HGR apparatus has been purposefully optimized for the measurement of hydrogen at the cost of deteriorated detection limits of other gases. An FT-IR spectrum of the offgas generated during P1S1-Test 8 is given in Figure 3-5.

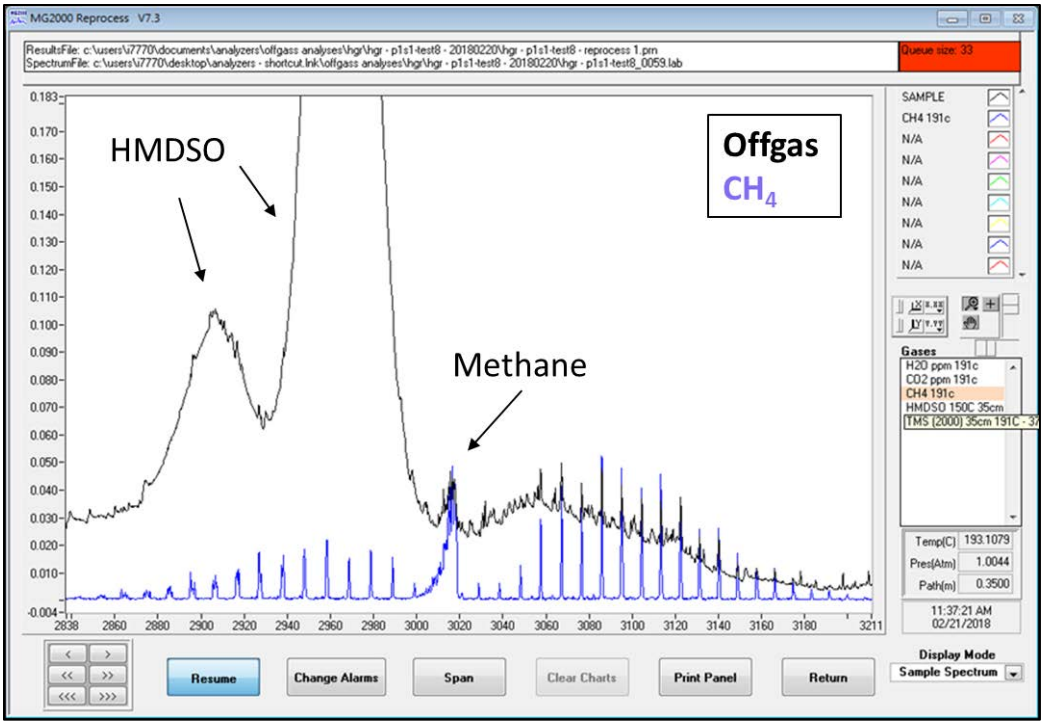

Figure 3-5. IR Spectra of Offgas from P1S1-Test 8. The black line is the IR spectrum sampled from the vapor space of the reaction. The blue line is a library spectrum of methane. Note that evidence of methane and HMDSO can be seen in the IR spectrum.

Additional testing was performed to evaluate the potential for hydrogen formation from other antifoam-related compounds, specifically propanal (a known side product of Antifoam 747 used in DWPF) and Xiameter AFE-1010 (chemically equivalent to H-10, an antifoam agent previously used in the CSTF evaporators). P1S1-Test 10 was conducted by charging approximately 100 mg/L of propanal to the Tank 38 simulant and heating to 100 °C under purge to detect hydrogen. This experiment yielded a notably higher HGR than previous testing, reaching as high as 1.3×10^{-5} ft^3 h^{-1} gal^{-1} before rapidly decreasing to a value of $9.3 \pm 1.5 \times 10^{-6}$ ft^3 h^{-1} gal^{-1} within two hours. Similarly, a relatively high HGR was achieved in P1S1-Test 7, wherein Xiameter AFE-1010 was charged to Tank 38 simulant at approximately 1000 mg/L. This experiment yielded an HGR of $2.3 \pm 0.4 \times 10^{-6}$ ft^3 h^{-1} gal^{-1}. Results for each of these experiments are displayed in Figure 3-6. It should be noted that trace amounts of octamethylcyclotetrasiloxane, a polydimethylsiloxane oligomer and known impurity in Xiameter AFE-1010, was observed in offgas streams from testing with Xiameter AFE-1010. This phenomenon is expected to be dependent upon the use of pure Xiameter AFE-1010 and is not expected from aged waste media.

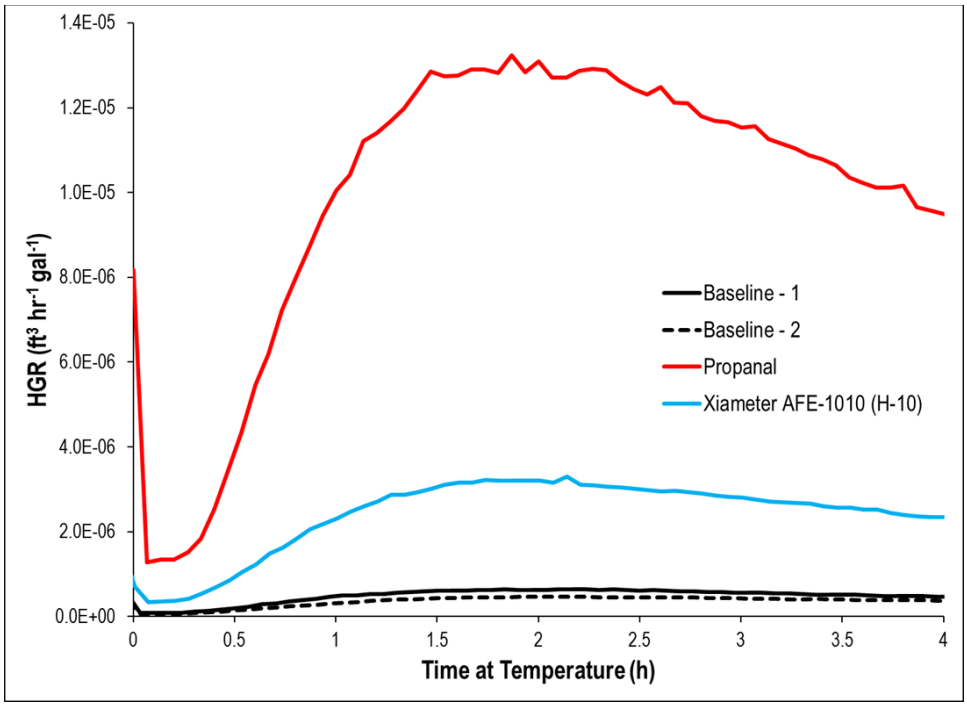

Figure 3-6. HGR Profiles of P1S1-Test 7 (Xiameter AFE-1010) and P1S1-Test 10 (Propanal).

TBP degradation products (butanol and dibutylphosphate) were also screened for hydrogen generation. P1S1-Test 11 was performed by charging approximately 200 mg of butanol per L of Tank 38 simulant. The HGR observed in this test was not statistically different from that seen in baseline testing, reaching 4.0 ± 0.6 × 10^{-7} ft^3 h^{-1} gal^{-1} at the end of 4 hours. Similar low rates were seen with DBP (P1S1-Test 12), which yielded an HGR of 4.1 ± 0.6 × 10^{-7} ft^3 h^{-1} gal^{-1}. These results are shown in Figure 3-7.

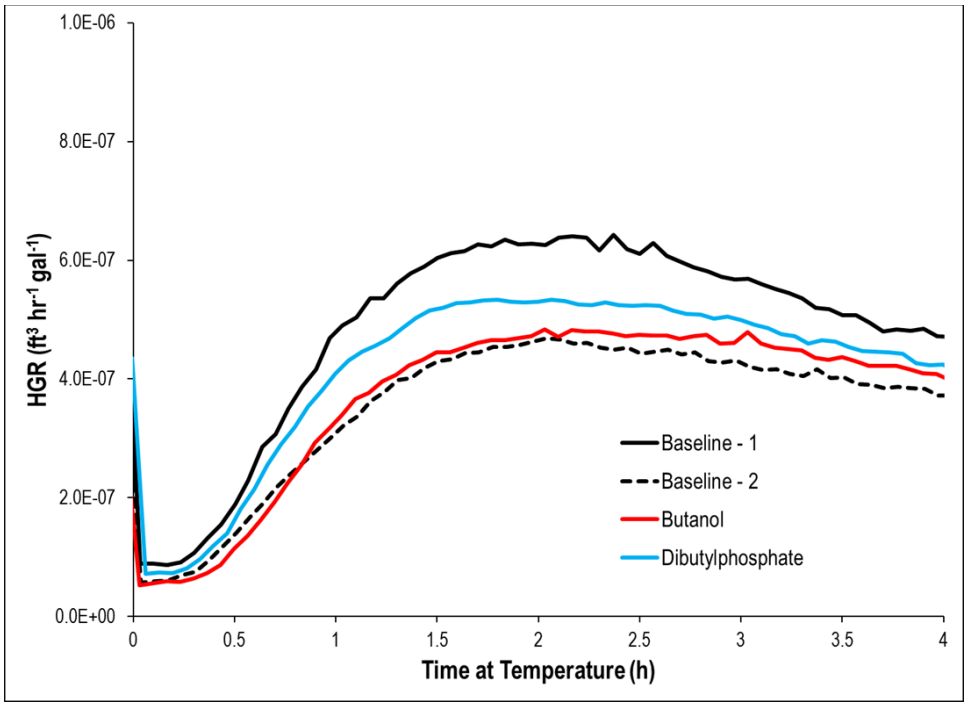

Figure 3-7. HGR Profiles of P1S1-Test 11 (Butanol) and P1S1-Test 12 (Dibutylphosphate).

Lastly, testing was performed to evaluate the potential of ion exchange resin degradation products to produce hydrogen. Three surrogate molecules were used to approximate the behavior of soluble resin degradation products expected after resin digestion with permanganate: terephthalic acid (P1S1-Test 14, added at 520 mg/L, used to study the HGR expected from the expected degradation product of the divinylbenzene monomers found in most resins), methylcarboxypyridinium (P1S1-Test 15, added at 390 mg/L, used to study the HGR expected from methylpyridine-containing resins employed in anion exchange columns), and sulfobenzoic acid (P1S1-Test 16, added at 615 mg/L, used to study the HGR expected from compounds containing sulfobenzoate, an expected degradation product of common cation exchange resins). Terephthalic acid and sulfobenzoic acid each yielded relatively low HGRs ($5.9 \pm 0.9 \times 10^{-7}$ ft^3 h^{-1} gal^{-1} and $5.0 \pm 0.8 \times 10^{-7}$ ft^3 h^{-1} gal^{-1}, respectively), similar to the baseline. However, methylcarboxypyridinium yielded a significantly higher HGR, reaching as high as $1.0 \pm 0.2 \times 10^{-5}$ ft^3 h^{-1} gal^{-1}. This observation suggests that methylpyridinium species are subject to high HGRs in tank farm conditions. Results of these experiments are shown in Figure 3-8.

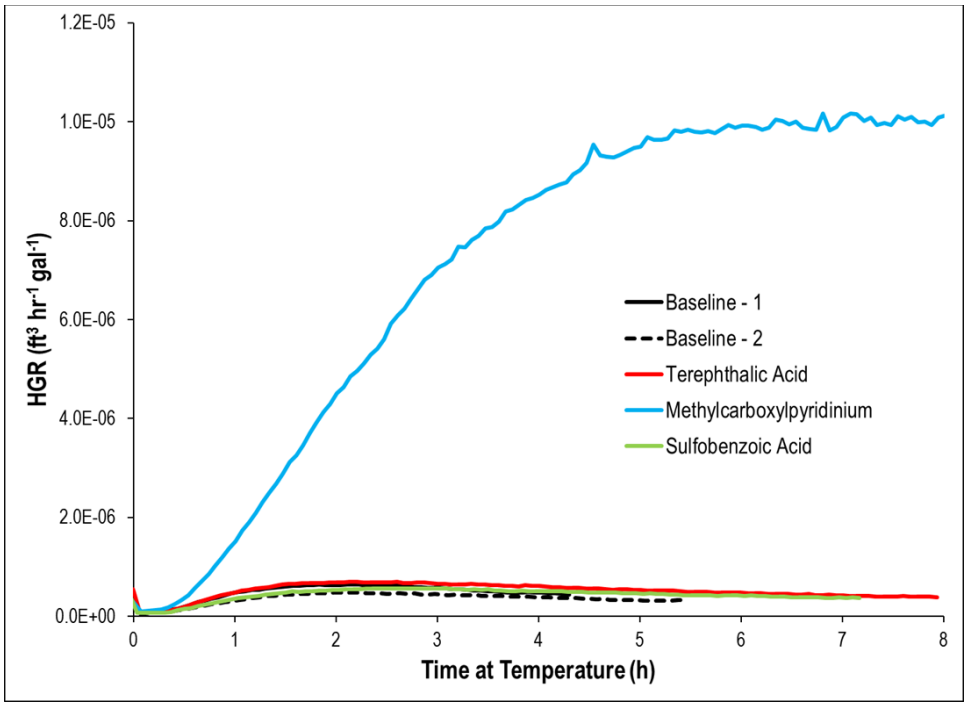

Figure 3-8. HGR Profiles of P1S1-Test 14 (Terephthalic Acid), P1S1-Test 15 (Methylcarboxypyridinium), and P1S1-Test 16 (Sulfobenzoic Acid).

The observed HGRs from P1S1-Test 1 through 17 and the corresponding 2σ uncertainties are given in Table 3-3.

Table 3-3. Observed HGRs from Preliminary Screening Experiments.

Test Name	Additive	Observed HGR (ft^3 h^{-1} gal^{-1})	2σ Uncertainty (ft^3 h^{-1} gal^{-1})
P1S1-Test 1	None	4.81E-07	7.54E-08
P1S1-Test 2	None	2.86E-07	4.48E-08
P1S1-Test 2B	None	4.58E-07	7.33E-08
P1S1-Test 2C	None	3.61E-07	6.09E-08
P1S1-Test 3A	Sodium Glycolate	5.36E-06	8.13E-07
P1S1-Test 3B	Sodium Glycolate	4.76E-06	7.22E-07
P1S1-Test 4	SME Supernatant	5.05E-06	7.72E-07
P1S1-Test 5	Sodium Formate	3.32E-07	5.79E-08
P1S1-Test 7	Xiameter AFE-1010	2.27E-06	3.59E-07
P1S1-Test 8	TMS	4.01E-07	5.95E-08
P1S1-Test 9	PEO	5.94E-07	9.11E-08
P1S1-Test 10	Propanal	9.26E-06	1.52E-06
P1S1-Test 11	Butanol	3.96E-07	6.30E-08
P1S1-Test 12	DBP	4.07E-07	6.41E-08
P1S1-Test 13	CSSX Organics	3.81E-07	6.04E-08
P1S1-Test 14	Terephthalic Acid	5.92E-07	9.41E-08
P1S1-Test 15	Methylcarboxypyridinium	1.01E-05	1.55E-06
P1S1-Test 16	Sulfobenzoic Acid	5.02E-07	7.72E-08
P1S1-Test 17	Formate+Oxalate+CSSX	5.88E-07	8.96E-08

Given the reaction rate information obtained from these tests, it is important to define a method for evaluation of reactivity. Such a method is available via existing thermolytic HGR prediction expressions. One such expression is the Hu equation used at the Hanford Facility,[9] given in Equation [3]:

$$HGR = \alpha_{thm} \cdot r_f \cdot [TOC] \cdot [Al]^{0.4} \cdot L_f \cdot e^{-E_{thm}/RT} [=] \frac{\text{mol H}_2}{\text{kg} \cdot \text{day}} \quad [3]$$

where,

α_{thm} is a pre-exponential constant equal to 3.94×10^9 mol H_2 kg^{-1} day^{-1},
r_f is a reactivity coefficient indicating the readiness with which hydrogen is formed in a certain condition,[f.1]
$[TOC]$ is the concentration of organic carbon in weight percent,
$[Al]$ is the concentration of aluminum in weight percent,
L_f is the mass fraction of the generating material that is in the liquid phase,
E_{thm} is the thermolytic activation energy, equal to 89,600 J mol^{-1},
R is the ideal gas constant, 8.314 J mol^{-1} K^{-1}, and
T is the temperature in K.

The Hu equation was developed by measuring both radioactive and simulant waste samples and is expected to apply to numerous organic compounds such as the complexants known to be in Hanford HLW. It is therefore reasonable to use as a first attempt at describing the reactivity of the organics examined in this work. To use the Hu reactivity coefficient, r_f, the Hu expression is modified to be used in HGR units reported at SRS in Equation [4]:

$$r_f = \frac{7.338 \cdot HGR_{obs}}{\rho_{sol'n} \cdot \alpha_{thm} \cdot [TOC] \cdot [Al]^{0.4} \cdot e^{-E_{thm}/RT}} \quad [4]$$

where,

HGR_{obs} is the observed HGR in ft^3 (at 25 °C, 1 atm) h^{-1} gal^{-1}, and
$\rho_{sol'n}$ is the density of the liquid in kg L^{-1}.

Note that the L_f term has been omitted in Equation [4]; this is because the liquid fractions of the reactions reported here are all equal to 1 (that is to say, they are all homogeneous solutions). Using Equation [4], the HGRs measured from each test, the measured density and aluminum concentration of each solution, and knowledge of added organic carbon and temperature used in each experiment, one may calculate the Hu reactivity factors for each organic compound investigated in this work. These values are given in Table 3-4 with 2σ uncertainty. Note that in the cases where "0" is given as a lower limit, the confidence interval of the measured HGR for that compound includes a value of 0 HGR.

[f.1] The r_f coefficient in the Hu equation applied to Hanford Facility HLW tanks is generally assigned a value of 0.3 for Single Shell Tanks containing older waste or a value of 0.6 for Double Shell Tanks containing fresher waste which may contain a higher fraction of energetic organic compounds.

Table 3-4. Calculated Hu Reactivity Factors for Each Organic Compound Tested in Initial Screening Experiments.

Compound	TOC (mg/L)	r_f (2σ)
Glycolate (Sodium Salt)	330	1.43 – 2.28
Glycolate (SME Product)	410	1.24 – 1.74
Sodium Formate	820	0 – 0.01
CSSX Solvent	60	0 – 0.18
Sodium Formate + CSSX Solvent + Sodium Oxalate	910	0.01 – 0.04
DBP	380	0 – 0.04
Butanol	130	0 – 0.10
TMS	100	0 – 0.13
PEO	360	0.02 – 0.11
Propanal	60	15.2 – 21.6
Xiameter AFE-1010	10	19.6 – 29.4
Sulfobenzoic Acid	220	0 – 0.13
Terephthalic Acid	370	0.02 – 0.11
Methylcarboxypyridinium	190	5.70 – 7.88

The results given in Table 3-4 suggest that the organics investigated during the preliminary screening process are not equally reactive toward the production of hydrogen. Most organics investigated (such as formate, CSSX solvent, DBP, butanol, and TMS) yielded no appreciable HGR over the baseline and, as a result, are suggested to have effectively zero reactivity, as can be seen in the reported r_f factors for these compounds. Polyethylene oxide and sodium oxalate (in the presence of formate and CSSX solvent) yield measurable HGRs relative to the organic-free baseline; however, the calculated r_f factors suggest that these compounds possess negligible reactivity. Sodium oxalate is expected to have zero reactivity toward the production of hydrogen due to its inherent lack of hydrogen atoms. Finally, some compounds exhibit a definite reactivity towards hydrogen production and should be evaluated further (such as glycolate, propanal, Xiameter AFE-1010, and methylcarboxypyridinium, a suspected degradation product of Reillex HPQ resin). The low reactivities exhibited by sulfobenzoic acid and terephthalic acid (r_f = 0 – 0.13) suggest that most of the expected degradation products from ion exchange resins (especially those employed in cation exchange) are not subject to high HGRs. However, given the positive indication of reactivity achieved from methylcarboxypyridinium (r_f = 5.7 – 7.9), other degradation products from anionic exchange resins employed historically at SRS (namely, Reillex HPQ and IONAC A-641) were proposed for further investigation.

Given the increased reactivity observed with the compounds glycolate (α-hydroxyethanoate, or $C_2H_3O_3$), propanal (propionaldehyde), Xiameter (10% blend of polydimethylsiloxane and octamethyldisiloxane in water), and resin degradation compounds (such as IONAC A-641 and Reillex HPQ, polydivinylbenzene-based resins with trimethylbenzylammonium and methylpyridinium modifiers, respectively), it was proposed to further develop an understanding of the parameters that drive the thermolysis of these compounds to establish a bounding thermolytic model.

3.2 Organic-Free Hydrogen Measurements

To better quantify the rates of hydrogen being released from each organic species as a function of temperature and solution matrix conditions, it is important to first understand the contribution of HGR due to "organic-free", or blank conditions (i.e., hydrogen release from simulant matrices when no added organic is present). Quantification of the "blank" HGR determining factors allows a calculation of thermolytic HGR from organic compounds according to the following expression:

$$HGR_{org}^{i} = HGR_{obs}^{i} - HGR_{blank}^{i} \quad [5]$$

where HGR_{org}^{i} is the contribution of organic thermolysis at condition i, HGR_{obs}^{i} is the observed generation rate of hydrogen at condition i, and HGR_{blank}^{i} is the contribution of other hydrogen generation mechanisms (such as thermolysis of trace organic impurities, residual corrosion of wetted metal internals, electrolysis, etc.) at condition i.

Several experiments were performed without added organic species across a wide range of salt concentrations and temperatures. These tests were performed using salt solution simulant with aluminum trinitrate nonahydrate, 50 wt % sodium hydroxide solution, sodium nitrite, sodium nitrate, sodium sulfate, sodium carbonate, and DI H_2O as sole ingredients (identical to ingredients used in test conditions with added organics present). The test conditions that were investigated in the absence of added organic are listed in Table 3-5. The test conditions identified here were conducted throughout the course of the experimental program described in this work. Specification of these concentration and temperature conditions is given in the run plan applicable to each sub set of test.

Table 3-5. Concentrations, Temperatures, and Results from Salt-Only HGR Testing.

Test Name	Al (M)	NO_2 (M)	NO_3 (M)	OH (M)	SO_4 (M)	CO_3 (M)	Temp (°C)	HGR ($ft^3\ h^{-1}\ gal^{-1}$)
P1S2-24	2.82E-01	1.53E+00	2.16E+00	4.07E+00	1.03E-01	2.32E-01	100	4.62E-07
BLANK-S	7.19E-02	2.33E+00	1.09E+00	2.52E+00	6.68E-02	6.16E-01	100	2.06E-07
BLANK-N	6.82E-02	2.22E+00	1.00E+00	2.54E+00	6.28E-02	5.89E-01	100	1.69E-07
BLANK-1	9.34E-02	2.31E+00	1.25E+00	2.86E+00	6.13E-02	6.54E-01	100	2.30E-07
BLANK-5	9.34E-02	2.31E+00	1.25E+00	1.89E+00	6.13E-02	6.54E-01	100	2.27E-07
BLANK-9	9.34E-02	2.31E+00	1.25E+00	2.86E+00	6.13E-02	6.54E-01	85	1.88E-07
BLANK-10	9.34E-02	2.31E+00	1.25E+00	2.86E+00	6.13E-02	6.54E-01	110	2.78E-07
GLY-1A	2.09E-01	1.40E+00	2.06E+00	4.21E+00	1.07E-01	2.21E-01	60	5.28E-08
GLY-2A	2.11E-01	1.46E+00	2.14E+00	4.21E+00	1.09E-01	2.31E-01	80	3.38E-07
GLY-4A	2.42E-01	2.16E+00	1.08E+00	4.14E+00	5.69E-02	2.30E-01	113	1.12E-06
P3-IAC-1D	4.19E-03	1.13E+00	2.63E+00	5.40E+00	4.67E-02	2.05E-01	95	2.04E-07
P3-IAC-2D	2.82E-02	7.72E-01	8.61E-02	1.04E+01	1.03E-02	4.33E-02	73	7.56E-08
P3-IAC-3D	4.45E-02	4.37E-01	2.64E+00	5.93E+00	1.04E-03	4.33E-02	89	2.83E-07
P3-IAC-4D	1.05E-01	2.30E+00	3.06E+00	1.70E+00	2.01E-01	4.56E-01	100	5.09E-07
P3-IAC-4E	1.05E-01	2.30E+00	3.06E+00	1.70E+00	2.01E-01	4.56E-01	100	3.13E-07
P3-IAC-5E	1.29E-01	3.46E-01	1.69E+00	1.99E+00	9.77E-02	1.71E-01	95	1.11E-07
P3-IAC-6D	4.60E-01	2.37E-01	3.48E+00	2.02E+00	9.16E-02	6.49E-01	109	1.66E-07
P3-IAC-7D	3.93E-01	1.90E+00	1.87E+00	6.85E+00	9.92E-02	8.99E-02	76	1.55E-07
Max	4.60E-01	2.33E+00	3.48E+00	1.04E+01	2.01E-01	6.54E-01	113	---
Min	4.19E-03	2.37E-01	8.61E-02	1.70E+00	1.04E-03	4.33E-02	60	---

The data in Table 3-5 were used to determine the functional dependence of a "blank" HGR expression on test conditions, according to the following model:

$$HGR_{blank} = k_{blank}\left[Al\right]^{\alpha}\left[NO_2\right]^{\beta}\left[NO_3\right]^{\gamma}\left[OH\right]^{\delta}\left[SO_4\right]^{\varepsilon}\left[CO_3\right]^{\phi} e^{-E_{blank}/RT} \quad [6]$$

where,

HGR_{blank} is the HGR from a salt solution mixture without added organic materials in $ft^3\ h^{-1}\ gal^{-1}$,
α, β, γ, δ, ε, and ϕ are unitless reaction order constants,
$[Al]$ is the concentration of aluminum in mol L^{-1},
$[NO_2]$ is the concentration of nitrite in mol L^{-1},
$[NO_3]$ is the concentration of nitrate in mol L^{-1},
$[OH]$ is the concentration of hydroxide in mol L^{-1},
$[SO_4]$ is the concentration of sulfate in mol L^{-1},
$[CO_3]$ is the concentration of carbonate in mol L^{-1},
k_{blank} is the empirical rate constant for hydrogen generation in $ft^3\ h^{-1}\ gal^{-1}$ $(L\ mol^{-1})^{\alpha+\beta+\gamma+\delta+\varepsilon+\phi}$, and
E_{blank} is the empirical apparent activation energy for hydrogen generation in J mol^{-1}.

The model given in Equation [6] was logarithmically linearized and linearly regressed according to the following form:

$$\ln HGR_{blank} = \ln k_{blank} + \alpha \ln[Al] + \ldots + \phi \ln[CO_3] - E_{blank}/RT \quad [7]$$

The JMP statistical modeling software package was used to linearly regress the data given in Table 3-5 according to the model equation shown in Equation [7]. A step-wise approach was taken to ensure the optimal selection of model parameters. The resulting optimized model expression is given in Equation [8].

$$HGR_{blank} = 1.890 \times 10^{-1} [NO_2]^{0.364} [NO_3]^{0.321} [OH]^{0.660} e^{-44{,}700/RT} \quad [8]$$

The expression given in Equation [8] is useful for predicting the mean HGR expected at given concentrations of nitrite, nitrate, and hydroxide and a given temperature. However, it is desirable to provide a conservative estimation of HGR^i_{org} such that the model generated from fitting calculated HGR contributions may be confidently used to establish a basis for safe waste tank operation. Therefore, when possible, predictions of the HGR contribution from baseline, blank conditions should be calculated at a one-sided, 95% confidence limit. An illustration of this point is made in Figure 3-9.

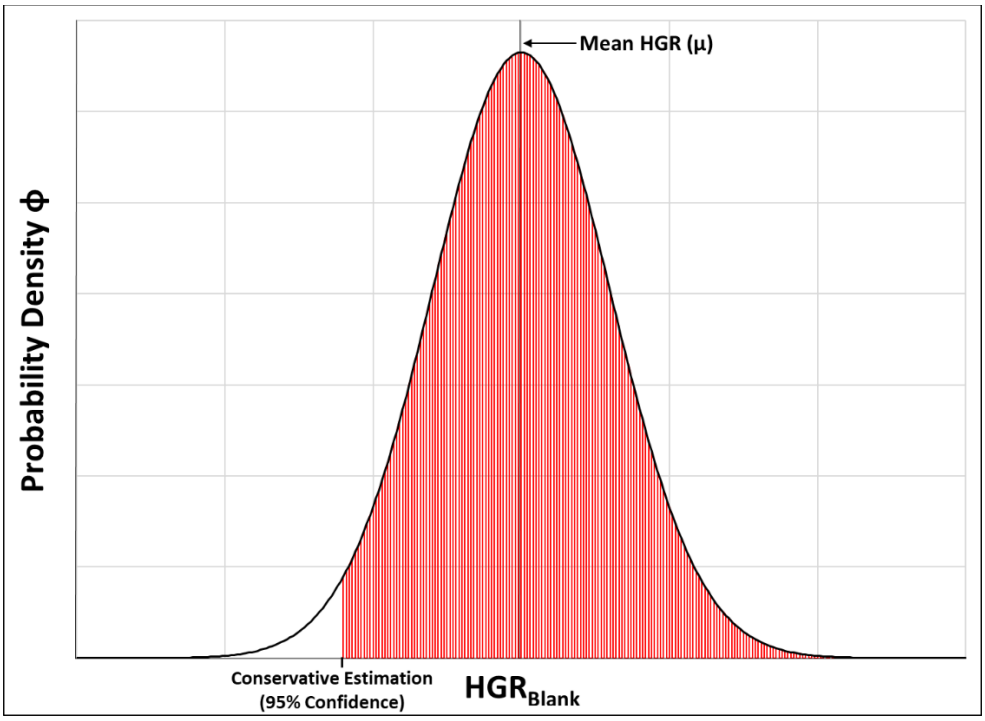

Figure 3-9. Illustration of a Lower, One-Sided 95% Confidence Interval Around a Normal Distribution. The normal distribution is situated around the mean HGR (μ) and distributed symmetrically such that the one-sided 95% confidence limit is equal to the corresponding two-sided 90% confidence limit.

Application of this desired 95% confidence limit may be derived from the data given in Table 3-5 and the blank HGR model fit given in Equation [8]. The 95% confidence limit of the blank HGR model is shown in Figure 3-10, as are measurements and mean predictions of the conditions listed in Table 3-5.

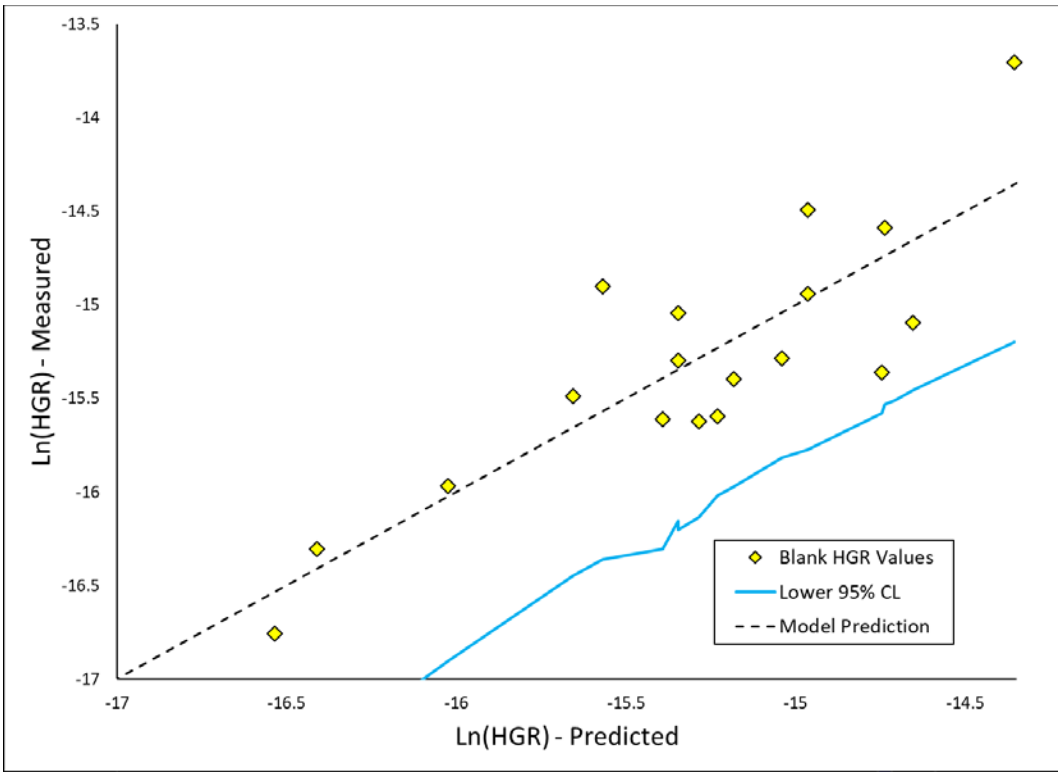

Figure 3-10. Measured HGR from Organic-Free Testing vs. HGR Predicted from the Blank HGR Model Given in Equation [8].

3.3 Glycolate

3.3.1 Model Generation Experiments

Forty-three HGR experiments were performed with sodium glycolate across varied salt solution concentrations. Two experiments were performed in the same Tank 38 simulant described above (P1S1-Test 3A and -3B). Fifteen experiments were performed across a D-Optimal[17] experimental design[18] to fully explore the chemical space pertinent to the SRS CSTF (P1S2-1 through -14). Eight experiments were performed at centroids in this chemical space; one at the logarithmic centroid (P1S2-15) and seven with varied glycolate loadings at the linear centroid (P1S2-16 through -19). Seven experiments were performed at Tank 38 conditions with single-component variations to demonstrate the impact of independently varying salt components (EX-1 through -7). Four additional experiments were performed at previously untested conditions to ensure model robustness (VAR-1 through -4). Three experiments were performed to measure HGR at composition regions predicted to be highly reactive (MAX-1 through -3). Four experiments were performed to examine the impact of temperature on thermolytic production of hydrogen from glycolate (GLY-1 through -4). The compositions and temperatures of each of these tests are given in Table 3-6. The measured HGR, predicted blank HGR at the 95% Confidence Level (CL), and adjusted HGR values are given in Table 3-7.

Table 3-6. HGR Test Conditions for Glycolate Model Generation.

Test Name	Al (M)	NO_2 (M)	NO_3 (M)	OH (M)	SO_4 (M)	CO_3 (M)	Na (M)	Glycolate (M)	Temp. (°C)
P1S2-1	6.67E-01	2.30E+00	1.89E+00	3.98E+00	7.85E-02	2.65E-01	9.53E+00	2.68E-02	100
P1S2-2	2.25E-03	1.78E+00	8.13E-02	1.12E+01	8.71E-03	1.30E-02	1.20E+01	2.90E-02	100
P1S2-3	2.14E-03	2.70E+00	7.29E-02	1.34E-01	<1.04E-03	5.86E-01	4.33E+00	2.71E-02	100
P1S2-4	8.26E-01	2.54E-01	2.69E+00	5.02E+00	1.46E-01	2.71E-01	9.18E+00	1.34E-02	100
P1S2-5	2.23E-03	2.63E+00	5.00E+00	1.37E-01	2.09E-01	1.05E-02	6.74E+00	1.37E-02	100
P1S2-6	2.98E-02	2.39E-01	7.06E-02	5.35E-02	2.04E-01	1.02E-02	8.70E-01	2.70E-02	100
P1S2-7	2.37E-03	2.37E-01	5.37E+00	4.66E-02	2.06E-01	5.69E-01	5.87E+00	1.33E-02	100
P1S2-8	2.23E-03	2.24E-01	8.05E-02	9.43E+00	<1.04E-03	3.38E-02	1.01E+01	1.33E-02	100
P1S2-9	2.15E-03	2.50E-01	1.22E+00	1.02E+01	3.14E-02	5.97E-03	1.33E+01	2.43E-02	100
P1S2-9A	2.29E-03	2.37E-01	1.36E+00	1.06E+01	2.73E-02	1.18E-02	1.15E+01	1.34E-02	100
P1S2-10	2.51E-02	2.39E-01	6.55E-02	1.26E-01	1.08E-03	9.24E-03	5.00E-01	2.69E-02	100
P1S2-11	2.11E-03	2.72E+00	5.10E+00	1.25E-01	<1.04E-03	1.37E-02	7.79E+00	1.36E-02	100
P1S2-12	2.10E-03	2.39E-01	6.34E+00	1.25E-01	1.49E-03	5.64E-01	6.87E+00	2.68E-02	100
P1S2-13	2.80E-03	2.70E+00	6.84E-02	1.16E-01	2.50E-01	5.86E-01	4.44E+00	2.70E-02	100
P1S2-14	7.26E-01	2.50E+00	1.66E+00	5.52E+00	<1.04E-03	1.37E-02	9.83E+00	1.37E-02	100
P1S2-15	4.19E-02	7.83E-01	5.92E-01	1.32E+00	1.02E-02	6.93E-02	2.53E+00	1.37E-02	100
P1S2-16	2.58E-01	1.34E+00	2.02E+00	4.07E+00	9.60E-02	2.08E-01	8.79E+00	2.71E-02	100
P1S2-16A	2.59E-01	1.30E+00	2.16E+00	4.24E+00	1.02E-01	2.29E-01	8.53E+00	2.72E-02	100
P1S2-16B	2.13E-01	1.34E+00	2.16E+00	4.45E+00	1.03E-01	2.27E-01	6.92E+00	1.34E-02	100
P1S2-17	2.80E-01	1.44E+00	2.08E+00	4.24E+00	1.05E-01	2.25E-01	9.31E+00	2.72E-02	100
P1S2-17A	2.05E-01	1.35E+00	2.16E+00	4.32E+00	1.05E-01	2.28E-01	6.74E+00	1.37E-02	100
P1S2-18A	2.57E-01	1.33E+00	1.98E+00	4.24E+00	1.07E-01	2.25E-01	9.40E+00	1.35E-02	100
P1S2-19	2.72E-01	1.42E+00	2.18E+00	4.24E+00	1.10E-01	2.25E-01	9.09E+00	6.70E-03	100
EX-1	7.45E-02	2.43E+00	1.23E+00	2.67E+00	6.29E-02	6.43E-01	6.79E+00	7.10E-03	100
EX-2	<1.11E-04	2.41E+00	1.20E+00	2.69E+00	6.15E-02	6.33E-01	6.22E+00	7.00E-03	100
EX-3	7.86E-02	<2.17E-03	1.17E+00	2.53E+00	5.93E-02	6.19E-01	4.70E+00	6.85E-03	100
EX-4	7.34E-02	2.41E+00	2.84E-01	2.59E+00	6.11E-02	6.26E-01	5.65E+00	6.95E-03	100
EX-5	7.67E-02	2.46E+00	1.19E+00	2.11E-01	6.15E-02	6.29E-01	4.65E+00	7.00E-03	100
EX-6	7.30E-02	2.43E+00	1.17E+00	2.60E+00	<1.04E-03	6.19E-01	6.31E+00	7.00E-03	100
EX-7	8.23E-02	2.41E+00	1.18E+00	2.54E+00	6.24E-02	5.66E-03	5.52E+00	7.10E-03	100

Test Name	Al (M)	NO_2 (M)	NO_3 (M)	OH (M)	SO_4 (M)	CO_3 (M)	Na (M)	Glycolate (M)	Temp. (°C)
VAR-1	9.64E-04	1.65E+00	8.16E-01	1.19E+01	1.76E-02	2.38E-03	1.20E+01	6.95E-03	100
VAR-2	1.00E-01	5.72E-01	2.84E+00	5.70E+00	8.05E-02	8.23E-02	7.48E+00	6.95E-03	100
VAR-3	1.04E-03	2.46E-01	1.39E+00	9.91E+00	<1.04E-03	3.11E-02	1.00E+01	6.80E-03	100
VAR-4	7.75E-02	2.39E-01	6.35E-01	5.79E+00	<1.04E-03	5.16E-01	6.79E+00	7.00E-03	100
MAX-1	1.05E-03	1.72E+00	9.69E-01	1.06E+01	<1.04E-03	2.47E-02	1.19E+01	6.90E-03	100
MAX-2	9.97E-04	2.48E-01	1.15E+00	1.07E+01	<1.04E-03	3.86E-02	1.10E+01	6.95E-03	100
MAX-3	9.97E-04	2.46E-01	3.34E+00	5.11E+00	1.08E-01	2.66E-02	7.39E+00	6.85E-03	100
GLY-1	2.09E-01	1.40E+00	2.06E+00	4.21E+00	1.07E-01	2.21E-01	8.48E+00	1.49E-02	60
GLY-2	1.96E-01	1.40E+00	2.05E+00	4.21E+00	1.07E-01	2.24E-01	8.66E+00	1.42E-02	80
GLY-3	2.03E-01	1.44E+00	2.08E+00	4.18E+00	1.09E-01	2.25E-01	8.66E+00	1.42E-02	100
GLY-4	2.30E-01	1.22E+00	2.03E+00	4.12E+00	9.16E-02	2.30E-01	8.13E+00	1.37E-02	113

Table 3-7. HGR Test Results for Glycolate Model Generation.

Test Name	Observed HGR ($ft^3\ h^{-1}\ gal^{-1}$)	Predicted HGR from Blank (95% CL) ($ft^3\ h^{-1}\ gal^{-1}$)	Adjusted Thermolytic HGR ($ft^3\ h^{-1}\ gal^{-1}$)
P1S2-1	3.10E-05	1.87E-07	3.08E-05
P1S2-2	3.73E-05	9.22E-08	3.72E-05
P1S2-3	4.36E-08	2.04E-09	4.16E-08
P1S2-4	3.34E-05	9.77E-08	3.33E-05
P1S2-5	< 8.51E-08	1.36E-08	N/A
P1S2-6	< 8.77E-08	2.61E-10	N/A
P1S2-7	< 8.22E-07	1.56E-09	N/A
P1S2-8	4.91E-05	3.53E-08	4.91E-05
P1S2-9	2.30E-05	1.09E-07	2.29E-05
P1S2-9A	5.17E-05	1.11E-07	5.16E-05

Test Name	Observed HGR ($ft^3\ h^{-1}\ gal^{-1}$)	Predicted HGR from Blank (95% CL) ($ft^3\ h^{-1}\ gal^{-1}$)	Adjusted Thermolytic HGR ($ft^3\ h^{-1}\ gal^{-1}$)
P1S2-10	< 2.56E-08	6.38E-10	N/A
P1S2-11	< 8.64E-08	1.26E-08	N/A
P1S2-12	3.07E-07	4.89E-09	3.02E-07
P1S2-13	< 8.12E-08	1.69E-09	N/A
P1S2-14	4.06E-05	2.18E-07	4.04E-05
P1S2-15	8.86E-08	3.54E-08	5.32E-08
P1S2-16	1.95E-05	1.61E-07	1.93E-05
P1S2-16A	3.33E-05	1.66E-07	3.31E-05
P1S2-16B	1.80E-05	1.72E-07	1.78E-05
P1S2-17	2.65E-05	1.70E-07	2.63E-05
P1S2-17A	2.25E-05	1.70E-07	2.23E-05
P1S2-18A	1.70E-05	1.63E-07	1.68E-05
P1S2-19	1.03E-05	1.72E-07	1.01E-05
EX-1	1.83E-06	1.30E-07	1.70E-06
EX-2	1.31E-06	1.29E-07	1.18E-06
EX-3	3.90E-07	N/A	N/A
EX-4	1.26E-06	7.05E-08	1.19E-06
EX-5	2.56E-08	1.19E-08	1.37E-08
EX-6	2.04E-06	1.26E-07	1.91E-06
EX-7	1.45E-06	1.24E-07	1.33E-06
VAR-1	2.73E-05	2.15E-07	2.71E-05
VAR-2	2.15E-05	1.51E-07	2.13E-05
VAR-3	2.77E-05	1.11E-07	2.76E-05
VAR-4	1.27E-05	6.45E-08	1.26E-05
MAX-1	1.66E-05	2.19E-07	1.64E-05
MAX-2	3.71E-05	1.08E-07	3.70E-05
MAX-3	1.78E-05	1.03E-07	1.77E-05
GLY-1	7.03E-07	2.61E-08	6.77E-07
GLY-2	4.59E-06	7.42E-08	4.52E-06
GLY-3	1.91E-05	1.69E-07	1.89E-05
GLY-4	2.25E-05	2.41E-07	2.23E-05

Note that six of the HGR values listed in Table 3-7 (for tests P1S2-5, -6, -7, -10, -11, and -13) are reported as inequalities. This is due to hydrogen measurements that were below the limit of detection for the GC (1 ppm) at the conditions employed for the testing.

The analyses and results given in Table 3-6 and Table 3-7 were linearly regressed according to the following expressions:

$$HGR_{GLY} = k_0 \left[Al\right]^{\alpha} \left[NO_2\right]^{\beta} \left[NO_3\right]^{\gamma} \left[OH\right]^{\delta} \left[SO_4\right]^{\varepsilon} \left[CO_3\right]^{\phi} \left[Na\right]^{\mu} \left[C_{Gly}\right] e^{-E_A/RT} \quad [9]$$

$$\ln\left(\frac{HGR}{\left[C_{Gly}\right]}\right) = \ln\left(k_0 \left[Al\right]^{\alpha} \left[NO_2\right]^{\beta} \left[NO_3\right]^{\gamma} \left[OH\right]^{\delta} \left[SO_4\right]^{\varepsilon} \left[CO_3\right]^{\phi} \left[Na\right]^{\mu} e^{-E_A/RT}\right) \quad [10]$$

$$\ln\left(\frac{HGR}{\left[C_{Gly}\right]}\right) = \ln k_0 + \alpha \ln\left[Al\right] + \ldots + \mu \ln\left[Na\right] - \frac{E_A}{RT} \quad [11]$$

where,

HGR_{GLY} is the HGR expected from thermolysis of glycolate in $ft^3\ hr^{-1}\ gal^{-1}$,
α, β, γ, δ, ε, ϕ, and μ are effective reaction order constants (unitless),
k_0 is a pre-exponential rate constant in $ft^3\ hr^{-1}\ gal^{-1}\ (L\ mol^{-1})^{1+\alpha+\beta+\gamma+\delta+\varepsilon+\phi+\mu}$,
$\left[Na\right]$ is the concentration of sodium in mol L^{-1},
$\left[C_{Gly}\right]$ is the concentration of carbon from glycolate in mol L^{-1},
E_A is the effective activation energy in J mol^{-1},
R is the ideal gas constant, 8.314 J mol^{-1} K^{-1}, and
T is the temperature in K.

Note that the expressions given in Equations [9] through [11] inherently rely on a few assumptions. First, these expressions assume that only the components shown (aluminum, nitrite, nitrate, hydroxide, sulfate, carbonate, and sodium) have a meaningful impact on thermolytic HGR from glycolate. This assumption is made based on the assessment by Ashby *et al.*[10] that the primary hydrogen-producing pathways available to glycolate in caustic tank waste media are largely aluminum-catalyzed. Therefore, only species that are generally present in CSTF in great enough quantities to coordinate to a significant fraction of the available aluminum are considered. Second, the expressions assume that HGR may be adequately described by a single term (rather than a combination of terms). This assumption is consistent with the accepted approach for developing an empirical expression that describes reaction rates under several conditions. Finally, the expressions assume that the impact of glycolate on HGR is strictly linear (that is to say, an increase in glycolate concentration causes a proportional increase in HGR). This behavior has been demonstrated by Ashby *et al.*[10] and is the basis for the organic thermolysis assumptions made to support the Hanford flammability program.

A step-wise linear regression was performed on the data given in Table 3-6 to generate a simple expression that well describes the HGRs observed from testing (this process is demonstrated in Appendix B). The following model expression was regressed using JMP 11.2:

$$\ln\left(\frac{HGR}{[C_{Gly}]}\right) = 11.085 + 0.369\ln[NO_3] + 1.366\ln[OH] + 1.755\ln[Na] - \frac{9194}{T} \quad [12]$$

This expression may be rearranged and simplified to allow for the calculation of predicted HGR as a function of species concentrations and liquid temperature. The product of this rearrangement is given in Equation [13].

$$HGR_{GLY} = 6.518\times10^{4}[NO_3]^{0.369}[OH]^{1.366}[Na]^{1.755}[C_{Gly}]e^{-76,400/RT} \quad [13]$$

The expression given in Equation [13] suggests that the concentrations of nitrate, hydroxide, and sodium have the largest impact on glycolate HGR. Temperature is also predicted to have a significant impact, yielding an apparent activation energy of 76.4 kJ mol^{-1}.

The data given in Table 3-6 and Table 3-7 may be evaluated against the model described in Equations [12] and [13] to assess the goodness of fit. The results of this assessment are given in Figure 3-11.

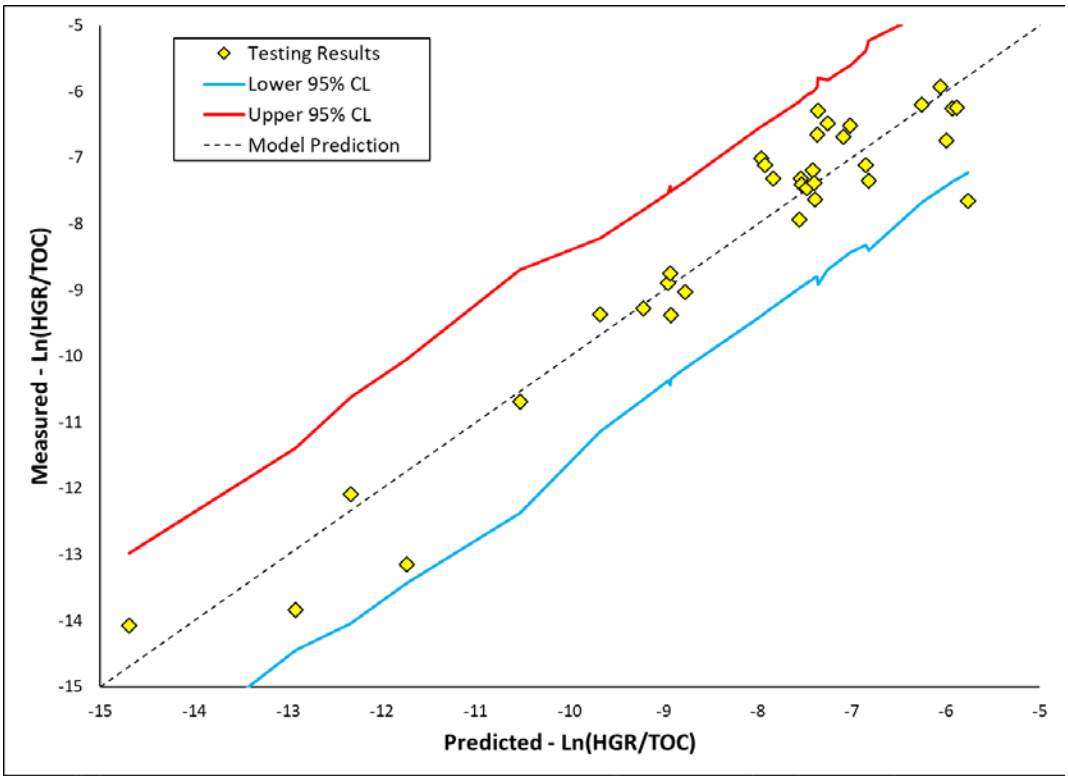

Figure 3-11. Scatterplot of HGR Measurements vs. Values Predicted from Equation [12].

The data shown in Figure 3-11 generally fall within the 95% confidence limit for a single prediction generated by the model given in Equation [12].

3.3.2 Model Validation Experiments

Seven experimental conditions were designed to evaluate the interim model for thermolytic HGR due to glycolate. These conditions were chosen by D-optimally selecting the best of 20,000 possible conditions across CSTF concentration and temperature space.[19] It should be noted that the ranges of concentrations and temperatures covered by this validation set do not fully evaluate the extreme ranges applicable to the CSTF due to the requirement that the D-optimal points must predict measurable HGRs ($>4\times10^{-8}$ $ft^3\ h^{-1}\ gal^{-1}$). The conditions of these seven tests are given in Table 3-8. The observed HGRs in the presence of glycolate, the expected organic-free HGR contribution, and the adjusted thermolytic HGRs are given in Table 3-9.

Table 3-8. HGR Test Conditions for Glycolate Model Validation and Improvement.

Test Name	Al (M)	NO_2 (M)	NO_3 (M)	OH (M)	SO_4 (M)	CO_3 (M)	Na (M)	Glycolate (M)	Temp. (°C)
P3-GLY-1	3.74E-03	1.19E+00	2.44E+00	5.41E+00	6.13E-02	1.95E-01	9.57E+00	3.05E-03	95
P3-GLY-2	3.34E-02	9.98E-01	1.14E-01	1.22E+01	5.54E-03	2.38E-02	1.35E+01	7.45E-03	73
P3-GLY-3	4.89E-02	4.61E-01	2.45E+00	5.88E+00	1.33E-01	1.44E-02	9.96E+00	1.20E-02	89
P3-GLY-4	1.04E-01	2.78E+00	3.16E+00	1.80E+00	2.35E-02	4.00E-01	9.00E+00	9.60E-03	100
P3-GLY-5	1.19E-01	3.72E-01	1.60E+00	2.07E+00	1.52E-01	1.48E-01	5.22E+00	2.92E-03	95
P3-GLY-6	4.04E-01	2.54E-01	3.16E+00	2.02E+00	1.83E-01	4.93E-01	8.35E+00	7.60E-03	109
P3-GLY-7	4.15E-01	2.13E+00	1.81E+00	6.12E+00	1.82E-02	1.05E-01	1.18E+01	5.90E-03	76

Table 3-9. HGR Test Results for Glycolate Model Validation and Improvement.

Test Name	Observed HGR ($ft^3\ h^{-1}\ gal^{-1}$)	Predicted HGR from Blank (95% CL) ($ft^3\ h^{-1}\ gal^{-1}$)	Adjusted Thermolytic HGR ($ft^3\ h^{-1}\ gal^{-1}$)
P3-GLY-1	6.98E-06	1.57E-07	6.82E-06
P3-GLY-2	7.60E-06	3.17E-08	7.57E-06
P3-GLY-3	1.60E-05	8.98E-08	1.59E-05
P3-GLY-4	1.75E-06	1.39E-07	1.61E-06
P3-GLY-5	1.49E-07	4.54E-08	1.04E-07
P3-GLY-6	3.25E-06	7.95E-08	3.17E-06
P3-GLY-7	7.87E-06	8.55E-08	7.78E-06

The results from the seven validation points are plotted against the model predicted HGRs in Figure 3-12. Results from validation testing are plotted in green.

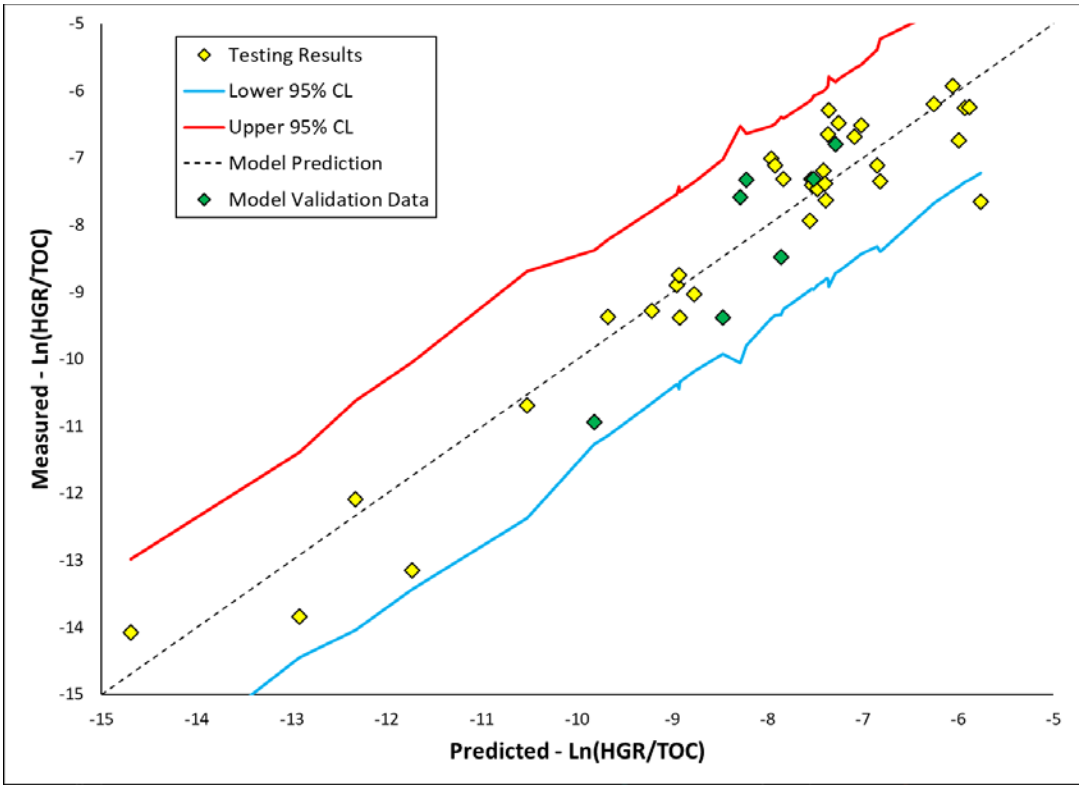

Figure 3-12. Plot of Measured HGRs from Model Generation (Yellow) and Validation (Green) Tests for Glycolate vs. Predicted HGRs According to Interim Model Shown in Equation [12].

As is clear from Figure 3-12, the interim model for the thermolytic HGR due to glycolate is sufficiently robust to account for the measurements made during validation testing. All seven test results fall within the 95% confidence interval of a single prediction made by the interim model.

Given the addition of seven data points gathered at concentration and temperature ranges previously unexplored, it is safe to assume that a more robust model for thermolytic HGR from glycolate may be attained by including the validation data set with the model generation data set and fitting an improved model by linear regression. The model achieved by this inclusion is given in Equation [14].

$$\ln\left(\frac{HGR}{[C_{GLY}]}\right) = 6.795 + 1.936\ln[Na] + 0.314\ln[NO_3] + 1.380\ln[OH] - \frac{7752}{T} \qquad [14]$$

All HGR results from glycolate testing are plotted against the model prediction calculated by Equation [14] in Figure 3-13.

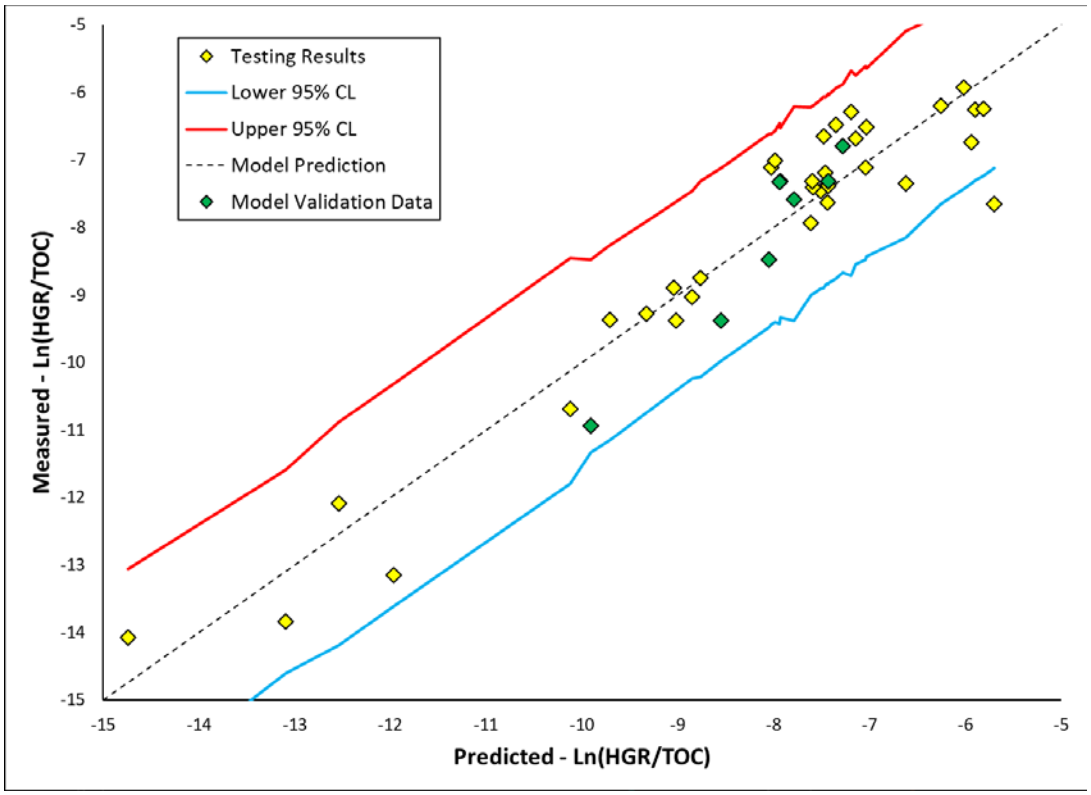

Figure 3-13. Plot of Measured HGRs from Model Generation (Yellow) and Validation (Green) Tests for Glycolate vs. Predicted HGRs According to Final Model Shown in Equation [14].

The scatterplot in Figure 3-13 suggests that the majority of variation in glycolate HGR data is well-described by the revised model expression in Equation [14]. This expression is simplified in Equation [15].

$$HGR_{GLY} = 8.934\times10^{2}\left[Na\right]^{1.936}\left[NO_3\right]^{0.314}\left[OH\right]^{1.380}\left[C_{GLY}\right]e^{-64{,}400/RT} \quad [15]$$

The inclusion of the validation data during model regression seems to have little impact on the mechanistic parameters of the empirical HGR expression, resulting in factors of 1.936, 0.314, and 1.380 for the apparent reaction orders of sodium, nitrate, and hydroxide, respectively (compared to the values of 1.755, 0.369, and 1.366 obtained from the interim model fit). The most significant changes are seen in the apparent pre-exponential rate constants and activation energies, 8.934×10^{2} and 64,400 J mol^{-1}, respectively (compared to the values of 6.518×10^{4} and 76,400 J mol^{-1} obtained from the interim model fit).

Given the added robustness from inclusion of the seven validation data points, the modified model expression given in Equation [15] was further evaluated against extreme temperature and salt concentration conditions. This evaluation is described in the next section.

3.3.3 High Boiling Point (Tank 30) Simulant Experiments

During the course of HGR measurements performed for this study, characterization results from a Tank 30 sample (HTF-30-18-96) were made available that suggested the presence of a notably high concentration of aluminum (1.98 M).[20] Given that multiple literature sources report a dependence of organic thermolysis on aluminum, it was proposed to perform a test case in which glycolate thermolysis could be studied in the presence of high aluminum concentrations.[21] This test was performed using a simulant mixture designed to

mimic the concentrations in Tank 30. The measured concentrations of salt species in the Tank 30 simulant are given in Table 3-10. Note the presence of KCl at approximately 0.1 M, which was deliberately added as a tracer compound for liquid volume. Note also that sodium aluminate was used to generate this material (rather than aluminum nitrate, used in previous testing) to accommodate the relatively low ratio of nitrate to aluminum (2.24:2.49).

Table 3-10. Composition of Tank 30 Simulant.

Component	Concentration (M)
Na	1.69E+01
Al	2.49E+00
NO_2	2.56E+00
NO_3	2.24E+00
OH	9.87E+00
SO_4	9.61E-03
CO_3	6.10E-02
K	1.08E-01
Cl	8.82E-02
$C_2H_3O_3$	6.66E-03

To determine the HGR from the simulant prepared "as-is" in the absence of glycolate, a blank measurement was performed in which 1 L of Tank 30 simulant was prepared in the HGR measurement apparatus and heated to 100 °C for HGR measurement. Once this measurement was complete, the temperature was decreased to 80 °C and 60 °C for subsequent measurements at reduced temperatures. After the conclusion of the 60 °C measurement, the mixture was heated to its boiling point (determined to be approximately 134 °C) and measured. A plot of the measured HGR and temperature as a function of time is given in Figure 3-14.

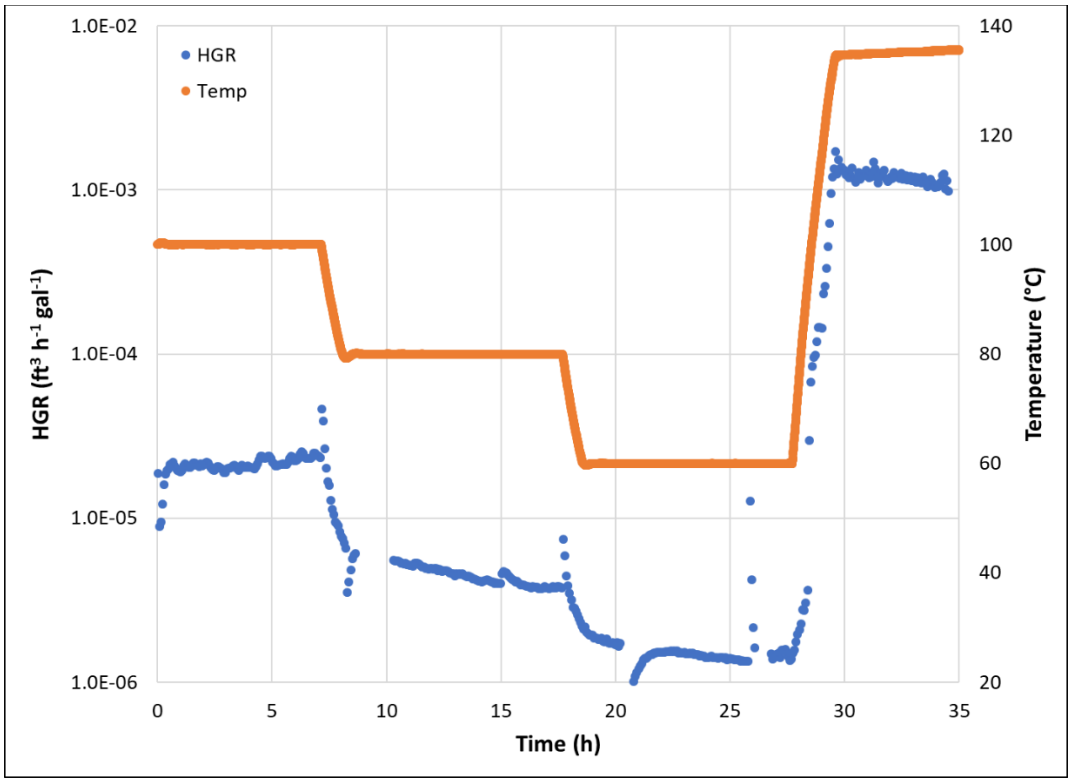

Figure 3-14. HGR (blue, in $ft^3\ h^{-1}\ gal^{-1}$) and Temperature (orange, in °C) as a Function of Time During the Glycolate-Free Tank 30 Simulant Experiment.

The HGRs measured from the Tank 30 simulant in the absence of glycolate were 2.40×10^{-5} $ft^3\ h^{-1}\ gal^{-1}$, 3.78×10^{-6} $ft^3\ h^{-1}\ gal^{-1}$, 1.36×10^{-6} $ft^3\ h^{-1}\ gal^{-1}$, and 1.23×10^{-3} $ft^3\ h^{-1}\ gal^{-1}$ at 100 °C, 80 °C, 60 °C, and 134 °C, respectively. The increase of HGR with respect to increasing temperature is consistent with thermolytic hydrogen generation. It is possible that the hydrogen generated in this test is the result of 1) thermolysis of organic impurities often found in sodium aluminate, or 2) corrosive hydrogen generation due to chloride pitting of the corrosion-resistant alloys employed in testing.

Testing with Tank 30 simulant material was also performed with sodium glycolate.[21] 474 mg/L glycolate (added as sodium glycolate) was added to a liter of the simulant and tested using the HGR measurement apparatus following the same temperature profile as the glycolate-free experiment. The resulting HGRs and temperatures of the glycolate-added test are given in Figure 3-15.

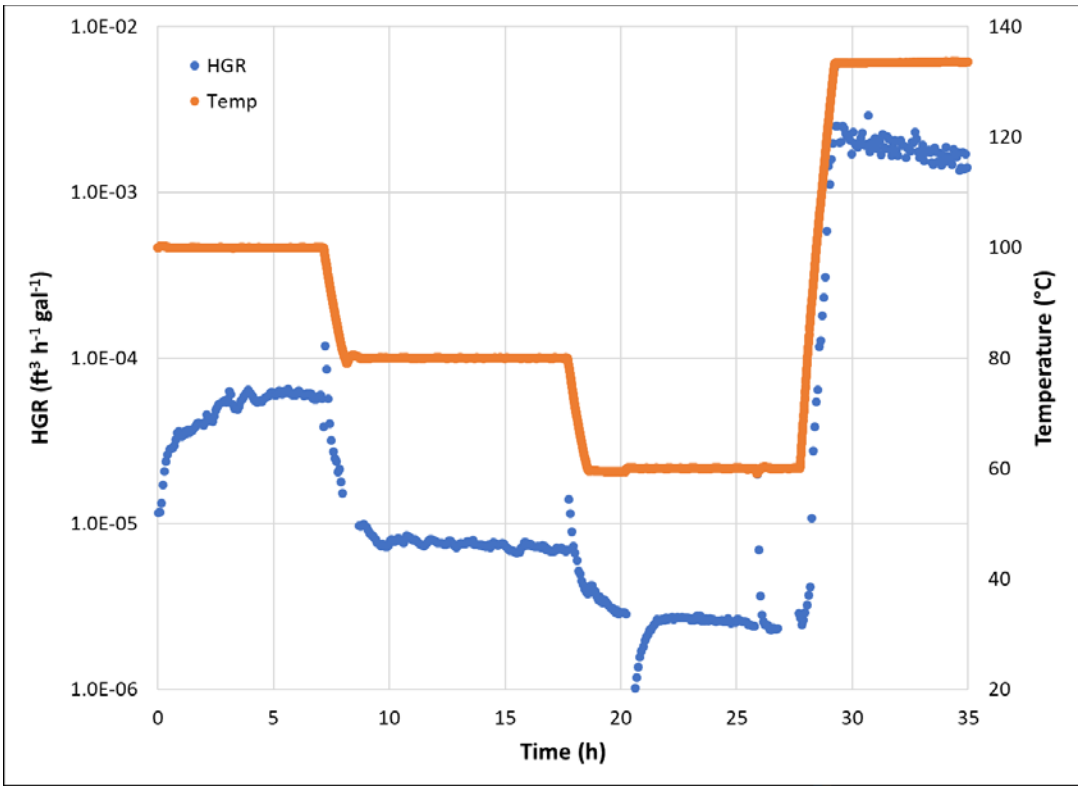

Figure 3-15. HGR (blue, in $ft^3\ h^{-1}\ gal^{-1}$) and Temperature (orange, in °C) as a Function of Time During the Glycolate-Added Tank 30 Simulant Experiment.

Results from the glycolate-added HGR measurements are universally higher than those seen in the absence of glycolate. Values of 5.82×10^{-5} $ft^3\ h^{-1}\ gal^{-1}$, 6.97×10^{-6} $ft^3\ h^{-1}\ gal^{-1}$, 2.50×10^{-6} $ft^3\ h^{-1}\ gal^{-1}$, and 2.02×10^{-3} $ft^3\ h^{-1}\ gal^{-1}$ were observed in the presence of 474 mg/L of glycolate at 100 °C, 80 °C, 60 °C, and 134 °C, respectively.

Given that the observed HGRs in the presence of glycolate are universally higher than the HGRs observed in the absence of glycolate, it is proposed that the difference in these rates is equal to the thermolytic generation of hydrogen from glycolate. The adjusted glycolate HGRs (as calculated by difference) are given in Table 3-11.

Table 3-11. Observed HGRs With and Without Glycolate and Glycolate-Attributable HGR from Tank 30 Simulant Testing.

Temperature (°C)	HGR with Glycolate ($ft^3\ h^{-1}\ gal^{-1}$)	HGR from Blank ($ft^3\ h^{-1}\ gal^{-1}$)	Adjusted HGR ($ft^3\ h^{-1}\ gal^{-1}$)
100	5.82E-05	2.40E-05	3.42E-05
80	6.97E-06	3.78E-06	3.19E-06
60	2.50E-06	1.36E-06	1.14E-06
134 (boiling)	2.02E-03	1.23E-03	7.90E-04

The adjusted HGRs from Table 3-11 may be plotted against temperature in an Arrhenius plot to determine the effective activation energy of the hydrogen-producing reaction in the thermolysis of glycolate in Tank 30 simulant. This exercise is performed in Figure 3-16.

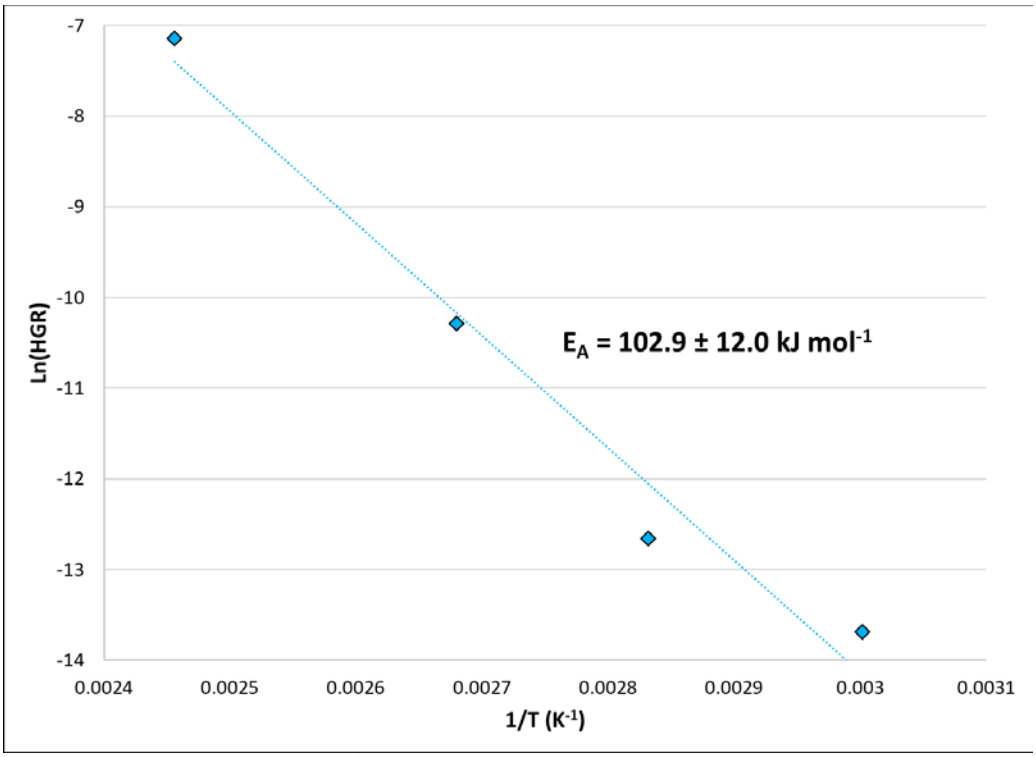

Figure 3-16. Arrhenius Plot of Glycolate-Attributable HGR.

The effective activation energy of the thermolytic production of hydrogen from glycolate in Tank 30 conditions, as calculated from the slope of the Arrhenius plot in Figure 3-16, is approximately 103 kJ mol^{-1}. The fact that the four points derived from the data in Table 3-11 are not well described by a straight line in Figure 3-16 suggests that more than one mechanism for hydrogen generation may be relevant at the conditions tested in the Tank 30 simulant.

These results may be evaluated against the proposed glycolate model (discussed earlier). This evaluation is displayed graphically in Figure 3-17.

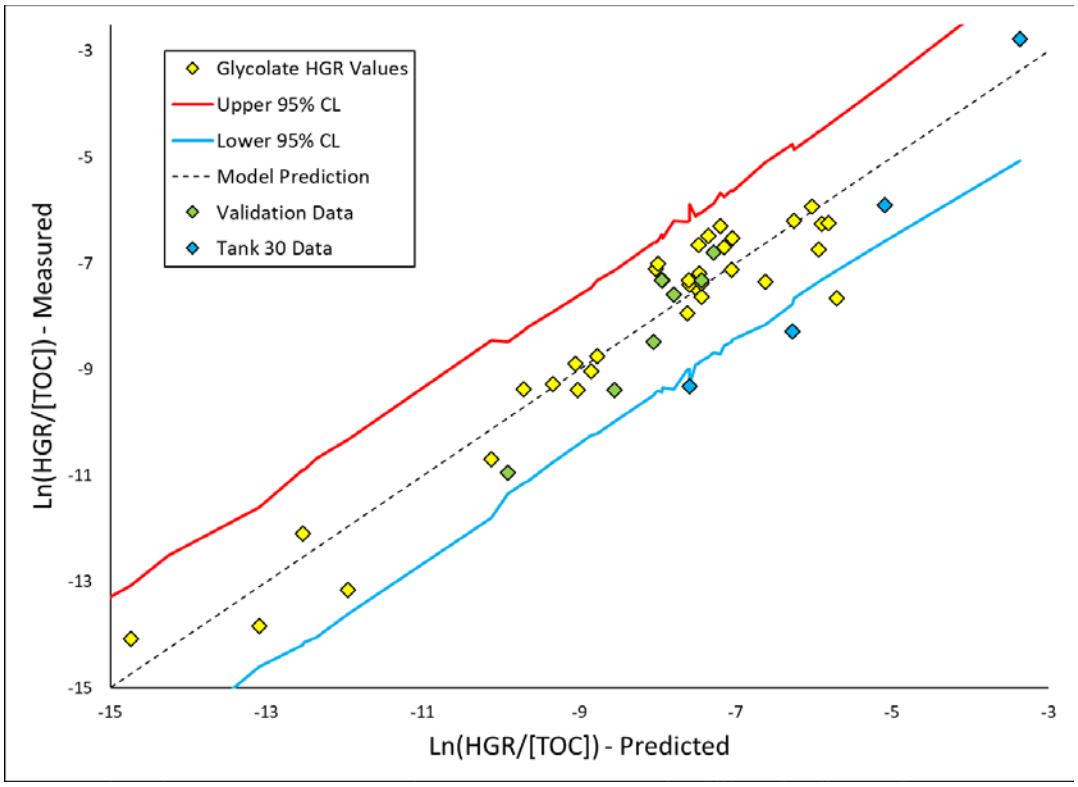

Figure 3-17. Evaluation of Tank 30 Simulant Test Results Against the Empirical Glycolate HGR Model Shown in Equation [14].

The results from testing with Tank 30 simulant (blue diamonds) seem to agree relatively well with the model predictions, with all four results falling below the 95% upper confidence limit. This suggests that the extreme extrapolations performed in this test series (high aluminum concentrations, high temperatures) are adequately protected by the proposed glycolate thermolysis model.

While the Tank 30 simulant results are adequately bounded by the empirical model given in Equation [15], it should be noted that the apparent activation energy employed in Equation [15] (64.4 kJ mol^{-1}) is significantly lower than that observed in Tank 30 simulant testing (102.9 kJ mol^{-1}). This difference suggests that the empirical model generated for thermolytic production of hydrogen from glycolate may underpredict HGRs at temperatures higher than those observed during Tank 30 simulant testing (>134 °C). The quality of extrapolation to higher temperatures may be improved by incorporating the results from Tank 30 simulant testing into the existing glycolate HGR model. The temperature-modified expression resulting from this incorporation is given in Equation [16].

$$\ln\left(\frac{HGR}{[C_{GLY}]}\right) = 13.347 + 1.520\ln[Na] + 0.282\ln[NO_3] + 1.441\ln[OH] - \frac{9903}{T} \qquad [16]$$

The incorporation of Tank 30 simulant data into the temperature-modified glycolate model shown in Equation [16] has minimal impact on the functional dependence of salt concentrations on HGR, with reaction order constants of sodium, nitrate, and hydroxide changing by -21%, -10%, and +4%, respectively. However, the values of the pre-exponential factor and the apparent activation energy are modified significantly (increasing from 8.934×10^{2} and 64.4 kJ mol^{-1} to 6.262×10^{5} and 82.3 kJ mol^{-1}, respectively).

These parameters agree more closely with the observations made by Hu (E_a = 89.6 kJ mol^{-1})[9] and Ashby (E_a = 113 kJ mol^{-1}).[10]

The results from all glycolate-containing simulant experiments are evaluated against the temperature-modified glycolate expression (Equation [16]) in Figure 3-18.

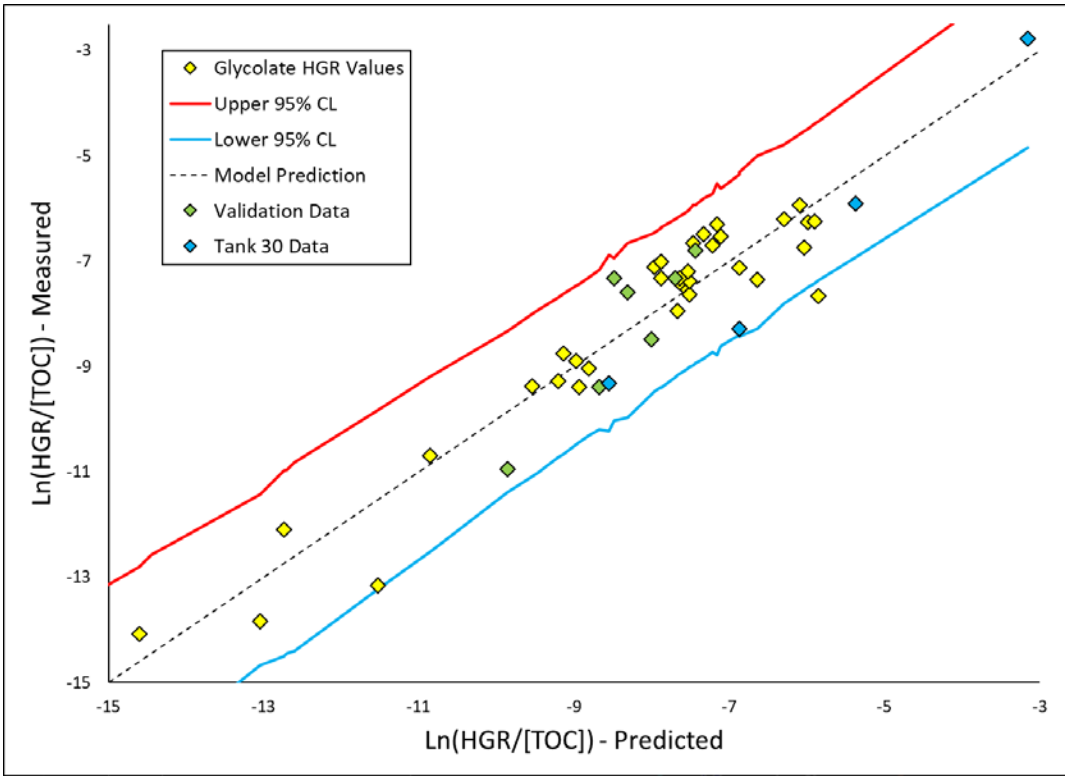

Figure 3-18. Plot of Measured HGRs from Model Generation (Yellow), Validation (Green), and Tank 30 Simulant (Blue) Tests for Glycolate vs. Predicted HGRs According to the Temperature-Modified Glycolate Model Shown in Equation [16].

The data in Figure 3-18 exhibit an improved fit of glycolate HGR measurements to a model expression, with all but one of the experimental results falling within the 95% confidence limits of the temperature-modified glycolate HGR expression.

The temperature-modified glycolate HGR expression given in Equation [16] may be simplified for ease of implementation. This expression is given in Equation [17].

$$HGR_{GLY} = 6.262\times10^{5}\left[Na\right]^{1.520}\left[NO_3\right]^{0.282}\left[OH\right]^{1.441}\left[C_{GLY}\right]e^{-82{,}300/RT} \qquad [17]$$

Given the increased quality of fit attained by the temperature-modified glycolate model (simplified in Equation [17]), it is recommended that this expression be used to approximate thermolytic HGR attributable to glycolate in caustic tank waste media. This expression is evaluated against measurements performed in radioactive waste media later in this report (Section 3.3.4.5).

3.3.4 Interactions with Other Components in Waste Tanks

Most of the testing performed to date focused on understanding the impacts of major salt components on glycolate thermolysis in tank waste media. However, it is prudent to justify this subset of species by performing exploratory tests to establish the relevance or irrelevance of other components on HGR. The exploratory tests performed in support of this effort are described herein.

3.3.4.1 Testing with Sludge Solids

Approximately 10 grams of Sludge Batch (SB) 9 simulant sludge solids were isolated by centrifuging 100 grams of SB9 sludge simulant and decanting the supernatant phase. These solids were added to a liter of the D-Optimal experiment design centroid simulant[18] along with 1 gram of glycolate to assess the impact of sludge solids on glycolate HGR. The solids loading of 1 wt % was targeted as a theoretical maximum according to waste tank evaporator operation criteria. The resulting HGR from this experiment is shown in Figure 3-19.

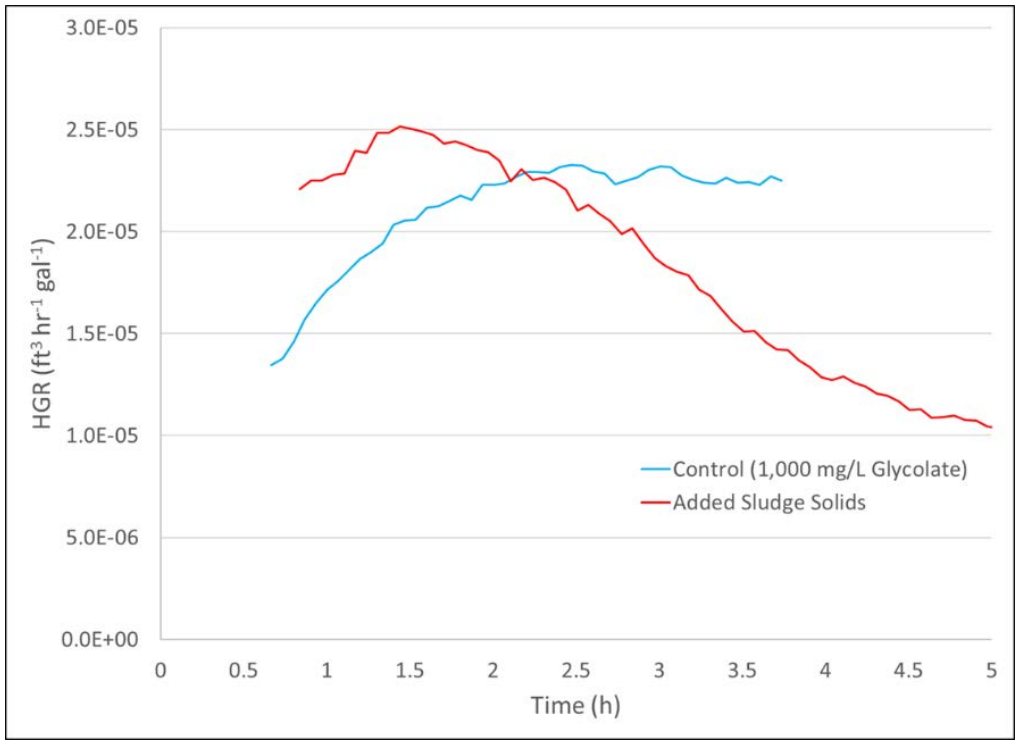

Figure 3-19. HGR from 1,000 mg/L Glycolate as a Function of Time in the Presence (Red) and Absence (Blue) of SB9 Sludge Solids (1 wt%).

While the solids-free control experiment seemed to increase and stabilize at a final HGR value, the experiment with 1 wt % sludge solids exhibited an initial peak followed by a rapid decrease in HGR. This is consistent with the notion that sludge solids (largely insoluble oxides, such as MnO_2) consume the glycolate via non-hydrogen producing reactions (such as oxidation similar to that seen in DWPF CPC simulations).[22] If such reactions were to occur, they would be expected to diminish the glycolate available to make hydrogen.

Given that this result suggests sludge solids lower the effective HGR, it would be reasonable to assume that a "solids-free" expression would be bounding of supernatant phases in contact with sludge solids. Therefore, it is recommended that sludge solids should not be considered when developing an expression for HGR,

understanding that when solids are present (e.g., during periods of mixing), the HGR predicted by said expression will be conservative.

3.3.4.2 Testing with Hg

In an attempt to explore the impacts of mercury on glycolate HGR, a second experiment was performed using the D-Optimal centroid simulant whereby 430 mg/L of mercury was added as mercuric nitrate monohydrate ($Hg(NO_3)_2 \cdot H_2O$).[18] Upon addition, it was noted that a yellow solid immediately formed in the reaction mixture. This solid was speculated to be insoluble mercuric oxide (HgO). The results of this test are given in Figure 3-20.

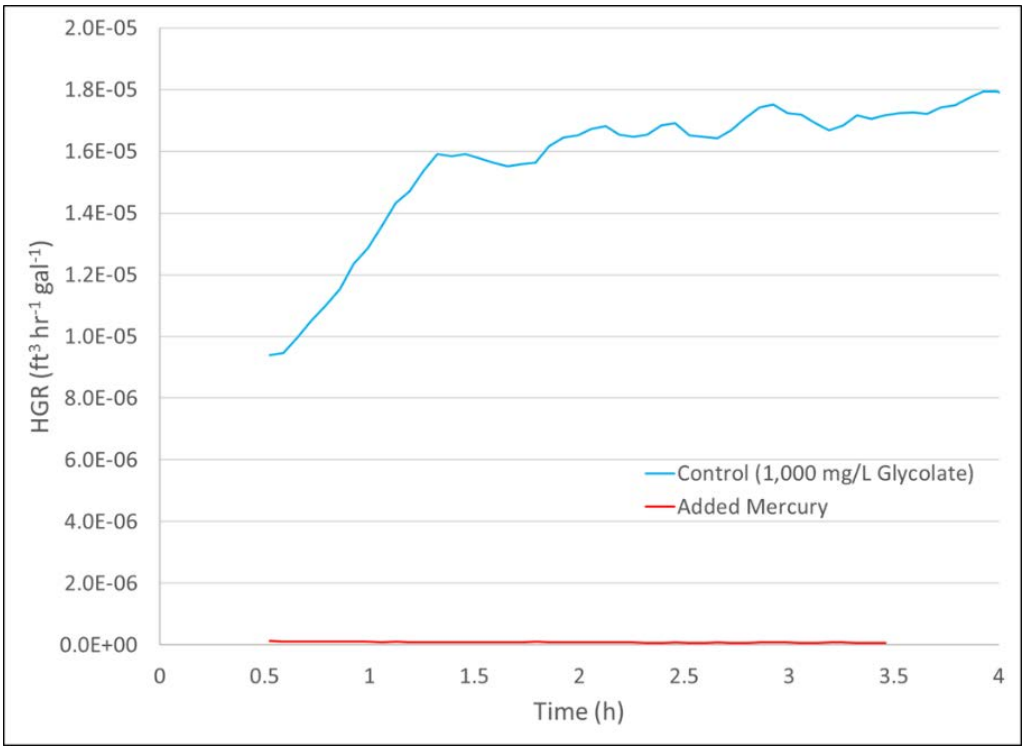

Figure 3-20. HGR from 1,000 mg/L Glycolate as a Function of Time in the Presence (Red) and Absence (Blue) of Mercury (430 mg Hg/L, added as $Hg(NO_3)_2 \cdot H_2O$).

The addition of mercuric nitrate to the reaction mixture seems to have a significant impact on the HGR from glycolate, decreasing the measured value from ~1.8×10^{-5} ft^3 hr^{-1} gal^{-1} to less than 1×10^{-7} ft^3 hr^{-1} gal^{-1}. Unlike the HGR measurement in the presence of sludge solids where the reaction rate was gradually slowed, the addition of mercuric nitrate at 430 mg Hg/L appears to have stopped the hydrogen generation reaction almost entirely. It is currently unclear what mechanisms are involved in this process. Given that 1) 430 mg Hg/L is relatively high compared to mercury concentrations expected in supernatant waste tank media, 2) this test is believed to be unrepresentative (with respects to the impacts of mercury on liquid-phase chemical reactions) due to the formation of insoluble mercury as mercuric oxide, and 3) the HGR from glycolate is diminished considerably in the presence of this component, it is recommended that this behavior not be included in HGR model development with the understanding that if such compounds are present in radioactive waste streams, the generated model will be conservative. However, it is also recommended that further investigation be made into this mechanism to assess alternative methods of mitigating thermolytic HGR.

3.3.4.3 Testing with Other Lewis Acids (Si and B)

Literature reports from Ashby *et al.*[10] suggest that the primary reaction mechanism for glycolate thermolysis resulting in hydrogen generation is due to a catalytic reaction involving aluminate anion as a Lewis acid binding site for nitrite anion. Once activated, the nitrited aluminum can react with glycolate to form a nitrosylated species that then undergoes degradation to form a hydrogen-generating intermediate aldehyde. The full mechanism proposed by Ashby is given in Figure 3-21.

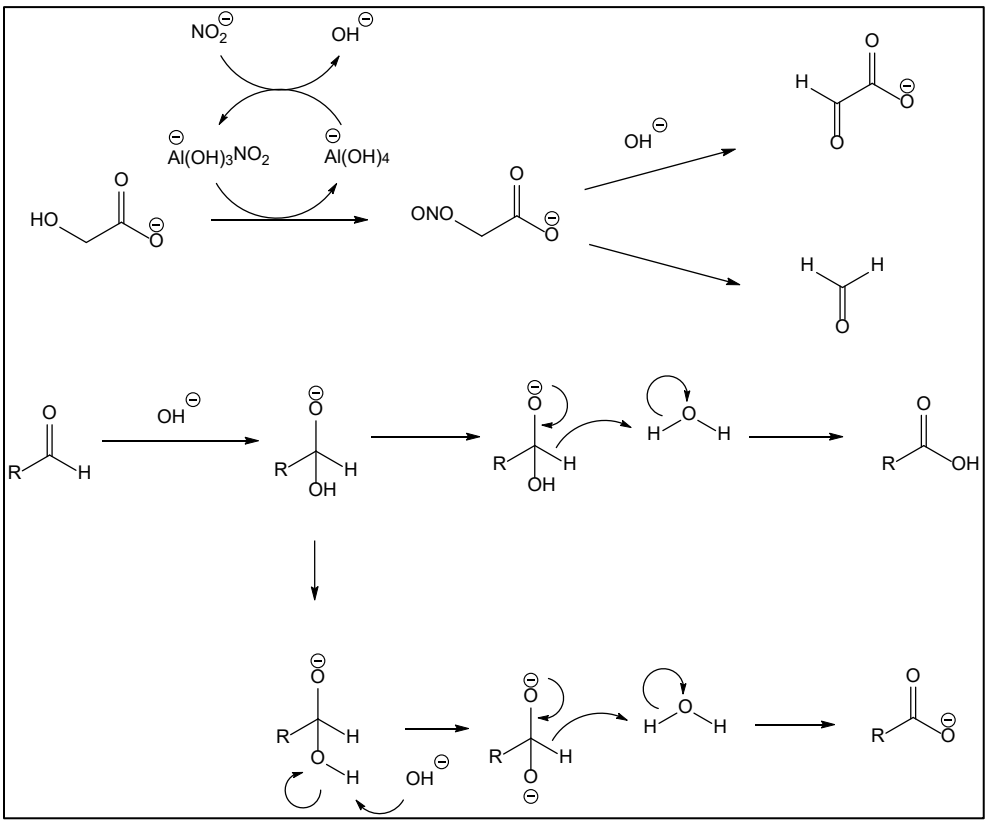

Figure 3-21. Mechanism of Aluminum-Catalyzed Thermolytic Production of Hydrogen from Glycolate Theorized by Ashby *et al.*[10]

Through the tracking of ^{13}C-labeled compounds and some rudimentary kinetics experiments, Ashby *et al.*[10] was able to determine the mechanism shown in Figure 3-21 and hypothesized that the rate limiting step was the interaction of glycolate with the nitrited aluminum species. The possibility of this interaction having an impact on glycolate thermolysis suggests that other Lewis acid-type metals may have an impact on HGR from glycolate. Boron, silicon, and iron are of particular interest.

Testing with sludge solids (described above) revealed that trace amounts of iron in caustic tank waste media (only a small fraction of the iron in SRS waste is water-soluble) had no appreciable impact on glycolate thermolysis at concentrations of interest. However, effects from Si and B had not been determined. Therefore, a screening experiment was conducted in which 190 mg/L of boron and 130 mg/L of silicon were added along with 1,000 mg/L of glycolate to the D-optimal centroid simulant to determine if these known Lewis acids had any influence on glycolate thermolysis at concentrations of interest.[18] The result of that experiment is given in Figure 3-22.

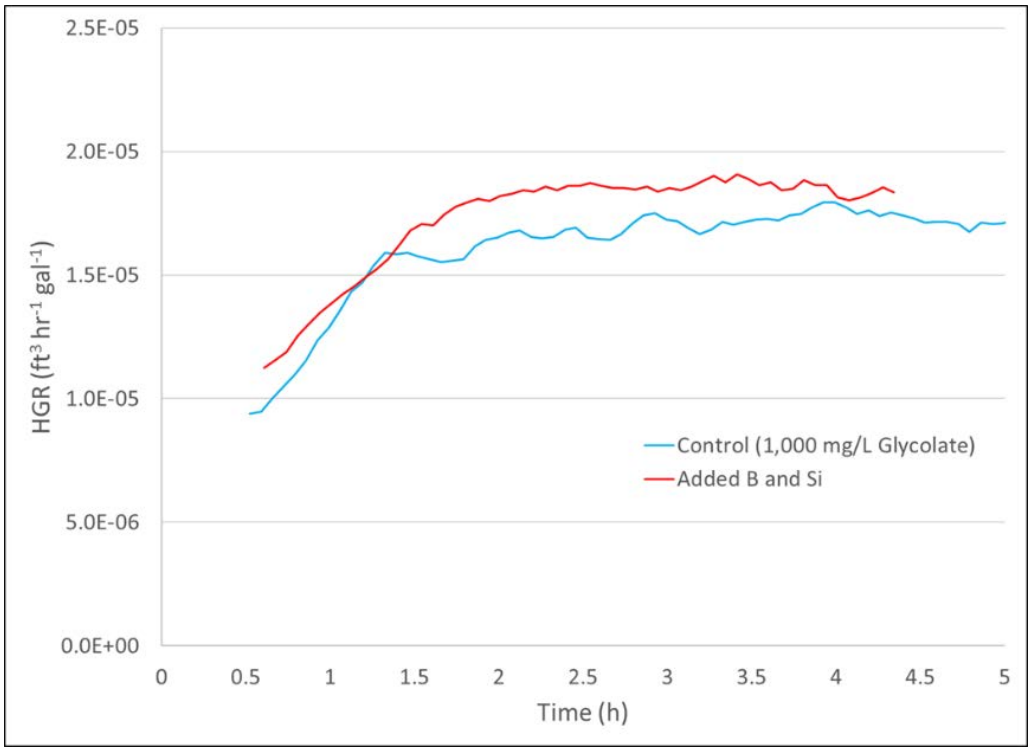

Figure 3-22. HGR from 1,000 mg/L Glycolate as a Function of Time in the Presence (Red) and Absence (Blue) of Boron and Silicon (190 and 130 mg/L, respectively).

The results shown in Figure 3-22 suggest that the presence of boron and silicon at 190 mg/L and 130 mg/L, respectively, have no appreciable impact on the production of hydrogen from glycolate. The HGR measurements obtained from each experiment are within experimental error and are therefore practically indistinguishable. It may then be concluded that B and Si terms may be omitted from expressions describing glycolate HGR.

3.3.4.4 Testing with Noble Metals (Ag, Pd, Rh, and Ru)

It has been known for several years that noble metals have an appreciable impact on the chemistry of reducing acids in the DWPF CPC. While the conditions in the CPC vary from basic (pH=12) to weakly acidic (pH=4), it may then be speculated that noble metals present in SRS waste (silver, palladium, rhodium, and ruthenium) could have an impact on glycolate chemistry at the higher pHs (pH>13) and sodium loadings ([Na]>1 M) present in the CSTF. A final screening experiment was performed to examine the impact of these noble metals on glycolate thermolysis. This test was conducted by charging silver, palladium, rhodium, and ruthenium to the D-Optimal centroid simulant at concentrations of 0.4 mg/L, 0.2 mg/L, 0.2 mg/L, and 1 mg/L (respectively) along with 1,000 mg/L of glycolate.[18] The results of this test are given in Figure 3-23.

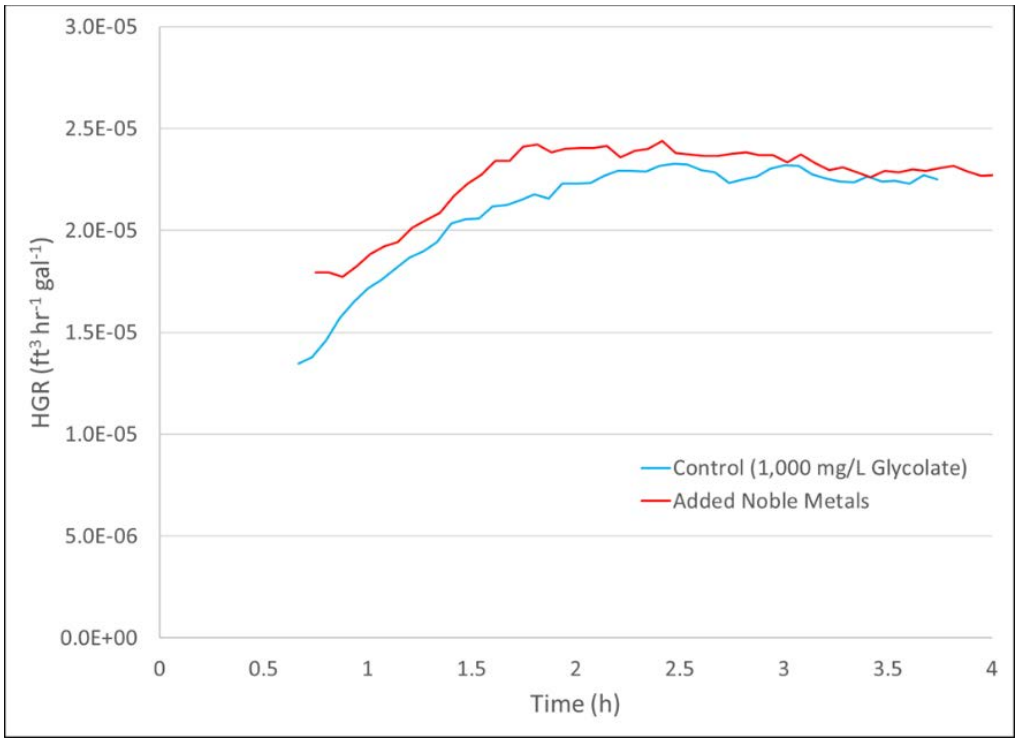

Figure 3-23. HGR from 1,000 mg/L Glycolate as a Function of Time in the Presence (Red) and Absence (Blue) of Silver, Palladium, Rhodium, and Ruthenium (0.4, 0.2, 0.2, and 1 mg/L, respectively).

The data in Figure 3-23 suggest that the presence of noble metals in caustic tank waste media have no appreciable impact on the production of hydrogen from glycolate. This finding is consistent with the observation that low pHs are generally required to observe hydrogen in the CPC. It is therefore concluded that effects from noble metals such as silver, palladium, rhodium, and ruthenium may be neglected when developing a thermolytic model for the production of hydrogen from glycolate.

3.3.4.5 Comparison to Glycolate HGR Measurements in Radioactive Waste

While developing the temperature-modified glycolate HGR model, SRNL was tasked with performing HGR measurements of select radioactive samples containing added glycolate as a separate validation data set.[23] Six tanks were identified for SRNL to perform HGR testing without and with added glycolate: 22, 28, 38, 39, 44, and 50.[24-27] To date, results from five of the six tests have been published in SRNL technical reports. No appreciable impact from added glycolate was observed in Tank 22 material. Glycolate impacts on HGR were observed, however, in Tanks 28, 38, and 39. Differences in Tank 50 testing in cases with and without added glycolate were not statistically significant and are not included in this analysis. The composition and condition information pertinent to HGR prediction, as well as the observed HGRs attributable to glycolate thermolysis, are given in Table 3-12. For comparison, additional data gathered from previous SRNL simulant studies[11] are also listed in Table 3-13 (HBP-75 through HBP-136, see Appendix A for further information), as are results reported in the chemical literature[10] (ASH-1 through ASH-4).

Table 3-12. Conditions and Results from Glycolate HGR Testing with Radioactive Waste.

Tank Number	Test Name	Nitrate (M)	Hydroxide (M)	Sodium (M)	TOC† (M)	Temp. (°C)	HGR ($ft^3\ h^{-1}\ gal^{-1}$)
38	Tk38-60	1.22E+00	3.00E+00	7.89E+00	4.19E-02	60	6.63E-08
	Tk38-80	1.22E+00	3.00E+00	7.89E+00	4.19E-02	80	9.99E-07
	Tk38-95	1.22E+00	3.00E+00	7.89E+00	4.19E-02	95	3.08E-06
	Tk38-B	1.22E+00	3.00E+00	7.89E+00	4.19E-02	111.5	9.99E-06
	Tk38-B2	1.22E+00	3.00E+00	7.89E+00	4.19E-02	111.5	1.07E-05
28	Tk28-70	1.85E+00	8.23E+00	1.30E+01	1.33E-02	70	7.5E-07
	Tk28-85	1.85E+00	8.23E+00	1.30E+01	1.33E-02	85	2.41E-06
	Tk28-100	1.85E+00	8.23E+00	1.30E+01	1.33E-02	100	1.09E-05
	Tk28-125	1.85E+00	8.23E+00	1.30E+01	1.33E-02	124.8	1.35E-04
39	Tk39-85	2.20E+00	1.79E+00	5.55E+00	5.33E-02	85	1.2E-07
	Tk39-100	2.20E+00	1.79E+00	5.55E+00	5.33E-02	100	7.6E-07
	Tk39-105	2.20E+00	1.79E+00	5.55E+00	5.33E-02	105.5	3.6E-06
22	Tk22-100	6.45E-02	1.89E-01	5.92E-01	3.20E-03	100	< 5.6E-08

†In testing with glycolate, the term TOC is used to described total organic carbon from glycolate.

Table 3-13. Conditions and Results from Glycolate HGR Testing in Previous Studies.

Test Name	Nitrate (M)	Hydroxide (M)	Sodium (M)	TOC (M)	Temp. (°C)	HGR ($ft^3\ h^{-1}\ gal^{-1}$)
ASH-1	2.59E+00	2.00E+00	9.42E+00	4.20E-01	120	4.46E-04
ASH-2	2.59E+00	2.00E+00	8.88E+00	4.20E-01	120	3.09E-04
ASH-3	2.59E+00	2.00E+00	9.31E+00	2.00E-01	120	2.29E-04
ASH-4	2.59E+00	2.00E+00	8.30E+00	4.20E-01	120	2.54E-04
HBP-75	3.20E+00	1.01E+01	1.75E+01	2.43E-01	75	2.63E-05
HBP-100	3.20E+00	1.01E+01	1.75E+01	2.43E-01	100	5.16E-04
HBP-120	3.20E+00	1.01E+01	1.75E+01	2.43E-01	120	4.08E-03
HBP-136	3.20E+00	1.01E+01	1.75E+01	2.43E-01	135.8	1.80E-02

Results from the tests listed in Table 3-12 and Table 3-13 are plotted against the values expected from the temperature-modified glycolate HGR expression (Equation [17]) in Figure 3-24.

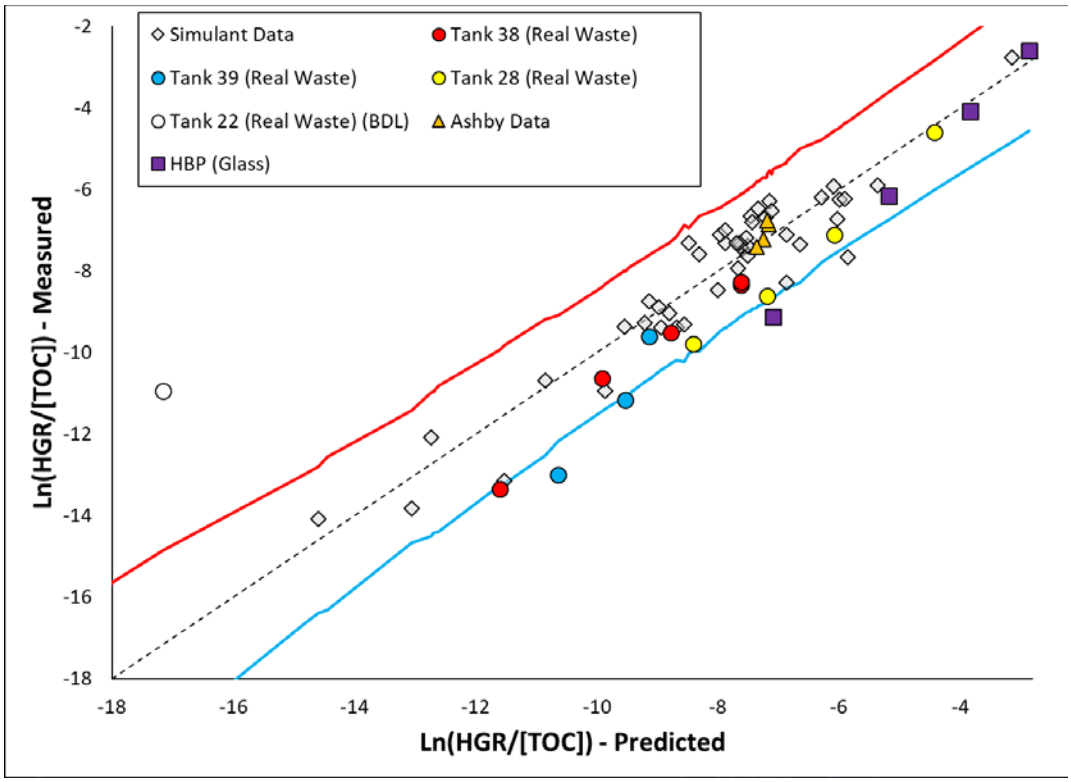

Figure 3-24. Plot of Measured HGRs from Simulant Experiments (Diamonds) and Radioactive Waste Samples (Circles) for Glycolate vs. Predicted HGRs According to the Temperature-Modified Glycolate Model Shown in Equation [17]. For comparison, results from previously-performed simulant experiments (squares) and literature-reported values (triangles) are also given.

The data shown in Figure 3-24 suggest that the temperature-modified glycolate HGR model sufficiently bounds the HGRs observed from glycolate in radioactive waste conditions. Results from testing with material from Tanks 28, 38, and 39 all fall below the model prediction line. A single experiment from Tank 22 is shown above the model prediction line: however, it should be noted that this experiment yielded no quantifiable hydrogen and is therefore listed as "below detection limit", or BDL. Improved detection methodology might be expected to yield lower detection limits, which would lower the artificially-high reported value.

Additional results from testing with simulants are also displayed in Figure 3-24. HGR measurements performed in 2017 with Tank 38 simulant in a glass vessel are shown as purple squares (designated as High Boiling Point - HBP) and literature results from work performed by Ashby *et al.*[10] are displayed as orange triangles (designated as Ashby). It should be noted that the values reported from Ashby are based on measurements of glycolate destruction rather than hydrogen formation and are therefore expected to be biased slightly high. It can be observed that all these simulant values fall below the upper 95% confidence limit, with roughly half of the results falling below the model prediction (50% of Ashby data, 75% of HBP data). Details pertaining to the performance of HBP testing in glass are given in Appendix A.

The quality of fit to radioactive waste data exhibited in Figure 3-24 suggests that the temperature-modified glycolate HGR model is sufficient to describe and bound the HGR expected from glycolate in radioactive caustic waste media. It is recommended that this model be used to estimate HGR from glycolate in future calculations. The use of this model to estimate glycolate HGR in CSTF flammability calculations is exhibited in Appendix C.

3.3.4.6 Extrapolation of Temperature-Modified Glycolate Model to Lower Temperatures (<60 °C)

The ability of the temperature-modified glycolate HGR model to be extrapolated to temperatures below those evaluated during testing can be assessed by considering the Arrhenius behavior observed from testing with radioactive waste samples. The modified Arrhenius plot shown in Figure 3-25 gives the natural log of the HGR measured from radioactive waste samples normalized by the concentration parameters specified in the temperature-modified glycolate HGR model vs the inverse of the absolute temperature. For reference, the model prediction values are also shown as a straight black line (dashed).

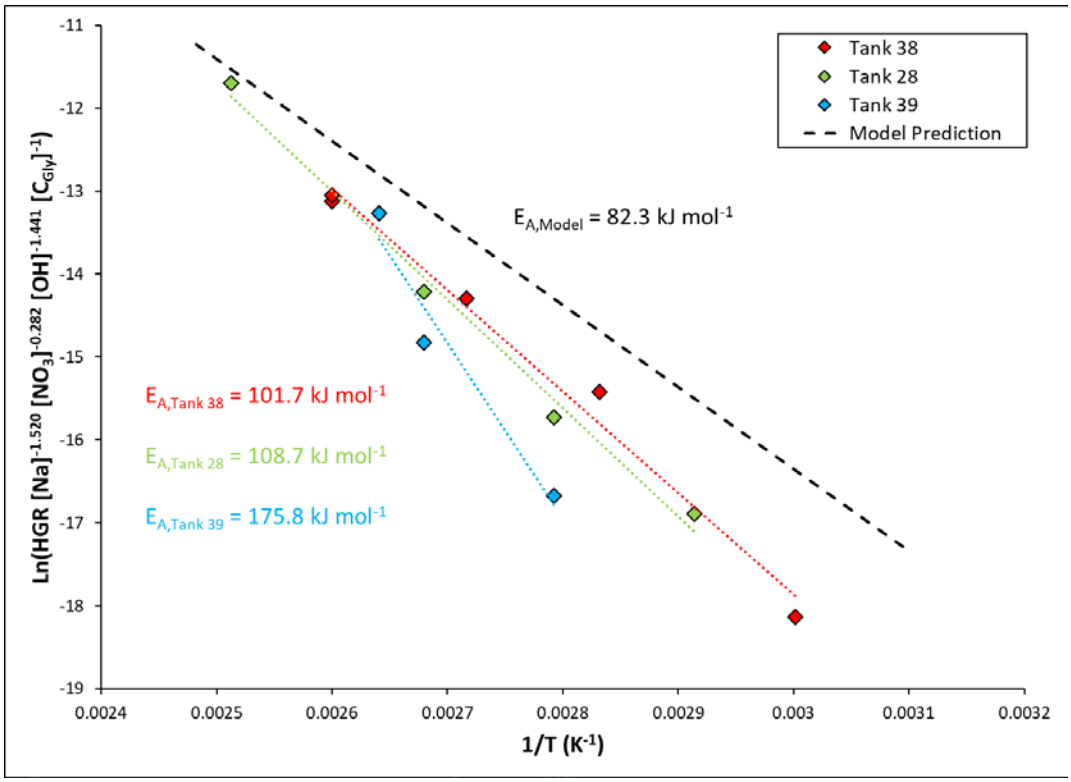

Figure 3

-25. Modified Arrhenius Plot of Glycolate HGRs Measured in Radioactive Waste Vs. Temperature-Modified Glycolate HGR Model Predictions.

The activation energies calculated from the best fit lines depicted in Figure 3-25 (101.7, 108.7, and 175.8 kJ mol^{-1} for Tanks 38, 28, and 39, respectively) are each higher than that predicted by the model expression (82.3 kJ mol^{-1}). These increased activation energies indicate that as temperature is decreased from the highest temperatures measured, the resulting decrease in HGR is greater than that expected from the model expressions. While this does indicate a failure of the model to accurately describe HGRs at lower temperatures, it suggests that extrapolations of predicted HGR to temperatures lower than those studied may be performed with minimal risk to the conservative assumptions made in model generation.

3.4 Xiameter AFE-1010

3.4.1 Model Generation Experiments

Ten experiments were performed to generate an interim model for thermolytic HGR from organic compounds derived from Xiameter AFE-1010.[28] These experiments were performed at conditions similar to those expected in Tank 38 at and around 100 °C. Test XIA-1 was conducted by adding Xiameter AFE-

1010 to a Tank 38 simulant directly and measuring the HGR at 100 °C. Tests XIA-2 through 7 were performed by adding Xiameter AFE-1010 to a variant of Tank 38 simulant in which a single component (aluminum, nitrite, nitrate, hydroxide, sulfate, or carbonate) concentration had been significantly altered. These tests were performed at organic concentrations and temperatures identical to those employed in XIA-1. In this way, it was expected that preliminary estimates of salt component impacts could be calculated by comparing HGR results from any two sets of experiments, as shown in Equations [18] and [19]:

$$\ln\left(\frac{HGR'}{HGR_0}\right) = \ln\left(\frac{k \times e^{-E/RT} \times \prod[i']^{\alpha_i}}{k \times e^{-E/RT} \times \prod[i_0]^{\alpha_i}}\right) = \alpha_i \ln\left(\frac{[i']}{[i_0]}\right); for\,[i'] \neq [i_0] \quad [18]$$

$$\alpha_i = \ln\left(\frac{HGR'}{HGR_0}\right) \Big/ \ln\left(\frac{[i']}{[i_0]}\right) \quad [19]$$

where,

HGR_0 is the HGR measured at the standard Tank 38 condition in $ft^3\ h^{-1}\ gal^{-1}$,

HGR' is the HGR measured when the concentration of component i is altered in $ft^3\ h^{-1}\ gal^{-1}$,

$[i_0]$ is the concentration of component i at the standard Tank 38 condition in mol L^{-1},

$[i']$ is the concentration of component i at the variant condition in mol L^{-1}, and

α_i is the reaction order of component i.

Tests XIA-2, 3, 4, 5, 6, and 7 were conducted to independently evaluate the impacts of aluminum, nitrite, nitrate, hydroxide, sulfate, and carbonate, respectively. In addition, test XIA-8 was performed in a Tank 38 simulant at 100 °C with approximately half of the organic loading employed in XIA-1. Finally, tests XIA-9 and 10 were performed using a Tank 38 simulant and an organic loading identical to that employed in XIA-1 at 85 °C and 110 °C, respectively, where 110 °C is the measured boiling point of the Tank 38 simulant employed in this testing. Table 3-14 lists the conditions (concentrations and temperatures) employed in these ten experiments. Table 3-15 lists the resulting HGR from each experiment, the expected contribution of organic-free simulant to HGR, and the adjusted HGR for each of the experiments described above.

Table 3-14. HGR Test Conditions for Xiameter Model Generation.

Test Name	Al (M)	NO_2 (M)	NO_3 (M)	OH (M)	SO_4 (M)	CO_3 (M)	Na (M)	TOC (M)	Temp. (°C)
XIA-1	9.23E-02	2.13E+00	1.11E+00	2.35E+00	5.11E-02	6.23E-01	7.13E+00	8.54E-04	100
XIA-2	2.29E-01	2.48E+00	1.15E+00	2.65E+00	6.85E-02	6.79E-01	7.74E+00	8.28E-04	100
XIA-3	7.93E-02	1.50E+00	1.16E+00	2.62E+00	7.05E-02	6.79E-01	6.70E+00	8.31E-04	100
XIA-4	9.75E-02	2.37E+00	2.71E-01	2.55E+00	5.72E-02	6.93E-01	6.31E+00	8.30E-04	100
XIA-5	9.60E-02	2.50E+00	1.60E+00	1.68E+00	<1.04E-03	6.93E-01	6.31E+00	8.39E-04	100
XIA-6	9.53E-02	2.28E+00	1.12E+00	2.54E+00	2.14E-02	6.66E-01	7.18E+00	8.42E-04	100
XIA-7	9.97E-02	2.35E+00	1.24E+00	2.71E+00	6.04E-02	2.20E-01	6.79E+00	8.31E-04	100
XIA-8	8.52E-02	2.26E+00	1.16E+00	2.61E+00	5.85E-02	6.39E-01	6.52E+00	4.21E-04	100
XIA-9	8.15E-02	2.61E+00	1.22E+00	2.71E+00	7.36E-02	7.23E-01	7.96E+00	8.19E-04	85
XIA-10	9.86E-02	2.35E+00	1.14E+00	2.78E+00	5.87E-02	6.33E-01	7.66E+00	8.39E-04	110

Table 3-15. HGR Test Results for Xiameter Model Generation.

Test Name	Observed HGR ($ft^3\ h^{-1}\ gal^{-1}$)	Predicted HGR from Blank (95% CL) ($ft^3\ h^{-1}\ gal^{-1}$)	Adjusted Thermolytic HGR ($ft^3\ h^{-1}\ gal^{-1}$)
XIA-1	1.40E-06	1.10E-07	1.29E-06
XIA-2	2.16E-06	1.27E-07	2.03E-06
XIA-3	2.09E-06	1.07E-07	1.98E-06
XIA-4	1.77E-06	6.78E-08	1.70E-06
XIA-5	9.55E-07	1.02E-07	8.53E-07
XIA-6	1.59E-06	1.19E-07	1.47E-06
XIA-7	1.35E-06	1.30E-07	1.22E-06
XIA-8	9.24E-07	1.23E-07	8.01E-07
XIA-9	8.62E-07	7.21E-08	7.90E-07
XIA-10	2.33E-06	1.83E-07	2.15E-06

The results from model generation testing with Xiameter AFE-1010 (shown in Table 3-14 and Table 3-15) were linearly regressed (according to the logarithmic methodology discussed earlier) using a stepwise fitting approach in JMP. The best-fit model is shown in Equation [20].

$$\ln\left(\frac{HGR}{[C_{XIA}]}\right) = 7.136 + 1.303\ln[OH] - \frac{5475}{T} \qquad [20]$$

The logarithmic model given in Equation [20] may be transformed for simple implementation, yielding the expression given in Equation [21]:

$$HGR_{XIA} = 1.256\times10^{3}[OH]^{1.303}[C_{XIA}]e^{-45{,}500/RT} \qquad [21]$$

The interim model developed for Xiameter AFE-1010 and its derivatives around Tank 38 conditions suggest that the most important factor in thermolytic HGR is the concentration of free hydroxide. The results of Xiameter model generation experiments given in Table 3-14 and Table 3-15 (as the natural logarithm of the HGR divided by the concentration of organic carbon added with Xiameter) are plotted against the model expression (as seen in Equation [20]) in Figure 3-26.

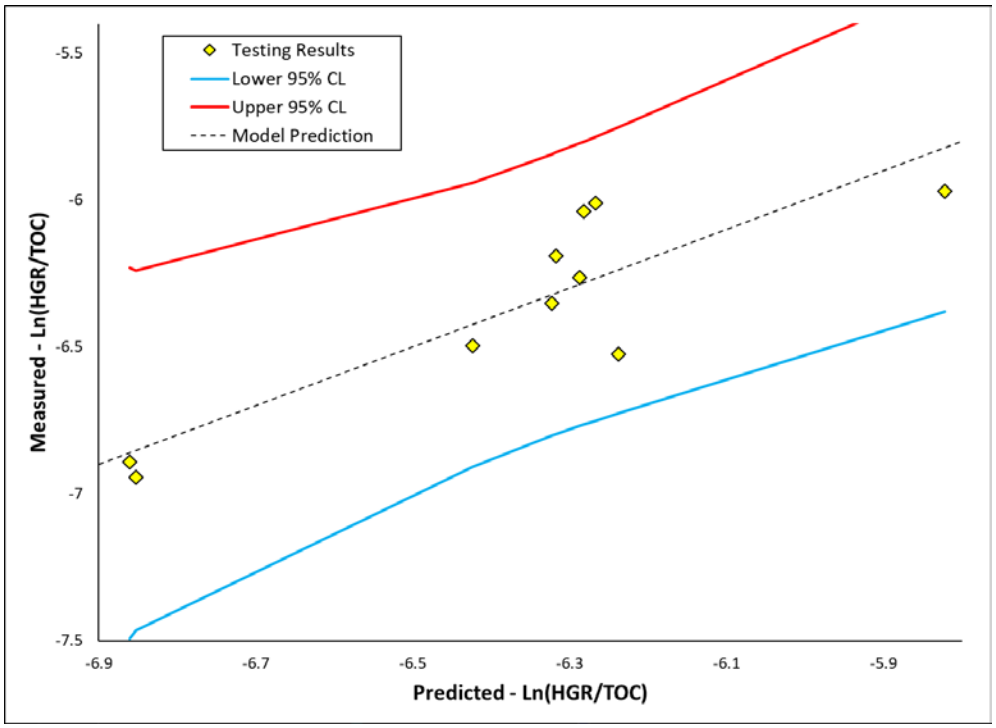

Figure 3-26. Plot of Measured HGRs from Model Generation Tests for Xiameter vs. Predicted HGRs According to Interim Model Shown in Equation [20].

The red and blue lines shown in Figure 3-26 are the upper and lower 95% confidence limits for a single prediction of HGR from the model equation shown in Equation [20]. The data in Figure 3-26 suggest that the HGRs measured around Tank 38 conditions are well captured within the uncertainty of the model equation given in Equation [20], which serves as an interim model for thermolytic HGR from Xiameter AFE-1010 to be validated and improved with additional data.

3.4.2 Model Validation Experiments

Seven experiments were designed to evaluate the applicability of the interim Xiameter model across the ranges of concentrations and temperatures available in the CSTF.[19] The conditions of these tests are identical to those employed for glycolate model validation. The concentrations and temperatures of these seven tests are given in Table 3-16. Observed HGR values, expected contributions from organic-free conditions, and the adjusted thermolytic HGR from these seven tests are given in Table 3-17.

Table 3-16. HGR Test Conditions for Xiameter Model Validation and Improvement.

Test Name	Al (M)	NO_2 (M)	NO_3 (M)	OH (M)	SO_4 (M)	CO_3 (M)	Na (M)	TOC (M)	Temp. (°C)
P3-XIA-1	3.93E-03	1.16E+00	2.58E+00	5.85E+00	6.07E-02	1.96E-01	1.07E+01	2.50E-04	95
P3-XIA-2	3.08E-02	9.37E-01	1.58E-01	1.25E+01	4.82E-03	2.82E-02	1.47E+01	3.00E-04	73
P3-XIA-3	5.00E-02	4.30E-01	2.63E+00	6.04E+00	1.15E-01	1.38E-02	1.01E+01	5.83E-04	89
P3-XIA-4	1.02E-01	2.61E+00	3.31E+00	1.78E+00	2.12E-02	3.96E-01	9.18E+00	5.35E-04	100
P3-XIA-5	1.25E-01	3.98E-01	1.92E+00	2.27E+00	1.78E-01	1.65E-01	5.70E+00	5.11E-04	95
P3-XIA-6	3.93E-01	2.63E-01	3.61E+00	2.29E+00	2.00E-01	5.53E-01	8.31E+00	5.94E-04	109
P3-XIA-7	4.37E-01	2.10E+00	1.95E+00	6.93E+00	1.62E-02	5.33E-02	1.22E+01	2.18E-04	76

Table 3-17. HGR Test Results for Xiameter Model Validation and Improvement.

Test Name	Observed HGR ($ft^3\ h^{-1}\ gal^{-1}$)	Predicted HGR from Blank (95% CL) ($ft^3\ h^{-1}\ gal^{-1}$)	Adjusted Thermolytic HGR ($ft^3\ h^{-1}\ gal^{-1}$)
P3-XIA-1	9.51E-07	1.64E-07	7.87E-07
P3-XIA-2	6.43E-07	3.60E-08	6.07E-07
P3-XIA-3	1.89E-06	9.00E-08	1.80E-06
P3-XIA-4	9.41E-07	1.37E-07	8.04E-07
P3-XIA-5	3.34E-07	5.37E-08	2.80E-07
P3-XIA-6	1.97E-06	9.20E-08	1.88E-06
P3-XIA-7	4.30E-07	9.27E-08	3.37E-07

The results from the seven interim Xiameter model validation tests are plotted against values predicted by the expression shown in Equation [20] in Figure 3-27.

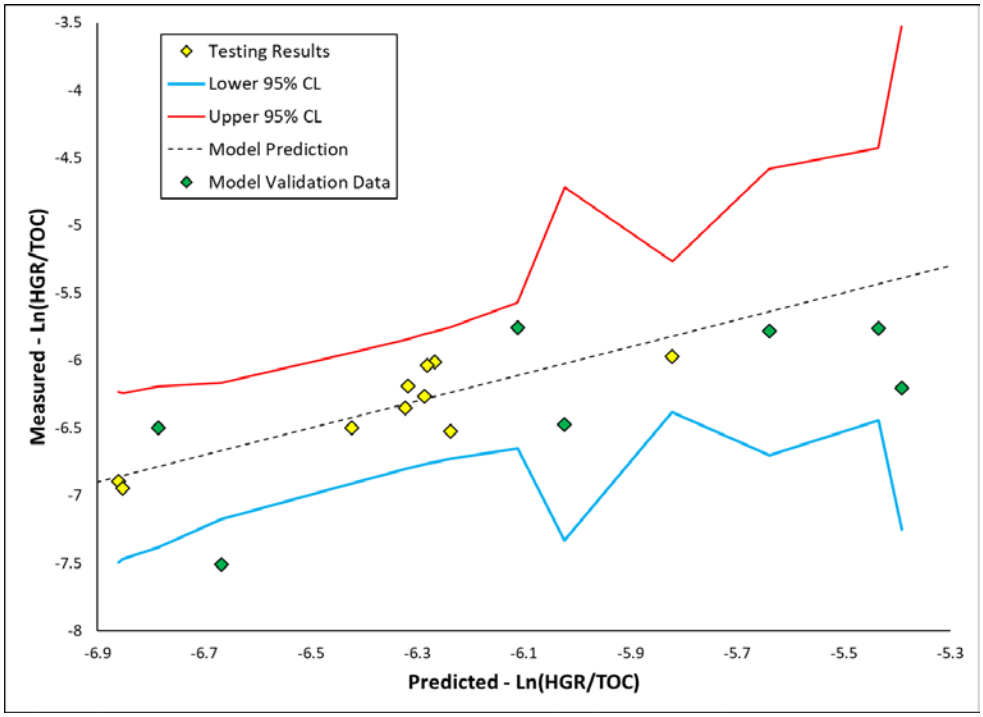

Figure 3-27. Plot of Measured HGRs from Model Generation (Yellow) and Validation (Green) Tests for Xiameter vs. Predicted HGRs According to Interim Model Shown in Equation [20].

First inspection of the data plotted in Figure 3-27 suggests that the interim Xiameter model well bounds the observed HGRs from the validation data set. The majority (six of seven) of the validation points fall within the 95% confidence interval of a single prediction from the model given in Equation [20], with the final point falling well below the model prediction. However, it should be noted that the model uncertainty around this validation seems to be significantly greater than around the model generation points. This behavior, while drastic, is not surprising given that the interim model for Xiameter thermolytic HGR was developed around Tank 38 conditions and the validation data set was designed to evaluate HGR across a generally larger set of concentration and temperature conditions available to CSTF operations. Such a model would be expected to give lower uncertainties for conditions similar to Tank 38 and higher uncertainties at conditions that are significantly removed from Tank 38.

As discussed previously for glycolate, the validation data set may be included for linear regression to generate a more robust model for Xiameter thermolytic HGR. The improved model obtained through the regression of this enhanced data set is given in Equation [22].

$$\ln\left(\frac{HGR}{[C_{XIA}]}\right) = 12.688 + 1.141\ln[OH] - \frac{7497}{T} \qquad [22]$$

The HGR results of all Xiameter testing are plotted against the enhanced model described in Equation [22] in Figure 3-28.

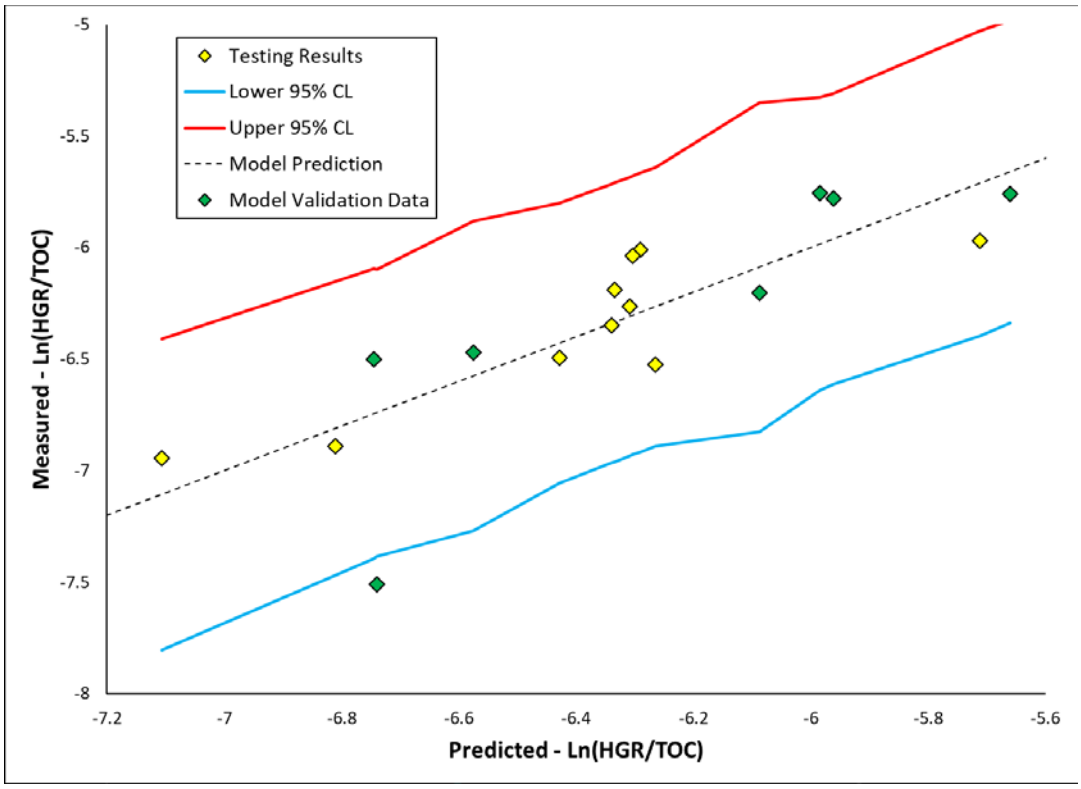

Figure 3-28. Plot of Measured HGRs from Model Generation (Yellow) and Validation (Green) Tests for Xiameter vs. Predicted HGRs According to Final Model Shown in Equation [22].

The data plotted in Figure 3-28 suggest that the majority of variation seen in results from Xiameter testing is described well by the enhanced model given in Equation [22]. It should also be noted that the model exhibits a general decrease in uncertainty around the validation data sets, indicating that the enhanced model may more readily be extrapolated to other regions in CSTF composition and temperature space.

The linearized model given in Equation [22] may be transformed for simple implementation, as is shown in Equation [23].

$$HGR_{XIA} = 3.238\times10^{5}\left[OH\right]^{1.141}\left[C_{XIA}\right]e^{-62{,}300/RT} \qquad [23]$$

Given the increase in robustness achieved by incorporating the validation data set into the linear model regression, it is recommended to use the expression given in Equation [23] to estimate the thermolytic HGR from Xiameter AFE-1010 in CSTF caustic waste media.

3.5 IONAC A-641 Ion Exchange Resin

3.5.1 Model Generation Experiments

Ten experiments (identical to those performed for Xiameter AFE-1010) were performed using IONAC A-641 digestion product to develop an interim model for thermolytic HGR from polystyrene-based resins.[28] The measured concentrations of chemical components used in these model development tests are given in Table 3-18. The observed HGRs, expected contribution from organic-free (blank) conditions, and adjusted thermolytic HGR values from these experiments are given in Table 3-19.

Table 3-18. HGR Test Conditions for IONAC A-641 Model Generation.

Test Name	Al (M)	NO_2 (M)	NO_3 (M)	OH (M)	SO_4 (M)	CO_3 (M)	Na (M)	TOC (M)	Temp (°C)
IAC-1	9.56E-02	2.30E+00	1.34E+00	2.68E+00	6.03E-02	6.24E-01	7.70E+00	2.29E-02	100
IAC-2	2.33E-01	2.09E+00	1.15E+00	2.79E+00	5.22E-02	5.16E-01	7.39E+00	2.26E-02	100
IAC-3	7.97E-02	1.31E+00	1.21E+00	2.43E+00	5.60E-02	5.53E-01	6.44E+00	2.35E-02	100
IAC-4	8.12E-02	2.24E+00	4.31E-01	2.39E+00	5.55E-02	5.46E-01	6.39E+00	2.39E-02	100
IAC-5	8.12E-02	2.20E+00	1.24E+00	1.74E+00	5.61E-02	5.49E-01	6.44E+00	2.41E-02	100
IAC-6	7.63E-02	2.24E+00	1.27E+00	2.61E+00	2.21E-02	5.63E-01	6.92E+00	2.37E-02	100
IAC-7	8.23E-02	2.24E+00	1.25E+00	2.80E+00	5.43E-02	1.86E-01	6.74E+00	2.41E-02	100
IAC-8	9.49E-02	2.39E+00	1.27E+00	2.71E+00	6.21E-02	6.06E-01	8.48E+00	1.26E-02	100
IAC-8A	8.75E-02	2.26E+00	1.13E+00	2.69E+00	5.93E-02	5.56E-01	8.48E+00	5.15E-03	100
IAC-9	7.71E-02	2.16E+00	1.23E+00	2.48E+00	5.45E-02	5.53E-01	8.18E+00	2.38E-02	85
IAC-10	8.19E-02	2.26E+00	1.27E+00	2.53E+00	5.87E-02	5.69E-01	8.31E+00	2.32E-02	110

Table 3-19. HGR Test Results for IONAC A-641 Model Generation.

Test Name	Observed HGR ($ft^3\ h^{-1}\ gal^{-1}$)	Predicted HGR from Blank (95% CL) ($ft^3\ h^{-1}\ gal^{-1}$)	Adjusted Thermolytic HGR ($ft^3\ h^{-1}\ gal^{-1}$)
IAC-1	2.52E-06	1.32E-07	2.39E-06
IAC-2	1.42E-06	1.25E-07	1.30E-06
IAC-3	1.40E-06	9.74E-08	1.30E-06
IAC-4	1.58E-06	7.76E-08	1.50E-06
IAC-5	7.09E-07	9.16E-08	6.17E-07
IAC-6	1.79E-06	1.26E-07	1.66E-06
IAC-7	1.59E-06	1.32E-07	1.46E-06
IAC-8	1.56E-06	1.32E-07	1.43E-06
IAC-8A	1.20E-06	1.24E-07	1.08E-06
IAC-9	2.85E-07	6.34E-08	2.22E-07
IAC-10	2.93E-06	1.77E-07	2.75E-06

The results from Table 3-19 were linearly regressed in a step-wise manner against the species concentration inputs given in Table 3-18. The best-fit model achieved from this regression is shown in Equation [24].

$$\ln\left(\frac{HGR}{[C_{IAC}]}\right) = 27.054 + 2.728\ln[OH] - \frac{14,623}{T} \quad [24]$$

This logarithmic model may be transformed, yielding the simplified expression in Equation [25].

$$HGR_{IAC} = 5.616\times10^{11}[OH]^{2.728}[C_{IAC}]e^{-121,600/RT} \quad [25]$$

The regressed model equation given in Equation [25] suggests that free hydroxide has the greatest influence on the production of thermolytic hydrogen from the digestion products of polystyrene-based resins like IONAC A-641. The results from model development testing are plotted against the interim model (given in Equation [24]) in Figure 3-29.

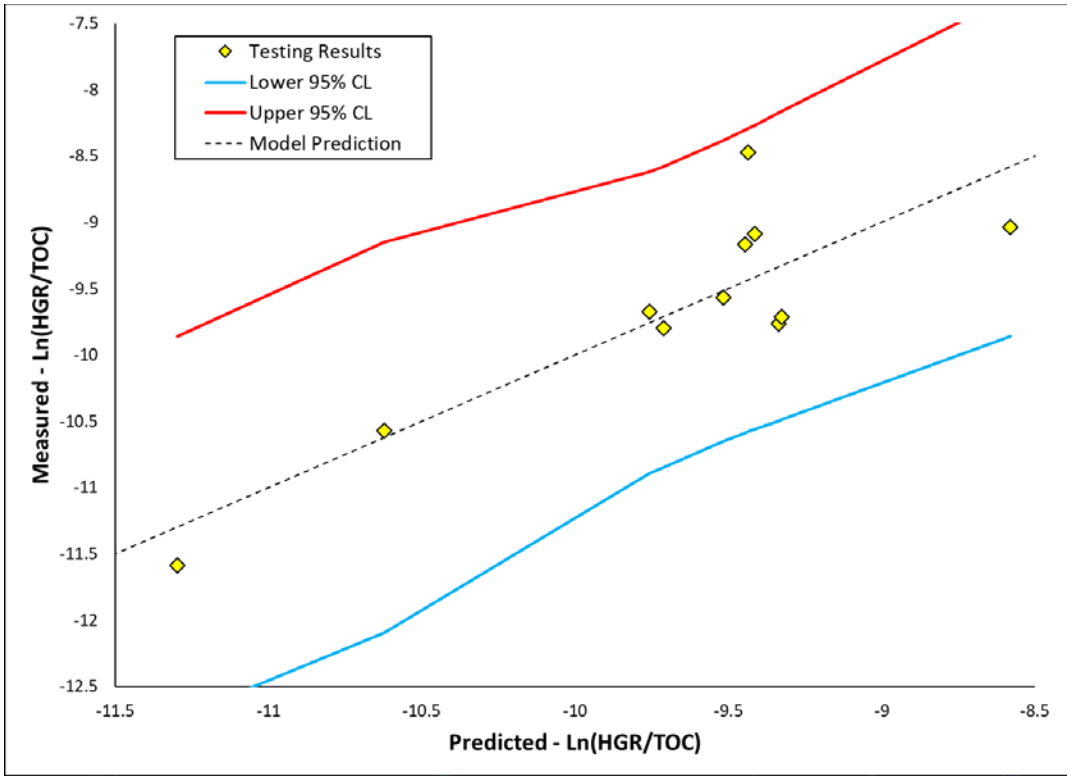

Figure 3-29. Plot of Measured HGRs from Model Generation Tests for IONAC vs. Predicted HGRs According to Interim Model Shown in Equation [24].

The data shown in Figure 3-29 suggest that the interim model development data are reasonably well-described by the model expression given in Equation [24]. This model is evaluated against additional data points and improved later in the following sections of this report.

3.5.2 Model Validation Experiments

3.5.2.1 Impact of Solids on Resin Digestion Material Thermolysis

Historically, much of the resin material employed in separations processes in H- and F-Canyons have been digested via oxidation by permanganate (the additions of undigested resin are not expected to be soluble in the supernatant phase of CSTF waste tanks). This process tends to generate an appreciable amount of MnO_2 solids, which is a known oxidizing agent for some organic compounds. These solids are transferred from the canyon digestion vessels to CSTF storage tanks along with resin digestion products. Previous HGR testing aimed at discerning HGRs from canyon transfer vessels and CSTF receipt vessels was conducted by adding resin digestion products along with MnO_2 solids as a single stream (replicating a single source of material). However, for the sake of a complete understanding of HGR due to organics from digested ion exchange resins, it is necessary to decouple the impact on HGR from added organic material from the anticipated impact of added oxidizing solids, as these solids would not necessarily be expected to follow the soluble resin digestion products throughout the CSTF tank farm. Furthermore, it is conceivable that the addition of an oxidizing solid along with a hydrogen-producing organic may confound the anticipated carbon-dependence on thermolytic HGR, as an increase in added resin digestion product would be expected to both increase and decrease the observed HGR due to the simultaneous increase in available organic carbon and carbon-reactive MnO_2.

Three sets of experiments were designed to evaluate 1) the influence of MnO_2 solids on thermolytic HGR from resin digestion products, and 2) the validity of an assumed first-order dependence of HGR on organic carbon. Each of the three sets of experiments was conducted at a single D-optimally selected composition/temperature condition identified for validation testing (as described previously for glycolate and Xiameter AFE-1010). The three conditions of interest were condition D (previously designated as P3-XXX-4), condition E (previously designated as P3-XXX-5), and condition F (previously designated as P3-XXX-6) from the validation data sets described earlier for glycolate and Xiameter. The first experiments from each set (P3-IAC-4, 5, and 6) were performed by adding the D-optimally selected aliquot of IONAC A-641 digestion product (with MnO_2 solids) to a liter of prepared simulant solution at condition D, E, and F compositions, respectively. The second experiments from each set (P3-IAC-4B, 5B, and 6B) were performed by first centrifuging the resin digestion product and decanting away the supernatant phase. Afterwards, aliquots of the same masses employed in the first tests (P3-IAC-4, 5, and 6) were drawn from the supernatant phase and charged to 1 L solutions of simulants at condition D, E, and F compositions, respectively. By comparing the first and second tests in each set, the effect of MnO_2 solids on thermolytic HGR from resin digestion products may be determined.

The penultimate experiments from each set (P3-IAC-4C, 5C, and 6C) were performed identically to the second experiments (P3-IAC-4B, 5B, and 6B) with a 50% reduction in added IONAC digestion product supernatant phase material. The final experiments from each set (P3-IAC-4D, 5E[f.2], and 6D) were performed by adding only salt solution simulant to the HGR apparatus with no added IONAC digestion product material. By comparing the results from the second, penultimate, and final experiments in each set, the basis for the TOC linearity assumption may be accepted or refuted.

Results from P3-IAC-4, P3-IAC-4B, P3-IAC-4C, and P3-IAC-4D are shown in Figure 3-30.

[f.2] The initial blank measurement for Condition E (P3-IAC-5D) was determined to be heavily influenced by anomalous hydrogen generation (in excess of that from organic-added measurements). Test P3-IAC-5E was performed to replace the unusable data from P3-IAC-5D.

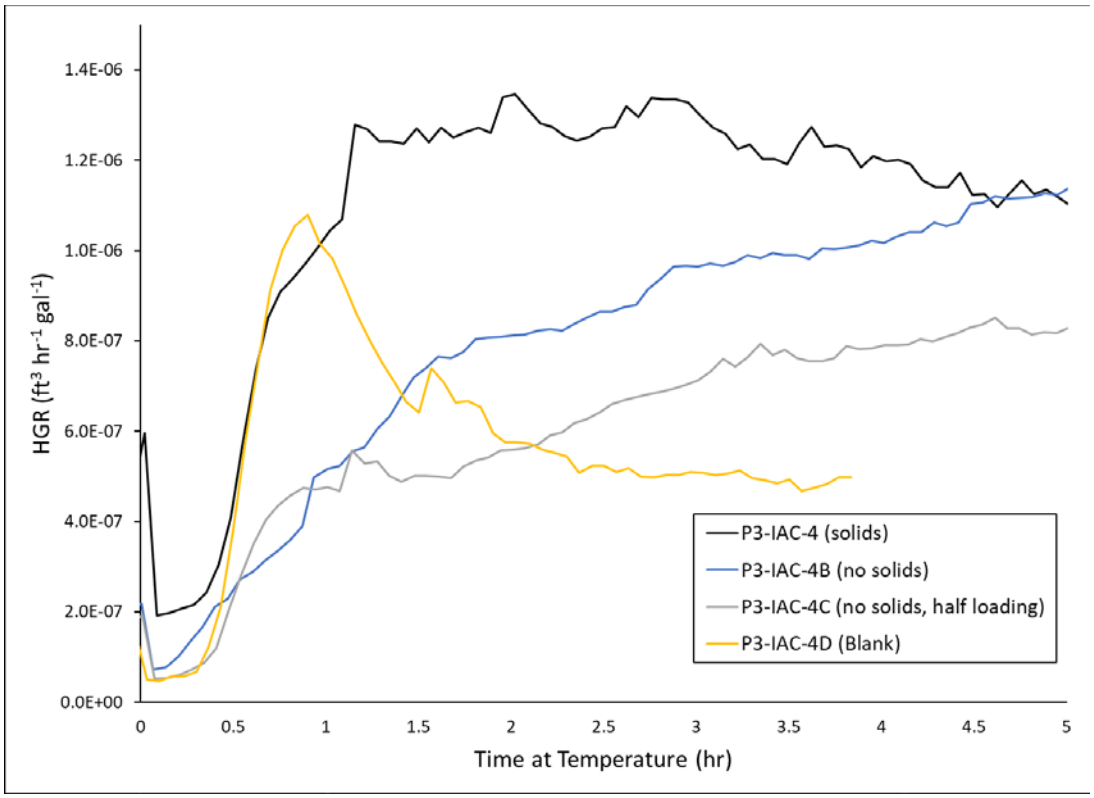

Figure 3-30. HGR Results from Condition D with Added IONAC Digestion Product Material.

The data shown in Figure 3-30 suggest that the presence of MnO_2 solids has no appreciable impact on thermolytic HGR from IONAC digestion materials. This stems from the observation that the observed HGR in the presence (P3-IAC-4) and absence (P3-IAC-4B) of solids gradually approaches 1.1×10^{-6} ft^3 h^{-1} gal^{-1} over time. Furthermore, the data suggest that the production rate of hydrogen is dependent on the concentration of organic material added. This is seen by the relative increase in HGR observed when doubling the amount of IONAC digestion product supernatant phase, rising from 8.0×10^{-7} ft^3 h^{-1} gal^{-1} (P3-IAC-4C) to 1.1×10^{-6} ft^3 h^{-1} gal^{-1}. Note also from the data shown in Figure 3-30 that the HGR attributable to IONAC-free simulant testing (P3-IAC-4D) represents a significant fraction of the observed HGR in tests with added IONAC material (P3-IAC-4, 4B, and 4C), approaching 4.0×10^{-7} ft^3 h^{-1} gal^{-1} over time.

Results from testing at condition E (P3-IAC-5, P3-IAC-5B, P3-IAC-5C, and P3-IAC-5E) are shown in Figure 3-31.

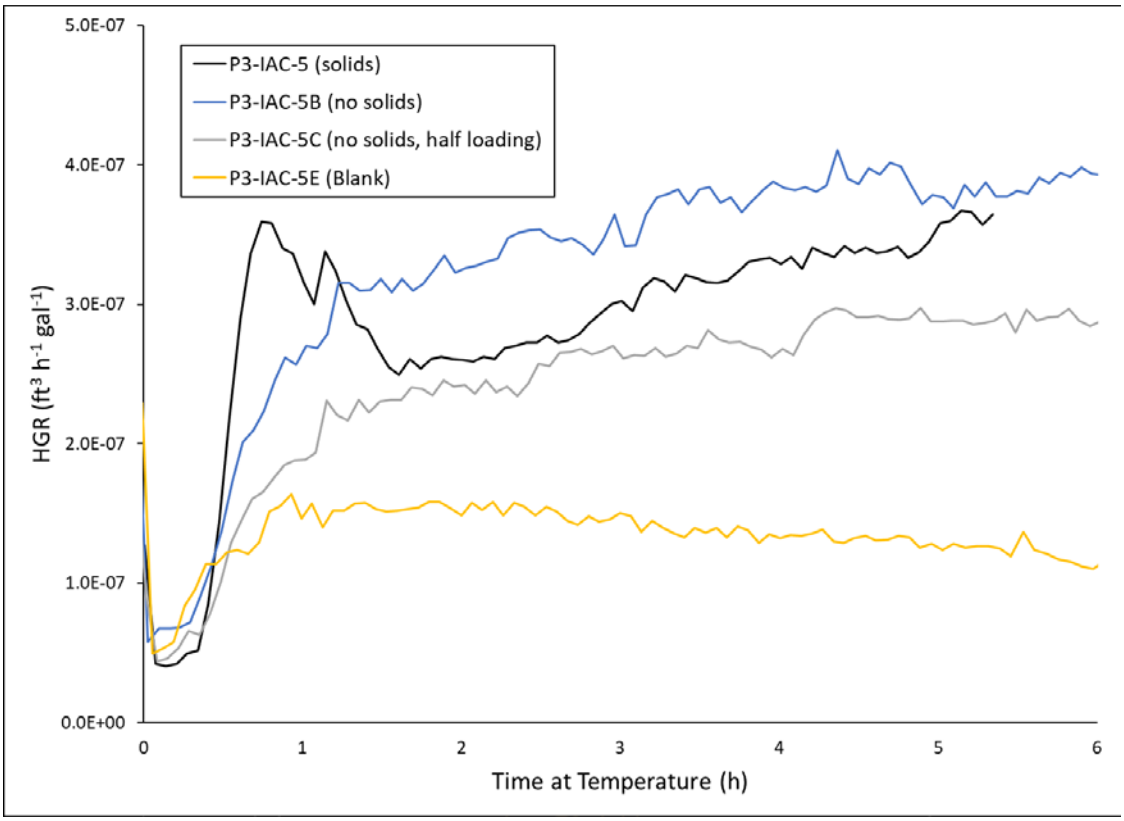

Figure 3-31. HGR Results from Condition E with Added IONAC Digestion Product Material.

Results shown in Figure 3-31 lead to similar conclusions as those seen in Condition D (Figure 3-30). Both tests with and without MnO_2 solids (P3-IAC-5 and P3-IAC-5B, respectively) trend towards values ($\geq 3.5\times10^{-7}$ ft^3 h^{-1} gal^{-1}) that are notably greater than the results from testing with a reduced loading of IONAC digestion product supernatant phase material (P3-IAC-5C, ~2.8×10^{-7} ft^3 h^{-1} gal^{-1}). Again, the HGR attributable to IONAC-free conditions appears to make up a substantial portion of the observed HGR (~1.1×10^{-7} ft^3 h^{-1} gal^{-1}).

Similar results for testing at condition F are given in Figure 3-32.

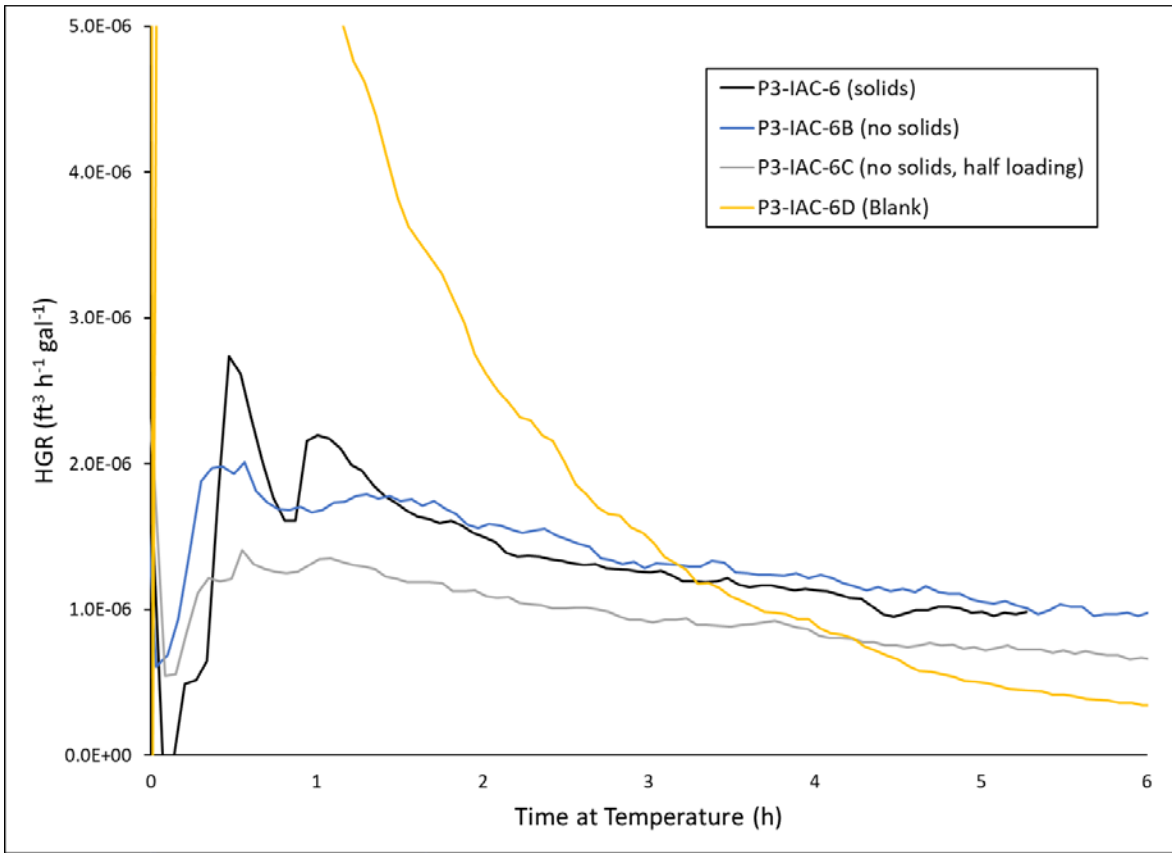

Figure 3-32. HGR Results from Condition F with Added IONAC Digestion Product Material.

Results for testing in condition F, shown in Figure 3-32, yield observations similar to those seen in conditions D and E. Testing with (P3-IAC-6) and without (P3-IAC-6B) MnO_2 solids yield nearly identical profiles, trending downward to approximately 1.2×10^{-6} ft^3 h^{-1} gal^{-1} at five hours. Similarly, testing with reduced IONAC digestion product supernatant phase material loadings exhibit decreased HGR, yielding approximately 0.9×10^{-7} ft^3 h^{-1} gal^{-1} at five hours. The test with no added IONAC material (P3-IAC-6D) exhibits a relatively high apparent HGR ($> 5\times10^{-6}$ ft^3 h^{-1} gal^{-1}) before decreasing to well below that observed for any of the tests containing IONAC material. It is believed that this temporary excursion is due to anomalous heating rod behavior stemming from scouring of the protective oxide layer during previous testing with Tank 30 simulant material with added chloride (Section 3.3.3) and is not representative of real behavior.

Given the results and observations from testing with IONAC material in the presence and absence of MnO_2 solids at standard and reduced loadings of organic carbon, it may be concluded that solid MnO_2 has no appreciable impact on the thermolytic HGR measured from resin digestion products. This result is intuitive, given that the organic compounds present in resin digestion products are formed by oxidation with MnO_4^-, which is a significantly more powerful oxidizing agent. The results discussed above also lead to the conclusion that thermolytic HGR is dependent on the concentration of available organic carbon, which is also intuitive given that the organic carbon is the expected fuel source for the hydrogen generation mechanisms present in caustic waste media.

3.5.2.2 Testing to Improve Thermolytic Model Equation

In addition to the nine IONAC-containing tests described above (P3-IAC-4, 4B, 4C, 5, 5B, 5C, 6, 6B, and 6D), four additional tests were performed to evaluate the validity of the interim IONAC model across the ranges of concentrations and temperatures applicable to CSTF waste.[19] These test conditions (including the three conditions (D, E, and F) identified above) were identical to those employed for glycolate and Xiameter model validations. The concentrations and temperatures used for these tests are given in Table 3-20. Observed HGR values, HGR expected from organic-free conditions, and the adjusted thermolytic HGRs are given in Table 3-21.

Table 3-20. HGR Test Conditions for IONAC Model Validation and Improvement.

Test Name	Al (M)	NO_2 (M)	NO_3 (M)	OH (M)	SO_4 (M)	CO_3 (M)	Na (M)	TOC (M)	Temp (°C)
P3-IAC-1	4.26E-03	1.24E+00	2.50E+00	5.57E+00	5.03E-02	1.95E-01	9.92E+00	2.33E-03	95
P3-IAC-2	3.30E-02	9.85E-01	1.27E-01	1.22E+01	5.22E-03	2.33E-02	1.47E+01	3.64E-03	73
P3-IAC-3	5.11E-02	4.54E-01	2.48E+00	5.99E+00	1.09E-01	1.46E-02	9.61E+00	3.63E-03	89
P3-IAC-4	1.12E-01	2.74E+00	3.13E+00	1.75E+00	2.28E-02	3.83E-01	8.48E+00	4.17E-03	100
P3-IAC-4B	1.05E-01	2.67E+00	3.21E+00	1.78E+00	2.24E-02	3.90E-01	8.96E+00	4.25E-03	100
P3-IAC-4C	1.05E-01	2.67E+00	3.21E+00	1.78E+00	2.24E-02	3.90E-01	8.96E+00	2.11E-03	100
P3-IAC-5	1.27E-01	4.11E-01	1.74E+00	2.30E+00	1.63E-01	1.66E-01	5.57E+00	4.34E-03	95
P3-IAC-5B	1.26E-01	3.93E-01	1.78E+00	2.21E+00	1.68E-01	1.62E-01	5.58E+00	4.32E-03	95
P3-IAC-5C	1.26E-01	3.93E-01	1.78E+00	2.21E+00	1.68E-01	1.62E-01	5.58E+00	2.14E-03	95
P3-IAC-6	3.93E-01	2.78E-01	3.47E+00	2.20E+00	1.96E-01	5.40E-01	8.35E+00	3.74E-03	109
P3-IAC-6B	4.01E-01	2.67E-01	3.48E+00	2.17E+00	1.93E-01	5.29E-01	8.36E+00	3.79E-03	109
P3-IAC-6C	4.01E-01	2.67E-01	3.48E+00	2.17E+00	1.93E-01	5.29E-01	8.36E+00	1.88E-03	109
P3-IAC-7	4.48E-01	2.28E+00	1.76E+00	7.30E+00	1.89E-02	7.13E-02	1.27E+01	4.41E-03	76

Table 3-21. HGR Test Results for IONAC Model Validation and Improvement.

Test Name	Observed HGR ($ft^3\ h^{-1}\ gal^{-1}$)	Predicted HGR from Blank (95% CL) ($ft^3\ h^{-1}\ gal^{-1}$)	Adjusted Thermolytic HGR ($ft^3\ h^{-1}\ gal^{-1}$)
P3-IAC-1	8.47E-07	1.62E-07	6.85E-07
P3-IAC-2	2.08E-07	3.30E-08	1.75E-07
P3-IAC-3	4.63E-07	9.03E-08	3.73E-07
P3-IAC-4	1.12E-06	1.35E-07	9.85E-07
P3-IAC-4B	1.17E-06	1.36E-07	1.03E-06
P3-IAC-4C	8.44E-07	1.36E-07	7.08E-07
P3-IAC-5	3.51E-07	5.33E-08	2.98E-07
P3-IAC-5B	3.83E-07	5.10E-08	3.32E-07
P3-IAC-5C	2.64E-07	5.10E-08	2.13E-07
P3-IAC-6	9.90E-07	9.08E-08	8.99E-07
P3-IAC-6B	7.83E-07	8.83E-08	6.95E-07
P3-IAC-6C	5.17E-07	8.83E-08	4.29E-07
P3-IAC-7	2.82E-07	9.51E-08	1.87E-07

The results from the 13 interim IONAC model validation tests are plotted against values predicted by the expression shown in Equation [24] in Figure 3-33.

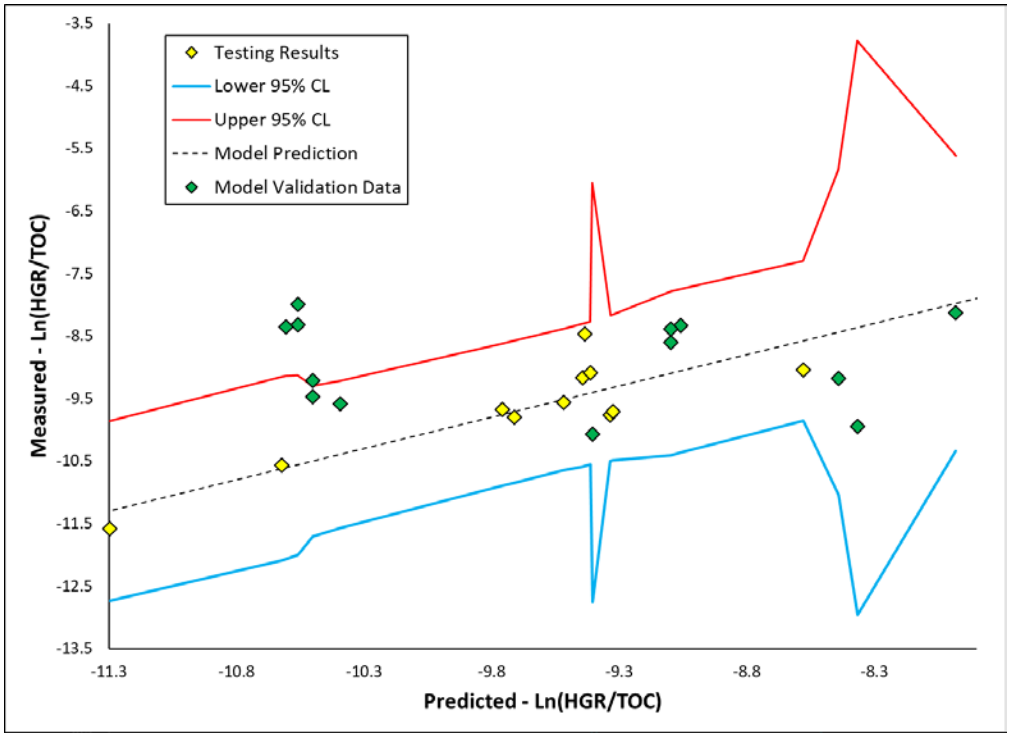

Figure 3-33. Plot of Measured HGRs from Model Generation (Yellow) and Validation (Green) Tests for IONAC vs. Predicted HGRs According to Interim Model Shown in Equation [24].

Upon inspection of the data shown in Figure 3-33, it seems that some of the validation data is not well described by the interim IONAC model. While most of the data from the validation set falls within the 95% confidence limit for a single measurement, test results from condition D (P3-IAC-4, P3-IAC-4B, and P3-IAC-4C) fall notably above the upper 95% confidence limit. Furthermore, model uncertainty around many of the validation points is relatively large, spanning several orders of magnitude at higher predicted rates. While an increase in uncertainty is expected at previously untested conditions, such large expansions in uncertainty upon extrapolation to other conditions are not desirable.

To generate a more robust model with less error, the results from the validation data set may be included during regression for the generation of an enhanced model. The revised IONAC model achieved through this regression is given in Equation [26].

$$\ln\left(\frac{HGR}{[C_{IAC}]}\right) = 14.123 + 0.542\ln[NO_3] + 1.065\ln[OH] - \frac{9151}{T} \qquad [26]$$

The HGR results of all IONAC testing are plotted against the enhanced model described in Equation [26] in Figure 3-34.

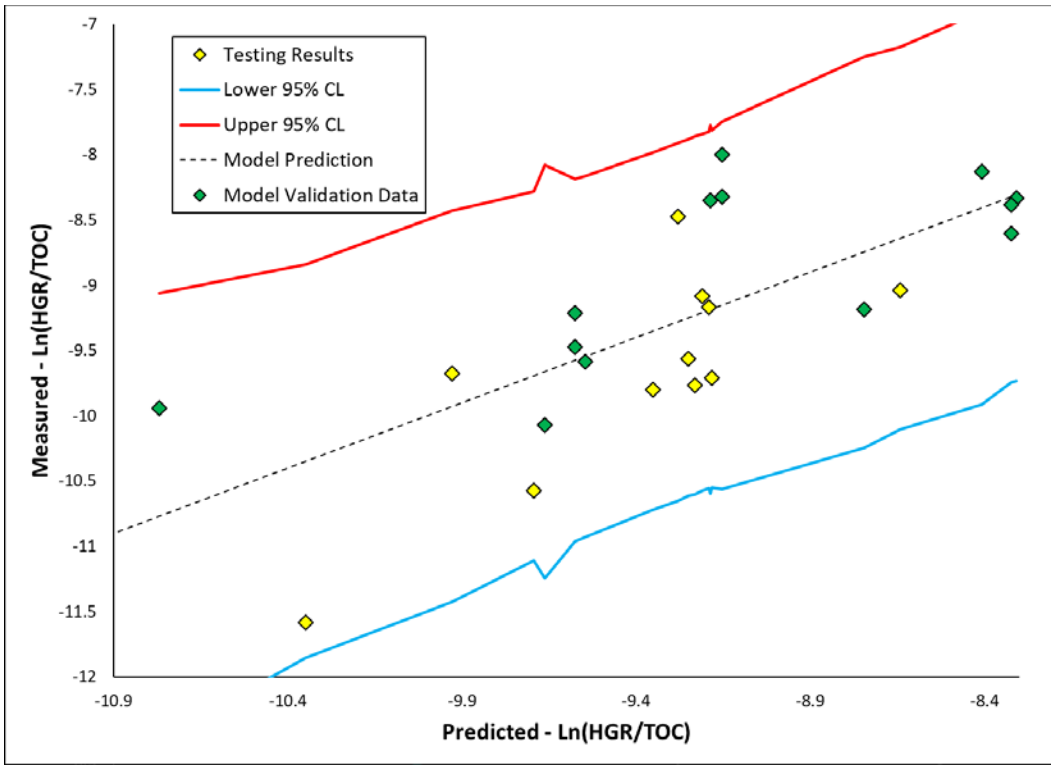

Figure 3-34. Plot of Measured HGRs from Model Generation (Yellow) and Validation (Green) Tests for IONAC vs. Predicted HGRs According to Final Model Shown in Equation [26].

The data plotted in Figure 3-34 suggest that the results from testing with IONAC digestion product material can be reasonably well bounded by the revised model given in Equation [26]. Furthermore, as was the case for the enhanced Xiameter model, the error around the validation data is greatly reduced in Figure 3-34 compared to that seen in Figure 3-33.

The linearized expression in Equation [26] may be simplified for ease of implementation. This transformed expression is given in Equation [27].

$$HGR_{IAC} = 1.361\times10^{6}\left[NO_3\right]^{0.542}\left[OH\right]^{1.065}\left[C_{IAC}\right]e^{-76{,}100/RT} \qquad [27]$$

Given that the model expression in Equation [27] is more robust than the interim model (Equation [25]), it is recommended to use Equation [27] to estimate the HGR attributable to digestion products from IONAC A-641 and similar ion exchange resins in CSTF caustic waste media.

3.6 Reillex HPQ Ion Exchange Resin

3.6.1 Model Generation Experiments

Ten Tank 38 variant experiments (RLX-1 through RLX-10), similar to those employed in Xiameter and IONAC model development, were performed to establish an interim model for thermolytic hydrogen generation due to the presence of digestion products from polyvinylpyridine-type resins, such as Reillex HPQ.[28] These experiments were performed by adding aliquots of Reillex HPQ digestion product material to 1 liter of Tank 38 variant simulant. Additionally, results from four previously-performed HGR experiments designed to support transfers of Reillex HPQ digestion product from H-Canyon to the SRS

CSTF (REI-3 through REI-6)[29] were incorporated into the model development data set. The species concentrations and conditions used during these tests are given in Table 3-22 and the observed, organic-free, and adjusted HGRs from each experiment are given in Table 3-23.

Table 3-22. HGR Test Conditions for Reillex HPQ Model Generation.

Test Name	Al (M)	NO_2 (M)	NO_3 (M)	OH (M)	SO_4 (M)	CO_3 (M)	Na (M)	TOC (M)	Temp (°C)
REI-3	1.18E-01	3.15E-01	1.98E+00	1.23E+00	N/A	N/A	3.53E+00	1.33E-04	100
REI-4	7.69E-01	2.58E+00	2.31E+00	7.41E+00	N/A	N/A	13.1E+01	1.33E-04	100
REI-5	1.18E-01	3.15E-01	1.98E+00	1.23E+00	N/A	N/A	3.53E+00	1.33E-04	80
REI-6	7.69E-01	2.58E+00	2.31E+00	7.41E+00	N/A	N/A	13.1E+01	1.33E-04	80
RLX-1	7.23E-02	2.39E+00	1.15E+00	2.61E+00	6.70E-02	6.63E-01	7.66E+00	6.29E-04	100
RLX-2	2.62E-01	2.30E+00	1.15E+00	2.49E+00	6.01E-02	6.36E-01	7.13E+00	6.23E-04	100
RLX-3	8.75E-02	1.28E+00	1.14E+00	2.54E+00	5.95E-02	6.43E-01	6.00E+00	6.23E-04	100
RLX-4	9.04E-02	2.35E+00	3.00E-01	2.61E+00	5.93E-02	6.49E-01	6.09E+00	6.29E-04	100
RLX-5	9.08E-02	2.35E+00	1.16E+00	1.73E+00	5.93E-02	6.53E-01	6.09E+00	6.37E-04	100
RLX-6	9.08E-02	2.52E+00	1.17E+00	2.78E+00	2.36E-02	5.99E-01	8.53E+00	6.30E-04	100
RLX-7	8.64E-02	2.50E+00	1.23E+00	2.80E+00	6.26E-02	2.00E-01	7.74E+00	6.27E-04	100
RLX-8	7.34E-02	2.50E+00	1.19E+00	2.68E+00	7.02E-02	6.79E-01	7.83E+00	3.14E-04	100
RLX-9	9.12E-02	2.56E+00	1.18E+00	2.82E+00	6.50E-02	6.09E-01	8.53E+00	6.40E-04	85
RLX-10	8.89E-02	2.37E+00	1.16E+00	2.75E+00	6.13E-02	5.89E-01	8.18E+00	6.28E-04	110

Table 3-23. HGR Test Results for Reillex HPQ Model Generation.

Test Name	Observed HGR ($ft^3\ h^{-1}\ gal^{-1}$)	Predicted HGR from Blank (95% CL) ($ft^3\ h^{-1}\ gal^{-1}$)	Adjusted Thermolytic HGR ($ft^3\ h^{-1}\ gal^{-1}$)
REI-3	5.0E-07	6.6E-08	4.34E-07
REI-4	3.6E-06	5.5E-07	3.05E-06
REI-5	2.8E-07	9.2E-08	1.88E-07
REI-6	9.2E-07	6.4E-07	8.56E-07
RLX-1	1.44E-06	1.25E-07	1.32E-06
RLX-2	3.00E-06	1.19E-07	2.88E-06
RLX-3	1.86E-06	9.75E-08	1.76E-06
RLX-4	1.13E-06	7.21E-08	1.06E-06
RLX-5	1.15E-06	9.10E-08	1.06E-06
RLX-6	1.27E-06	1.33E-07	1.14E-06
RLX-7	8.24E-07	1.36E-07	6.88E-07
RLX-8	8.60E-07	1.30E-07	7.30E-07
RLX-9	8.27E-07	7.29E-08	7.54E-07
RLX-10	1.85E-06	1.84E-07	1.67E-06

The results from Table 3-23 were linearly regressed against the condition inputs given in Table 3-22 to generate an interim model for thermolytic HGR from polyvinylpyridine-based resin digestion products. The best-fit model achieved from this step-wise regression is given in Equation [28].

$$\ln\left(\frac{HGR}{[C_{RLX}]}\right) = 9.835 + 0.984\ln[Al] - \frac{5098}{T} \quad [28]$$

The simplified version of the model given in Equation [28] is shown in Equation [29].

$$HGR_{RLX} = 1.868\times10^{4}[Al]^{0.984}[C_{RLX}]e^{-42{,}400/RT} \quad [29]$$

The interim model for thermolytic HGR from Reillex digestion material (given in Equation [29]) suggests that aluminum may have the greatest influence on the production rate of hydrogen. This result is markedly different from the observations of previously-developed interim models for Xiameter and IONAC organics, both of which suggested a strong impact from free hydroxide. The results from Reillex interim model generation testing are plotted against the model fit given in Equation [28] in Figure 3-35.

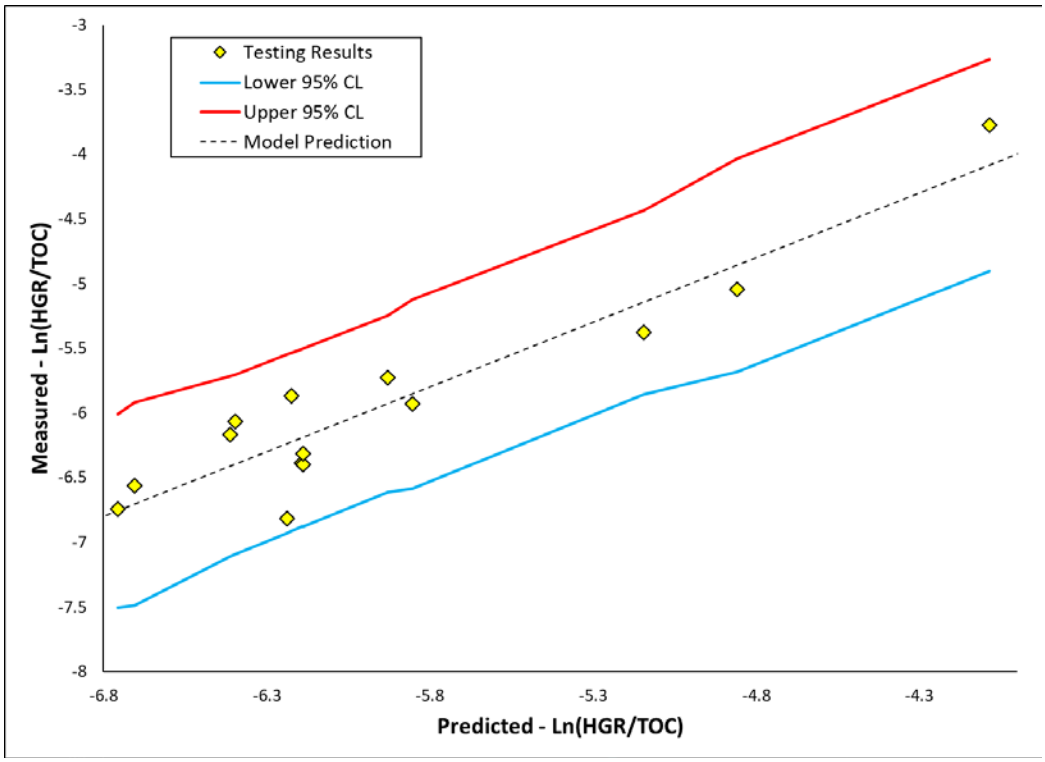

Figure 3-35. Plot of Measured HGRs from Model Generation Tests for Reillex vs. Predicted HGRs According to Interim Model Shown in Equation [28].

The data shown in Figure 3-35 suggest that the results from Reillex interim model generation testing are reasonably well-described by the best-fit model given in Equation [28]. This model is evaluated against additional data points later in this report.

3.6.2 Model Validation Experiments

Seven experiments were performed to assess the applicability of the interim Reillex model (Equation [29]) across the ranges of concentrations and temperatures possible in the CSTF.[19] The conditions in these tests are identical to those used to validate or refute the glycolate, Xiameter, and IONAC interim models. The concentrations and temperatures used in these tests are listed in Table 3-24. The observed HGR values from these experiments, as well as the expected contribution from organic-free conditions and the adjusted thermolytic HGRs for each condition are reported in Table 3-25.

Table 3-24. HGR Test Conditions for Reillex Model Validation and Improvement.

Test Name	Al (M)	NO_2 (M)	NO_3 (M)	OH (M)	SO_4 (M)	CO_3 (M)	Na (M)	TOC (M)	Temp. (°C)
P3-RLX-1	5.37E-03	1.15E+00	2.53E+00	5.57E+00	6.00E-02	1.99E-01	1.01E+01	3.48E-04	95
P3-RLX-2	3.35E-02	8.93E-01	1.33E-01	1.18E+01	5.96E-03	3.29E-02	1.14E+01	3.16E-04	73
P3-RLX-3	5.11E-02	4.30E-01	2.66E+00	6.02E+00	1.12E-01	1.42E-02	9.70E+00	2.79E-04	89
P3-RLX-4	1.01E-01	2.54E+00	3.23E+00	1.78E+00	2.20E-02	3.83E-01	9.18E+00	5.10E-04	100
P3-RLX-5	1.32E-01	3.93E-01	1.87E+00	2.19E+00	1.78E-01	1.68E-01	5.83E+00	4.98E-04	95
P3-RLX-6	4.15E-01	2.72E-01	3.69E+00	2.15E+00	1.55E-01	5.30E-01	8.44E+00	5.53E-04	109
P3-RLX-7	3.97E-01	1.93E+00	2.10E+00	6.91E+00	1.28E-02	1.11E-01	1.14E+01	2.10E-04	76

Table 3-25. HGR Test Results for Reillex Model Validation and Improvement.

Test Name	Observed HGR ($ft^3\ h^{-1}\ gal^{-1}$)	Predicted HGR from Blank (95% CL) ($ft^3\ h^{-1}\ gal^{-1}$)	Adjusted Thermolytic HGR ($ft^3\ h^{-1}\ gal^{-1}$)
P3-RLX-1	1.65E-06	1.59E-07	1.49E-06
P3-RLX-2	1.15E-06	3.18E-08	1.12E-06
P3-RLX-3	9.53E-07	9.01E-08	8.63E-07
P3-RLX-4	5.69E-07	1.34E-07	4.35E-07
P3-RLX-5	5.75E-07	5.15E-08	5.24E-07
P3-RLX-6	9.97E-07	9.01E-08	9.07E-07
P3-RLX-7	4.39E-07	9.18E-08	3.47E-07

The results from the seven interim Reillex model validation tests are plotted against values predicted by the expression shown in Equation [28] in Figure 3-36.

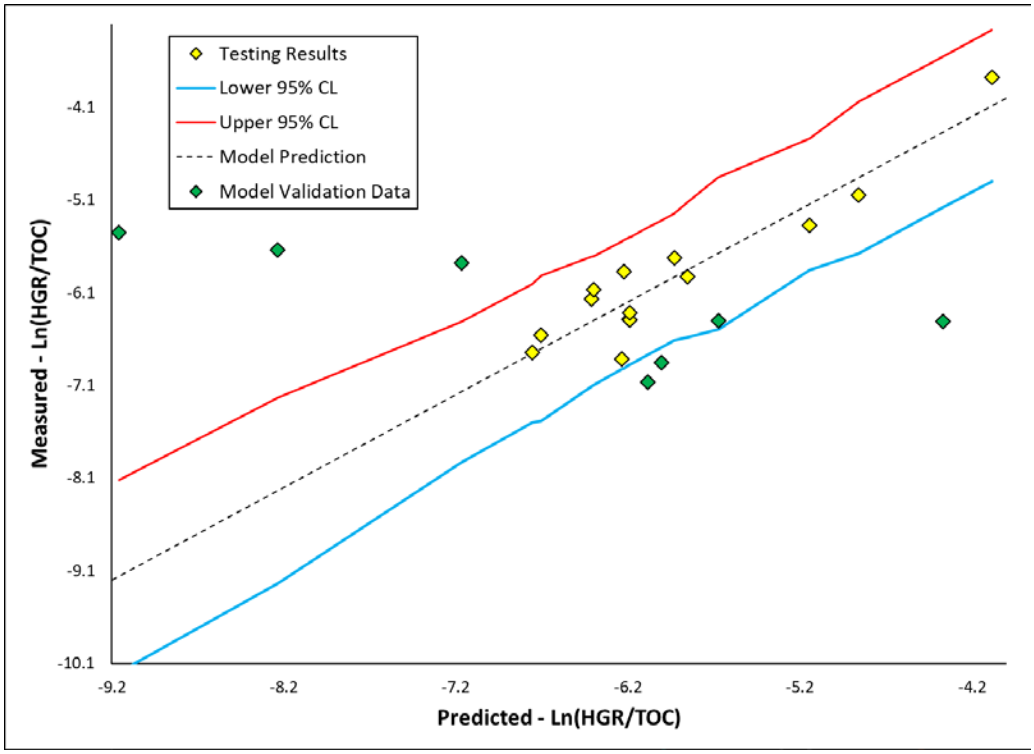

Figure 3-36. Plot of Measured HGRs from Model Generation (Yellow) and Validation (Green) Tests for Reillex vs. Predicted HGRs According to Interim Model Shown in Equation [28].

The data shown in Figure 3-36 suggests that the Reillex interim model validation tests are not well-described by the interim model given in Equation [28]. Only one of the seven validation tests fall within the 95% confidence limit for a single prediction. While three of the outliers fall below the lower confidence limit (suggesting that the condition is well-bound by the model, if not well-described), the other three outliers fall well above the upper 95% confidence limit and represent a significant short-coming of the interim Reillex model. As has been seen previously, some of the validation data points exhibit a higher degree of uncertainty than the model generation data set. This behavior is consistent with the extrapolation of model predictions from the model generation regime (Tank 38 and variants) to the model validation regime (total CSTF concentration ranges).

The validation data set may be included in the linear regression to improve the quality and robustness of the Reillex HGR model. The enhanced model achieved by including the validation data set in the linear regression is given in Equation [30].

$$\ln\left(\frac{HGR}{[C_{RLX}]}\right) = 2.096 + 0.891\ln[OH] - \frac{3363}{T} \qquad [30]$$

The HGR results of all Reillex testing are plotted against the enhanced Reillex model described in Equation [30] in Figure 3-37.

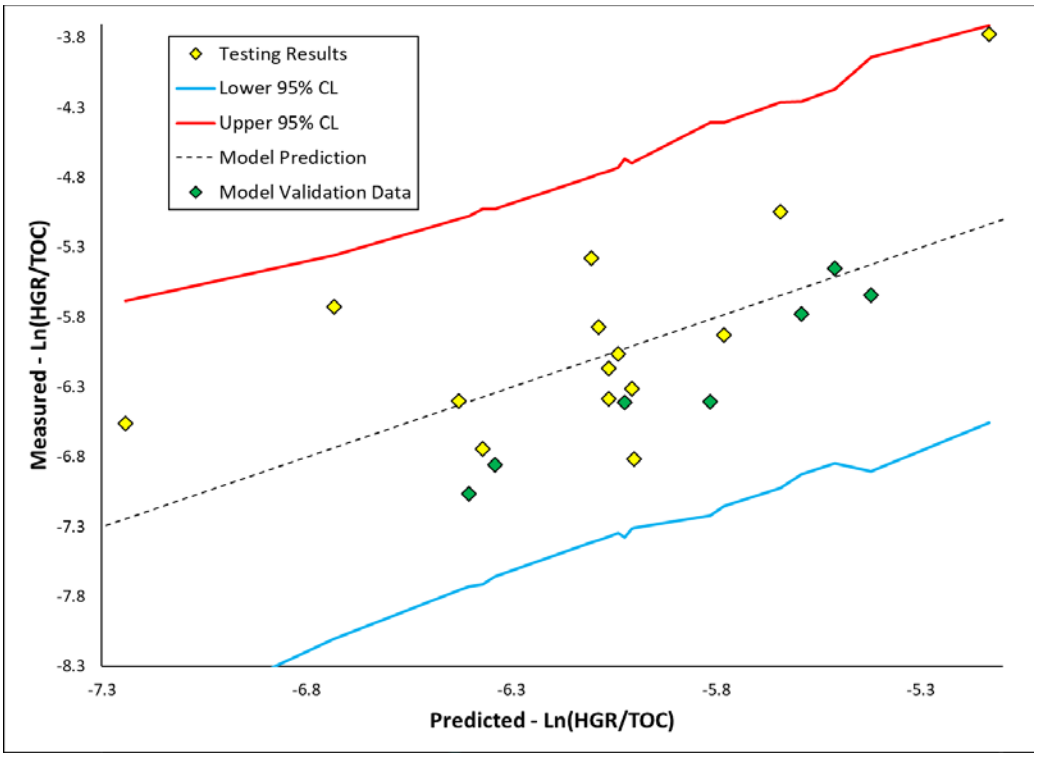

Figure 3-37. Plot of Measured HGRs from Model Generation (Yellow) and Validation (Green) Tests for Reillex vs. Predicted HGRs According to Final Model Shown in Equation [30].

The results plotted in Figure 3-37 show that the majority of testing with Reillex HPQ resin digestion product material are generally well-described by the model expression given in Equation [30]. All the original model generation data and the validation data sets fall within the 95% confidence limit for a single prediction.

The linearized model presented in Equation [30] is transformed for ease of implementation in Equation [31].

$$HGR_{RLX} = 8.134 \times [OH]^{0.891} [C_{RLX}] e^{-27{,}900/RT} \quad [31]$$

Given the improved fitting and robustness available with the revised model, it is recommended to use the expression given in Equation [31] to estimate the thermolytic HGR from the digestion products of Reillex HPQ and similar polyvinylpyridine-based resins in CSTF caustic waste media.

3.7 Propanal

An HGR test in Tank 38 simulant with 100 ppm of propanal added at 100 °C (identified as test PRO-1) was performed to evaluate the thermolytic potential of propanal and similar aldehydes. The concentrations of chemical species and temperature used in PRO-1 are given in Table 3-26.

Table 3-26. Concentrations and Conditions from Test PRO-1.

Parameter	Measured Value
Aluminum Concentration (M)	7.71E-02
Nitrite Concentration (M)	2.56E+00
Nitrate Concentration (M)	1.20E+00
Free Hydroxide Concentration (M)	2.70E+00
Sulfate Concentration (M)	7.14E-02
Carbonate Concentration (M)	7.19E-01
TOC from Propanal (M)	5.36E-03 (~100 ppm propanal)
Temperature (°C)	100

The results of this experiment are given in Figure 3-38.

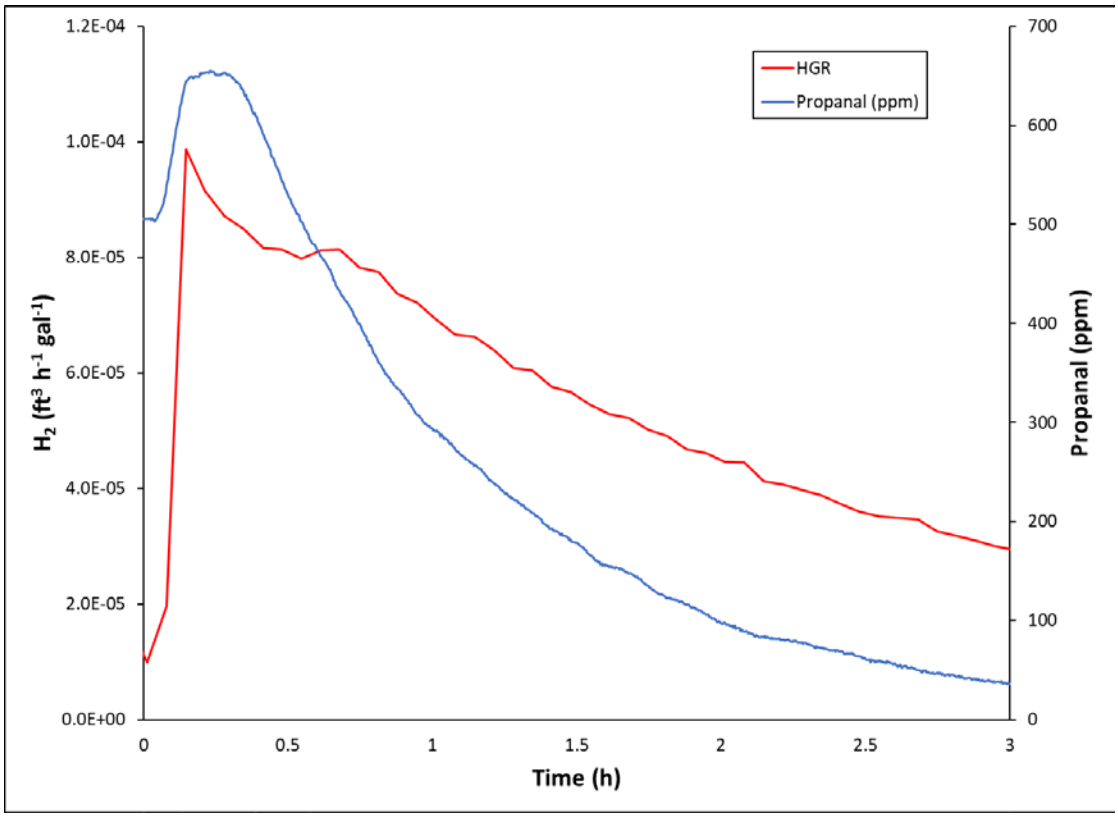

Figure 3-38. HGR and Propanal Offgas Results from PRO-1.

The data shown in Figure 3-38 reveal a few important observations. First, it is clear that the production rates of hydrogen from propanal greatly exceed those observed from other organics on a per-gram basis, reaching as high as 1.0×10^{-4} ft^3 h^{-1} gal^{-1} from 100 ppm of propanal. Second, a drastic decrease in HGR is observed over the course of three hours, diminishing by over an order of magnitude. The root of this decrease may be deduced from a third observation: the apparent presence (and time-dependent concentration) of propanal in the headspace. Following addition to the 100 °C Tank 38 simulant, the vapor-phase concentration of propanal immediately increases to over 600 ppm. Within 3 hours, the concentration of propanal in the vapor phase decreases to less than 50 ppm. The appearance and subsequent decrease of propanal in the vessel headspace suggest that propanal is easily lost to evaporation at a rate that rapidly

alters the liquid phase concentration of propanal. This is consistent with the relatively low atmospheric boiling point of propanal (48.8 °C).

Given the underlying assumptions used in the design of the HGR measurement apparatus used in this testing, the rapid decrease of liquid-phase propanal (due to both evaporation and thermolytic reaction) necessitates a modification in experimental design to accurately assess HGRs. Nine additional propanal HGR experiments were performed at variations of Tank 38 conditions, similar to those tests performed for Xiameter, IONAC, and Reillex model generation experiments.[28] These tests were performed by charging propanal to cooled simulant and mixing before heat is applied to maximize solubility and minimize loss from immediate evaporation. Tests PRO-2 through PRO-7 were performed by varying the loadings of salt species at 100 °C in the presence of 100 ppm of propanal. Test PRO-8 was performed by decreasing the propanal concentration to 50 ppm in Tank 38 simulant at 100 °C. Tests PRO-9 and PRO-10 were performed by measuring the HGR from 100 ppm of propanal in Tank 38 simulant at 85 °C and 70 °C, respectively. The concentrations and conditions employed in Tests PRO-2 through PRO-9 are listed in Table 3-27.

Table 3-27. Concentrations and Conditions from Tests PRO-2 Through PRO-10.

Test Name	Al (M)	NO_2 (M)	NO_3 (M)	OH (M)	SO_4 (M)	CO_3 (M)	TOC (M)	Temp (°C)
PRO-2	2.39E-01	2.50E+00	1.15E+00	2.64E+00	7.02E-02	6.86E-01	5.18E-03	100
PRO-3	7.78E-02	1.48E+00	1.16E+00	2.64E+00	7.02E-02	6.89E-01	5.33E-03	100
PRO-4	7.38E-02	2.48E+00	2.35E-01	2.63E+00	6.93E-02	6.79E-01	5.16E-03	100
PRO-5	7.82E-02	2.50E+00	1.15E+00	1.76E+00	7.04E-02	6.83E-01	5.29E-03	100
PRO-6	8.93E-02	2.41E+00	1.13E+00	2.84E+00	2.25E-02	6.16E-01	5.34E-03	100
PRO-7	9.38E-02	2.41E+00	1.16E+00	2.58E+00	5.84E-02	2.11E-01	5.25E-03	100
PRO-8	7.56E-02	2.63E+00	1.22E+00	2.77E+00	7.18E-02	7.19E-01	2.64E-03	100
PRO-9	7.67E-02	2.63E+00	1.21E+00	2.99E+00	7.15E-02	7.06E-01	5.26E-03	85
PRO-10	8.56E-02	2.24E+00	1.07E+00	2.85E+00	5.59E-02	1.14E+00	5.22E-03	70

HGR results for tests PRO-2 through PRO-7 are given in Figure 3-39.

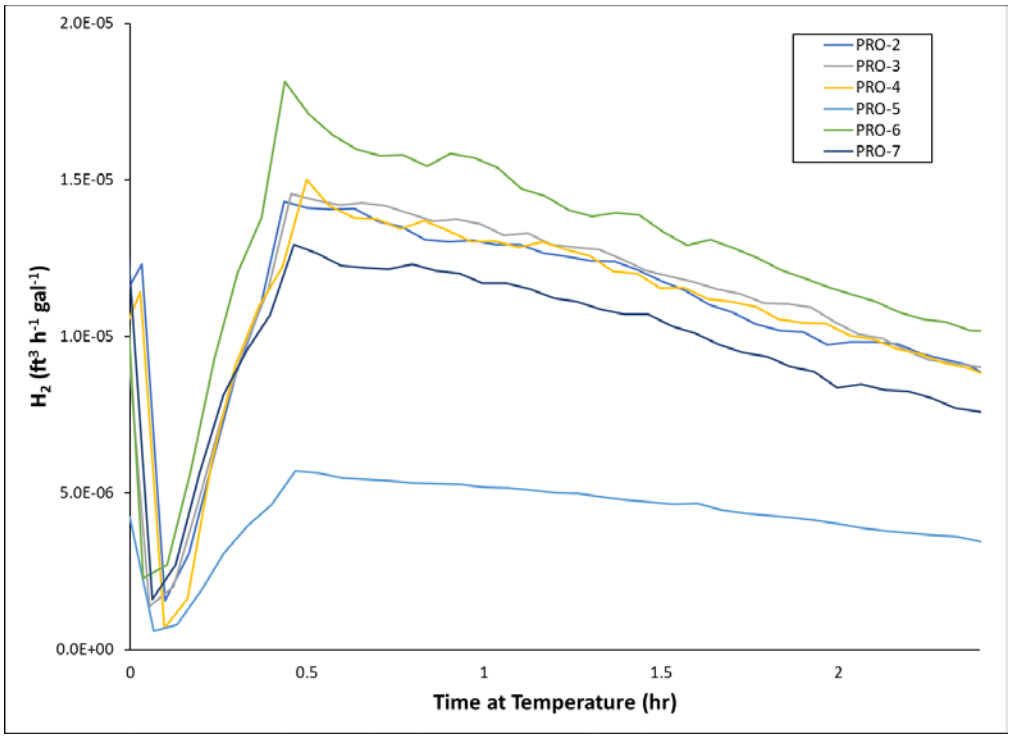

Figure 3-39. Impacts of Salt Species Concentrations on Propanal HGR.

The results in Figure 3-39 show that, except for hydroxide, changes in salt concentrations generally have little impact on thermolytic HGR from propanal. Results from PRO-2, 3, 4, 6, and 7 follow the same general trend, peaking at approximately 1.5×10^{-5} ft^3 h^{-1} gal^{-1} and rapidly decreasing to approximately 1.0×10^{-5} ft^3 h^{-1} gal^{-1} within three hours. However, results from PRO-5 (decreased hydroxide) exhibit a notably lower peak HGR (approximately 5×10^{-6} ft^3 h^{-1} gal^{-1}). These results suggest that changes in free hydroxide concentration have the greatest impact in thermolytic HGR from propanal.

Results from PRO-8 (50 ppm of propanal) are shown in Figure 3-40. The region of HGR observed in PRO-2, 3, 4, 6, and 7 (100 ppm of propanal) are shown for reference (red region enclosed by black lines).

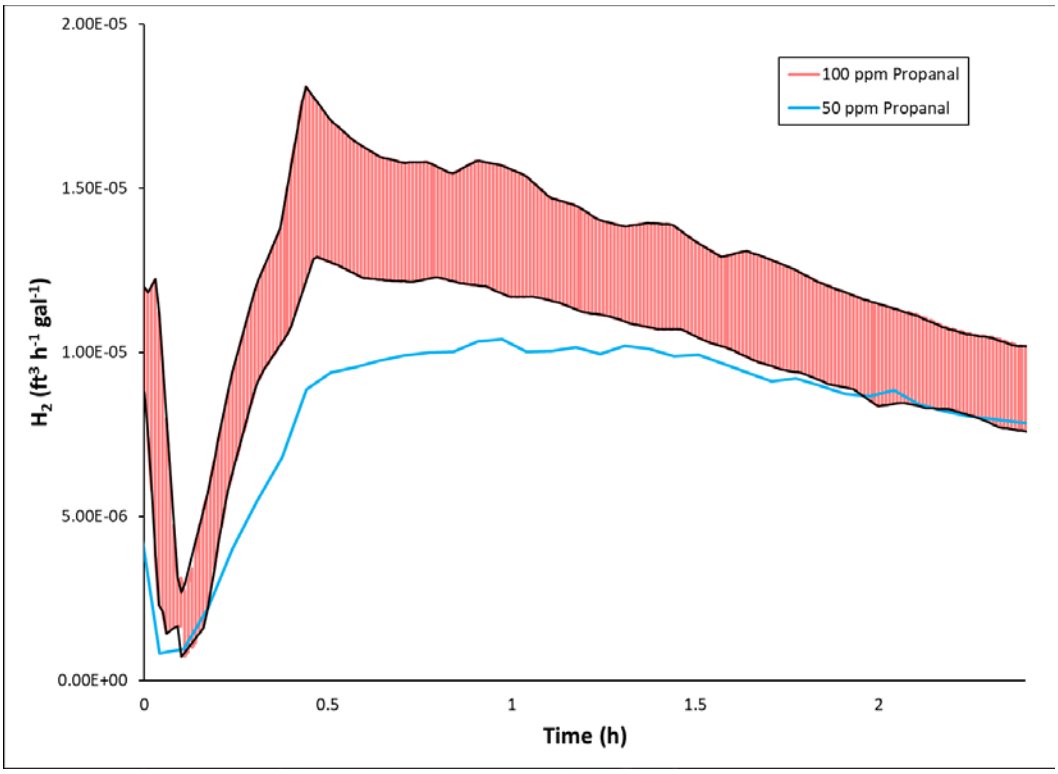

Figure 3-40. Impacts of Organic Carbon Concentration on Propanal HGR.

Results from Figure 3-40 suggest that a decrease in propanal concentration has a noticeable impact on HGR. This result is intuitive, given that propanal is the initiating reagent for hydrogen production. It should be noted that a decrease in initial liquid-phase propanal concentration would be expected to lead to a decreased rate of thermolytic hydrogen production as well as a decreased rate of propanal evaporation. This difference in effective rates of propanal disappearance would naturally be expected to have significant impacts on the time-dependent behavior of propanal thermolysis, making quantitative comparison difficult.

Results from tests PRO-9 (85 °C) and PRO-10 (70 °C) are given in Figure 3-41. HGR ranges experienced in tests PRO-2, 3, 4, 6, and 7 (100 °C) are also shown for reference.

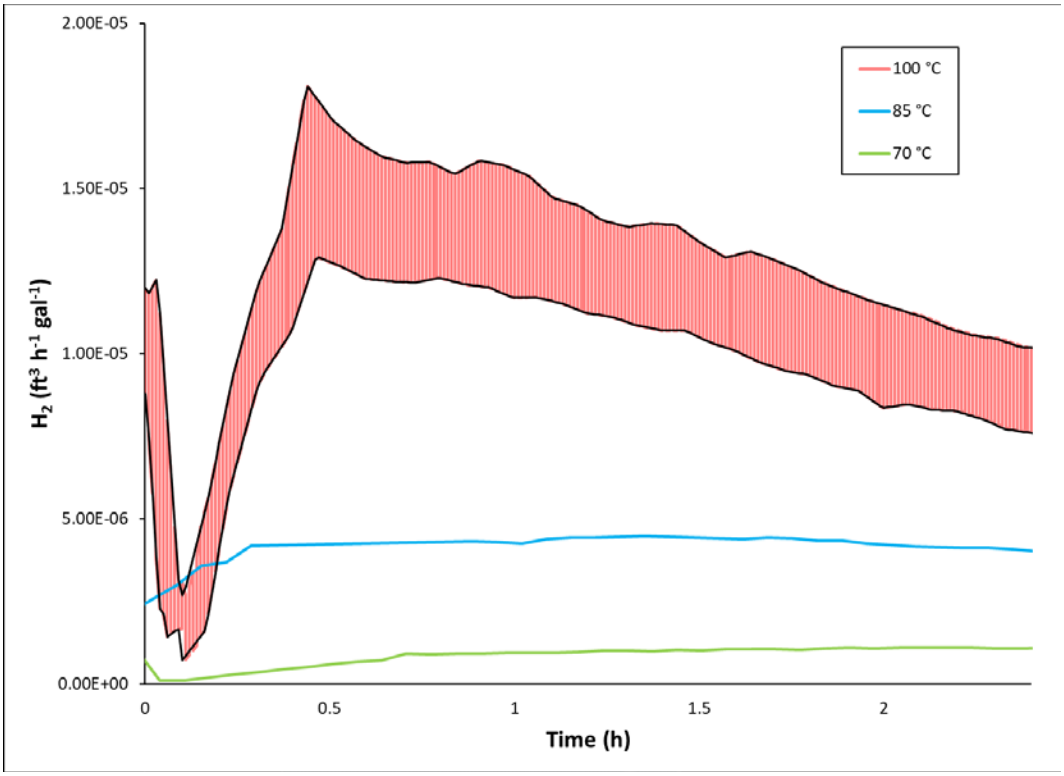

Figure 3-41. Impacts of Temperature on Propanal HGR.

Data in Figure 3-41 suggest that thermolytic production of hydrogen from propanal is strongly influenced by temperature. Testing with 100 ppm of propanal in Tank 38 simulant at 85 °C (PRO-9) yields an HGR of approximately 5×10^{-6} ft^3 h^{-1} gal^{-1}, three times less than the peak HGRs observed from testing at 100 °C. Furthermore, testing at 70 °C yields a significantly lower HGR, reaching approximately 1×10^{-6} ft^3 h^{-1} gal^{-1}. This observation is consistent with the concept of thermolytic production of hydrogen. It should be noted here that, similar to effects from changes in initial organic concentrations, changes in temperature affect both the thermolytic production rates of hydrogen as well as the evaporation rates of propanal. It is therefore difficult to obtain quantitative information describing the influence of temperature on HGR.

The observations that organic concentration, hydroxide concentration, and temperature are the most influential drivers for the thermolytic production of hydrogen from propanal is consistent with the Cannizzaro-type reaction mechanism outlined in Figure 3-21. A reaction expression consistent with the Cannizzaro mechanism is given in Equation [32] as a proposed basis for an HGR due to propanal thermolysis.

$$HGR_{PRO} = k_1\left[C_{PRO}\right]\left[OH\right]e^{-E_1/RT} + k_2\left[C_{PRO}\right]\left[OH\right]^2 e^{-E_2/RT} \qquad [32]$$

It is conceivable that dynamic reaction data from experiments PRO-2 through PRO-10 may be used to calculate the values of k_1, k_2, E_1, and E_2. If a quantitative model for propanal thermolysis is desirable, it is recommended to use the model expression shown in Equation [32] to regress reaction parameters from PRO-2 through PRO-10 HGR results.

Samples were drawn from the products of each test with propanal and submitted for Volatile Organic Analysis (VOA) to determine the amount of propanal lost at each condition. Results from these analyses are given in Table 3-28.

Table 3-28. Changes in Propanal Concentration During Propanal Testing.

Test Name	Propanal Concentration In Feed (mg/L)	Volatile Organic Analyte In Product (mg/L)	Change in Concentration (%)
PRO-1	104	<0.25	>99.76
PRO-2	100	<0.25	>99.75
PRO-3	103	<0.25	>99.76
PRO-4	100	<0.25	>99.75
PRO-5	102	<0.25	>99.75
PRO-6	103	---	---
PRO-7	102	<0.25	>99.75
PRO-8	51	<0.25	>99.51
PRO-9	102	<0.25	>99.75
PRO-10	101	---	---

The results presented in Table 3-28 suggest that effectively no propanal remains in simulant mixtures when subjected to temperatures of 85 °C or higher for 3 or more hours. This observation suggests that solutions with propanal concentrations of 50 ppm or less would lose effectively all its propanal after a single pass through a CSTF evaporator. Given this observation as well as the fact that propanal is introduced to the CSTF at concentrations typically much less than 50 ppm in very dilute recycle streams from DWPF, it may be assumed that propanal is not capable of concentrating to appreciable levels in CSTF waste and should not be considered when evaluating the buildup of hydrogen from thermolysis in CSTF waste tanks.

3.8 Synergistic Interactions of Organic Molecules

Until now, only contributions from individual organic species to HGR have been considered. No assessment has been made as to the presence or influence of synergistic interactions when multiple organics are present (such as in CSTF waste media). The assumptions made thus far are that the total HGR attributable to organic thermolysis is equal to the sum of the contributions from each individual species, as shown in Equation [33].

$$HGR_{total} = HGR_{Gly} + HGR_{RLX} + \ldots = \sum_i HGR_i \quad [33]$$

Equation [33] may be rearranged to state a hypothesis that may be used to test for the presence of synergistic effects on thermolytic HGR is caustic waste media, as shown in Equation [34].

$$HGR_{total} - \sum_i HGR_i = \Delta \leq 0 \quad [34]$$

To evaluate this hypothesis, an experiment may be performed in which all relevant organic species are added to a single reaction mixture in amounts capable of producing hydrogen. The HGR from this "combined organic" test (HGR_{total}) may then be evaluated against the measured HGRs from tests where each organic was added individually at an identical concentration to an identical mixture at the same

temperature (HGR_i). The measured HGR from each organic may then be summed together ($\sum_i HGR_i$) and subtracted from the combined organic test result to calculate the observed difference (Δ). According to the expression given in Equation [34], three possibilities arise from this comparison:

1. The value of Δ is calculated to be a positive number, indicating an apparent synergistic interaction from combining multiple organic species,
2. The value of Δ is calculated to be 0, indicating no net effect from combining multiple organic species, or
3. The value of Δ is calculated to be a negative number, indicating an apparent antagonistic interaction from combining multiple organic species.

Four conditions from the seven validation tests performed for each organic described above were identified to screen for any sign of synergistic interactions: P3-YYY-3 (Condition C), P3-YYY-4 (Condition D), P3-YYY-5 (Condition E), and P3-YYY-6 (Condition F).[19] These conditions were used to perform four additional tests (designated as YYY = "ALL" tests) where all organic species were added to the same concentrations employed in validation testing.

The results from test P3-ALL-3 are shown in Figure 3-42. For comparison, the results from P3-RLX-3, P3-XIA-3, P3-GLY-3, and P3-IAC-3 are also shown. Additionally, the mathematical sum of the HGRs measured from each of the individual organic tests is shown (in red).

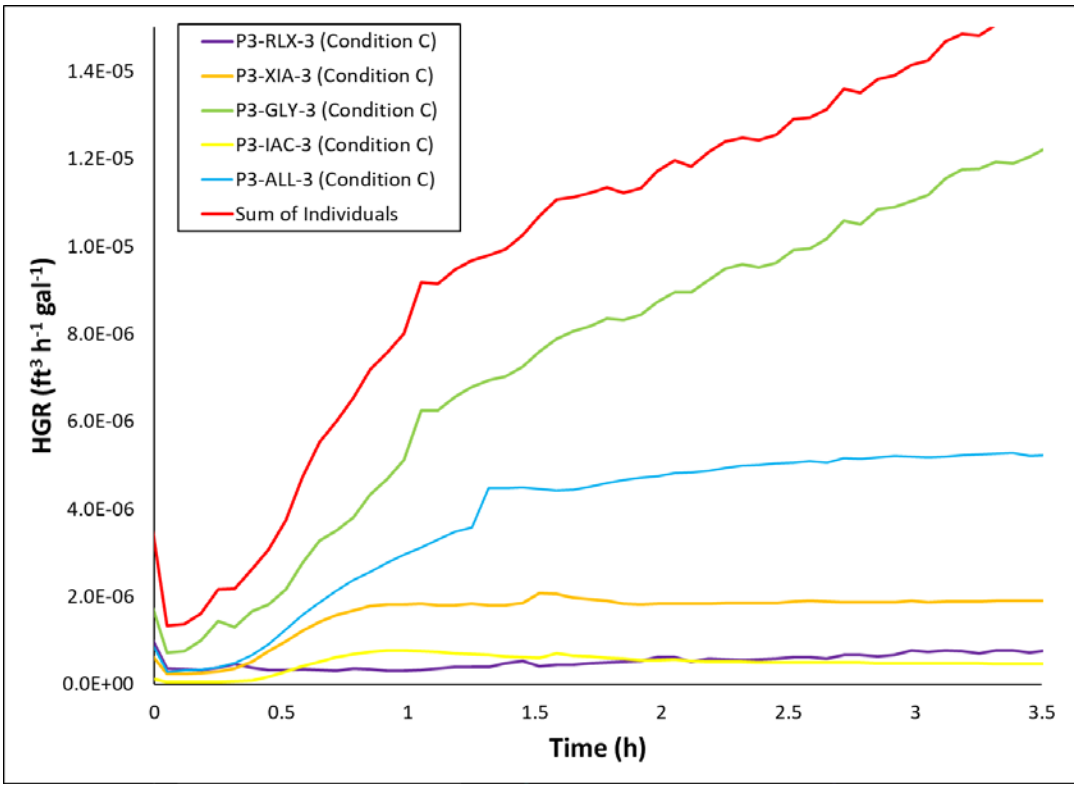

Figure 3-42. Results from Individual and Combined Organics Testing at Condition C.

The data shown in Figure 3-42 suggest that antagonistic effects ($\Delta < 0$) are present at the concentrations and temperature employed at Condition C, exhibited by the greater HGR expected by summation of individual organic results (compared to the observed HGR seen in the ALL test).

It is interesting to note that the observed HGR from the P3-ALL-3 test is not only lower than the value expected by summing the individual organic tests but is also lower than the HGR observed from glycolate as an individual species. Given that the glycolate concentrations, salt species compositions, and temperatures are the same in these experiments, it may be assumed that glycolate specifically experienced antagonistic effects when combined with the other organic species present in the ALL test.

It is hypothesized that the basis for this antagonistic interaction is the known tendency of glycolate HGR to be diminished in the presence of oxidizing solids. Glycolate HGR has been observed to be significantly decreased by the addition of sludge solids (as seen in Tank 38 screening experiments described in Section 3.3.4.1). A similar behavior may be expected when resin digestion byproducts (e.g., MnO_2 solids from permanganate oxidation of resin) are added along with glycolate. Given that glycolate is the greatest hydrogen producer in Condition C (by approximately an order of magnitude), it is reasonable to assume that glycolate oxidation by MnO_2 would have a significant impact on the observed HGR when all organics are present.

Results from similar tests at Condition D are shown in Figure 3-43.

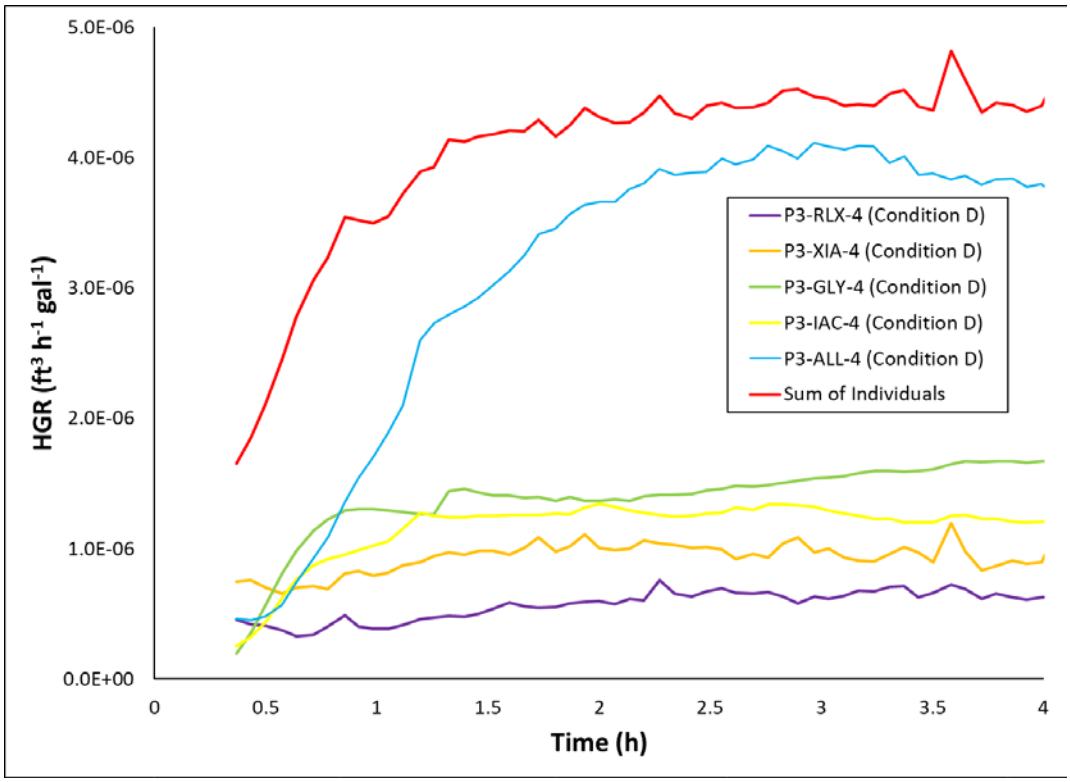

Figure 3-43. Results from Individual and Combined Organics Testing at Condition D.

Results from Figure 3-43 suggest a value of Δ slightly less than zero at Condition D. This result indicates a lack of synergistic interaction between glycolate, Xiameter AFE-1010, IONAC A-641 digestion products, and Reillex HPQ digestion products at any appreciable level. Note further that, while there is an apparent

decrease in HGR from the expected summation of individual contributors to that observed in the combined organics test, it cannot be determined what species, if any, are being antagonized in this mixture.

Results from additional combined organics testing at Condition E are shown in Figure 3-44.

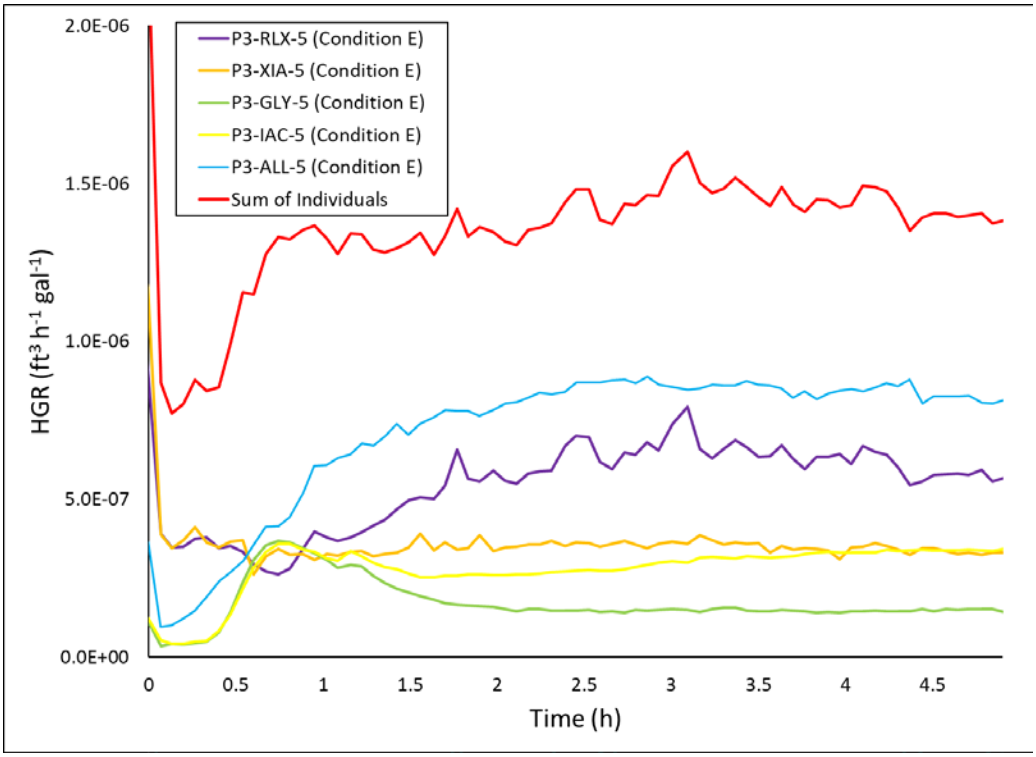

Figure 3-44. Results from Individual and Combined Organics Testing at Condition E.

Results from Figure 3-44 suggest a value of Δ less than zero at Condition E. This result indicates apparent antagonistic interaction between the added organic species at this composition and temperature. As was the case with Condition D, it is impossible to determine the source of the antagonistic interaction in Condition E based on the data in Figure 3-44 alone. However, it should be observed that the glycolate contribution (as expected based on results from P3-GLY-5) is smaller than the observed gap between the observed combined organics test and the expected summation value. This observation leads to the conclusion that MnO_2 oxidation of glycolate alone does not account for the observed antagonistic interactions at Condition E.

Results from the final combined organics test (Condition F) are shown in Figure 3-45.

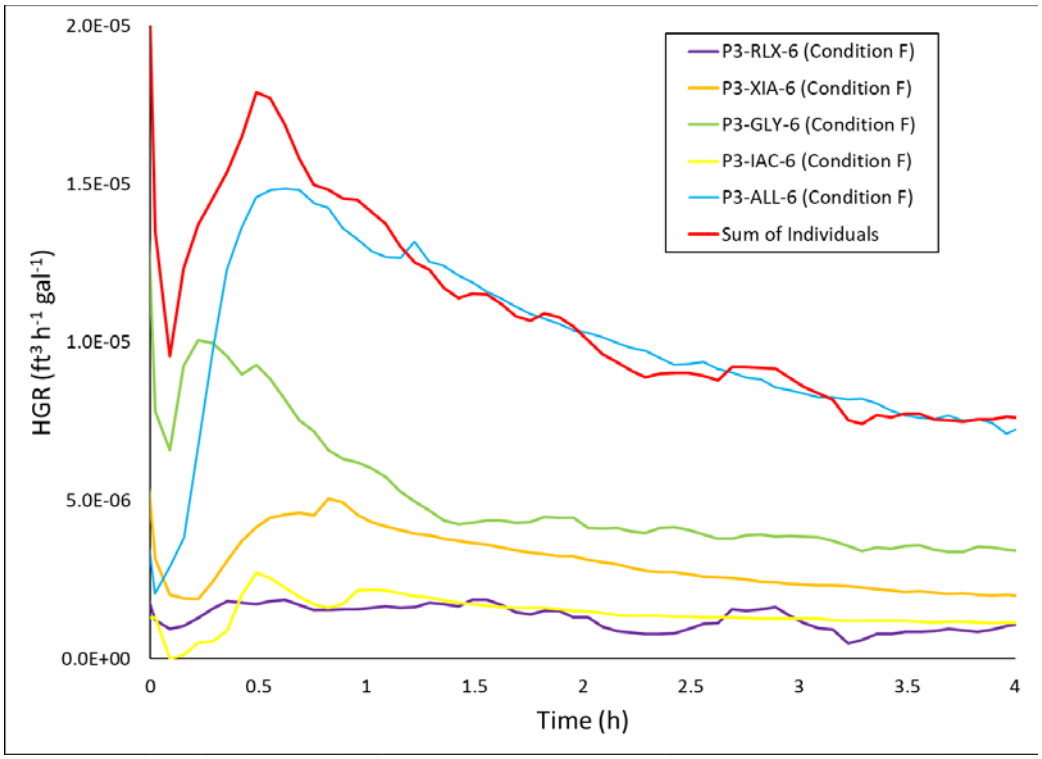

Figure 3-45. Results from Individual and Combined Organics Testing at Condition F.

Results from Figure 3-45 suggest of value of Δ very nearly equal to zero, suggesting that there is no observable effect from combining multiple organic species at Condition F.

It must be noted that the generation of CH_4 gas (approximately 30 ppm) was observed during the P3-ALL-6 test. This concentration corresponds to a methane generation rate of approximately 1.2×10^{-6} ft^3 h^{-1} gal^{-1}. Given that CH_4 was not detected in other P3-XXX-6 tests, it is unclear at this stage if the methane generation is due to the presence of multiple compounds capable of producing CH_4 at levels below our detection limit or if this phenomenon is due to some synergistic chemical interaction. While these combined organics tests are not representative of organics loadings in tanks within the CSTF, it is recommended that the generation rates of CH_4 be further studied to assess the potential generation rates in SRS waste.

The observations from testing at Conditions C, D, E, and F suggest that there are no synergistic effects on the HGR when combining reactive organic compounds in caustic waste media. Rather, there are signs of antagonistic effects in two of the four cases studies. This implies that an additive HGR model (such as that shown in Equation [33]) tends to be an accurate prediction of organic behavior in caustic media or to overpredict the HGR that would be observed. Given that conservative approximations are often preferred for the sake of preventing flammable build-up of hydrogen, it is recommended to retain an additive model rather than credit the apparent synergy observed in some cases. It is also recommended to assume no synergistic interactions are occurring, as none were identified during testing and none of relevance have been identified in the literature.

3.9 Generation of a Global TOC HGR Model

While the models generated in previous sections were developed across a wide variety of simulant compositions and temperatures, it should be noted that these models would, at best, only be expected to apply to cases where identical or similar organic species are employed (e.g., the final Xiameter model would

not necessarily be expected to adequately describe the HGR from tanks rich in resin digestion products, but may be adequate to describe the HGR from tanks rich in siloxane-based antifoaming agents). Rather, a global, TOC-based HGR model would be preferable to model equations developed for special cases of organics, where the thermolytic HGR attributable to organic compounds can be estimated regardless of species. Given the observation that each of the models developed above exhibit similar kinetic behaviors (near 1st-order dependence on hydroxide), it is reasonable to expect that a unifying global model with hydroxide dependence may be developed.

A few assumptions must be made to generate a global TOC HGR model that can be readily applied to radioactive waste media in SRS tank farms. Those assumptions and their corresponding justifications are listed below.

- *Thermolytic HGRs from Xiameter AFE-1010, IONAC A-641 resin, and Reillex HPQ resin digestion products are generally greater than those of other organic compounds present in the SRS tank farm*. This was shown to be the case in preliminary screening tests where measurements of Xiameter and resin surrogates were reported to be higher than HGRs observed from other organic species in identical simulant compositions and temperatures.
- *The mechanisms of organic thermolysis are empirically similar*. This assumption is apparently true given the near-linear dependence of hydroxide for each of the organics studied (hydroxide reaction order of 1.141 for Xiameter, 1.065 for IONAC, and 0.891 for Reillex).
- *The thermodynamic parameters of organic thermolysis are inherently species-dependent (rate constants and apparent activation energies cannot be universally assumed to adequately describe all organic thermolysis)*. This assumption is also apparently true, given the apparent activation energies of the organics described above (62.3 kJ mol^{-1} for Xiameter, 76.1 kJ mol^{-1} for IONAC, and 27.9 kJ mol^{-1} for Reillex). Note also that this assumption is intuitive, given that similar compounds (e.g. formaldehyde and propionaldehyde) would be expected to have similar mechanisms with different reaction rates.
- *Thermolytic HGRs from organics in radioactive waste are inherently lower than the HGRs predicted by the models described in previous sections*. This proposition is believed to be true for a couple of reasons. First, as was noted previously, the models developed in this report are generated from those species considered the most reactive in the CSTF. Given that radioactive waste in tanks are expected to contain blends of other, lower reactivity organics, HGR is expected to be inherently lower in radioactive waste on a "per TOC" basis. Furthermore, the testing performed in this study used freshly added (or freshly-digested, when applicable) organic materials, whereas organic present in the SRS tank farm have been present for much longer timeframes (generally on the order of years). Given that these organic materials are blends of several individual organic compounds (Xiameter is a mixture of several species and resin digestion processes oxidize pure resins into numerous organic products), it would be expected that the most reactive compounds added with the organic material degrade first, lowering the average HGR due to the increased relative contribution of less reactive compounds in radioactive waste.

The assumptions outlined above lead to the development of a relatively simple model for global model for HGR from any organic species in the SRS CSTF. This model is the product of a species-dependent rate constant, a species-independent function of supernatant composition, the concentration of organic carbon of interest, and an Arrhenius term utilizing a species-dependent apparent activation energy. This model expression is given in Equation [35].

$$HGR_{TOC} = k_{sd} \times f\left(\left[Na\right],\left[Al\right],\left[OH\right],etc.\right) \times \left[TOC\right] \times e^{-E_{sd}/RT} \qquad [35]$$

where,

HGR_{TOC} is the HGR attributable to organic thermolysis in any waste tank in $ft^3\ h^{-1}\ gal^{-1}$,
k_{sd} is the *species-dependent* rate constant in $ft^3\ h^{-1}\ gal^{-1}\ (L\ mol^{-1})^{1+f([Na],[Al],etc.)}$,
E_{sd} is the *species-dependent* apparent activation energy in $J\ mol^{-1}$,
$[TOC]$ is the concentration of total organic carbon in the waste tank of interest in $mol\ L^{-1}$, and
$f([Na],[Al],[OH],etc.)$ is the *species-independent* reaction mechanism function.

In this framework, it is important to first understand the nature of $f([Na],[Al],[OH],etc.)$ before it can be used to estimate the HGRs from radioactive waste. Under the assumptions specified above, the functionality of $f([Na],[Al],[OH],etc.)$ can be determined by evaluating the test results from each of the organics described above in a singular model regression (rather than determining the impacts of salt concentrations with individual regressions). This combined regression can be achieved by first assuming that the functional form of HGR (as observed from simulated organic testing and radioactive waste experiments) can be described by a simple kinetic expression, given in Equation [36].

$$HGR_i = k_i [Na]^{\alpha} [Al]^{\beta} [NO_2]^{\gamma} [NO_3]^{\delta} [OH]^{\varepsilon} [SO_4]^{\phi} [CO_3]^{\mu} [TOC] e^{-E_i/RT} \quad [36]$$

This model assumption may be linearized by taking the natural logarithm of each side of the equation, as has been shown. This exercise is repeated in Equation [37].

$$\ln\left(\frac{HGR_i}{[TOC]}\right) = \ln k_i + \alpha \ln[Na] + ... + \mu \ln[CO_3] - \frac{E_i}{RT} \quad [37]$$

The assumptions outlined above suggest that constants k_i and E_i are species-dependent and may not be applied to results from radioactive waste. However, the value of $f([Na],[Al],[OH],etc.)$ (expressed in Equation [36] as $f([Na],[Al],[OH],etc.) = [Na]^{\alpha} [Al]^{\beta} [NO_2]^{\gamma} [NO_3]^{\delta} [OH]^{\varepsilon} [SO_4]^{\phi} [CO_3]^{\mu}$) is assumed to be independent of organic species, and may be regressed independently from k_i and E_i.

It should be noted that it is impossible to regress three sets of data to the model shown in Equation [37] as written. This model must first be expanded to account for the fact that separate k_i and E_i values are expected for each organic. This modification is given in Equation [38].

$$\ln\left(\frac{HGR_i}{[TOC]}\right) = \ln k_i + \ln k_j + \ln k_k + \alpha \ln[Na] + ... + \mu \ln[CO_3] - \frac{E_i}{RT} - \frac{E_j}{RT} - \frac{E_k}{RT} \quad [38]$$

Note that an important criterion of the linear regression of multiple sets of data to the model proposed in Equation [38] is that the model must simplify to Equation [37] for each organic species i. This criterion may be satisfied by setting the values of $\ln k_j$, $\ln k_k$, E_j, and E_k to zero for each organic species i.

The simplification criterion may be met by utilizing a sparse input matrix during regression (rather than a complete input matrix, as has been used previously). An example of this calculation is given in Figure 3-46

for the case where m results of Xiameter tests, n results of IONAC tests, and p results of Reillex tests are being simultaneously regressed.

$$\vec{b} = \underline{A} \times \vec{x}$$

$$\begin{bmatrix} \ln\left(HGR/TOC\right)_1^{XIA} \\ \vdots \\ \ln\left(HGR/TOC\right)_m^{XIA} \\ \ln\left(HGR/TOC\right)_1^{IAC} \\ \vdots \\ \ln\left(HGR/TOC\right)_n^{IAC} \\ \ln\left(HGR/TOC\right)_1^{RLX} \\ \vdots \\ \ln\left(HGR/TOC\right)_p^{RLX} \end{bmatrix} = \begin{bmatrix} 1 & 0 & 0 & \ln[Na]_1^{XIA} & \cdots & \ln[CO_3]_1^{XIA} & 1/RT_1^{XIA} & 0 & 0 \\ \vdots & \vdots & \vdots & \vdots & \ddots & \vdots & \vdots & \vdots & \vdots \\ 1 & 0 & 0 & \ln[Na]_m^{XIA} & \cdots & \ln[CO_3]_m^{XIA} & 1/RT_m^{XIA} & 0 & 0 \\ 0 & 1 & 0 & \ln[Na]_1^{IAC} & \cdots & \ln[CO_3]_1^{IAC} & 0 & 1/RT_1^{IAC} & 0 \\ \vdots & \vdots & \vdots & \vdots & \ddots & \vdots & \vdots & \vdots & \vdots \\ 0 & 1 & 0 & \ln[Na]_n^{IAC} & \cdots & \ln[CO_3]_n^{IAC} & 0 & 1/RT_n^{IAC} & 0 \\ 0 & 0 & 1 & \ln[Na]_1^{RLX} & \cdots & \ln[CO_3]_1^{RLX} & 0 & 0 & 1/RT_1^{RLX} \\ \vdots & \vdots & \vdots & \vdots & \ddots & \vdots & \vdots & \vdots & \vdots \\ 0 & 0 & 1 & \ln[Na]_p^{RLX} & \cdots & \ln[CO_3]_p^{RLX} & 0 & 0 & 1/RT_p^{RLX} \end{bmatrix} \times \begin{bmatrix} \ln k_{XIA} \\ \ln k_{IAC} \\ \ln k_{RLX} \\ \alpha \\ \vdots \\ \mu \\ -E_{XIA} \\ -E_{IAC} \\ -E_{RLX} \end{bmatrix}$$

Figure 3-46. Linear Regression of All Simulant HGR Data to Determine Global Salt Species Dependence.

Once the input matrix and output vector (matrix $\underline{A}$ and vector $\vec{b}$, as shown in Figure 3-46) are determined, the solutions for the unknown parameter vector, $\vec{x}$, may be calculated using the linear algebraic formula given in Equation [39].

$$\vec{x} = \left(\underline{A}^T \times \underline{A}\right)^{-1} \times \left(\underline{A}^T \times \vec{b}\right) \quad [39]$$

This step may be performed iteratively (as was done previously for the individual organic models) to determine the optimal regression (defined as the simplest model capable of describing a majority (>85%) of the variation of the data. The result of this iteration yielded a simplistic model dependent only on the molar hydroxide concentration to an order near unity and on the molar TOC concentration to the first order, shown in Equation [40].

$$HGR_i = k_i [OH]^{0.925} [TOC_i] e^{-E_i/RT} \quad [40]$$

The values of k_i and E_i were simultaneously determined for each of the organics employed during these tests. The regressed values of those parameters are given in Table 3-29.

Table 3-29. Kinetic Parameters for Xiameter, IONAC, and Reillex Obtained During Global Model Regression.

Organic Species	k_i	E_i
Xiameter AFE-1010	1.607×10^{4}	52.4 kJ mol^{-1}
IONAC-A-641	7.237×10^{8}	94.2 kJ mol^{-1}
Reillex HPQ	1.149×10^{1}	29.1 kJ mol^{-1}

The results of the simulant tests described in this report are plotted against the regressed global model results in Figure 3-47.

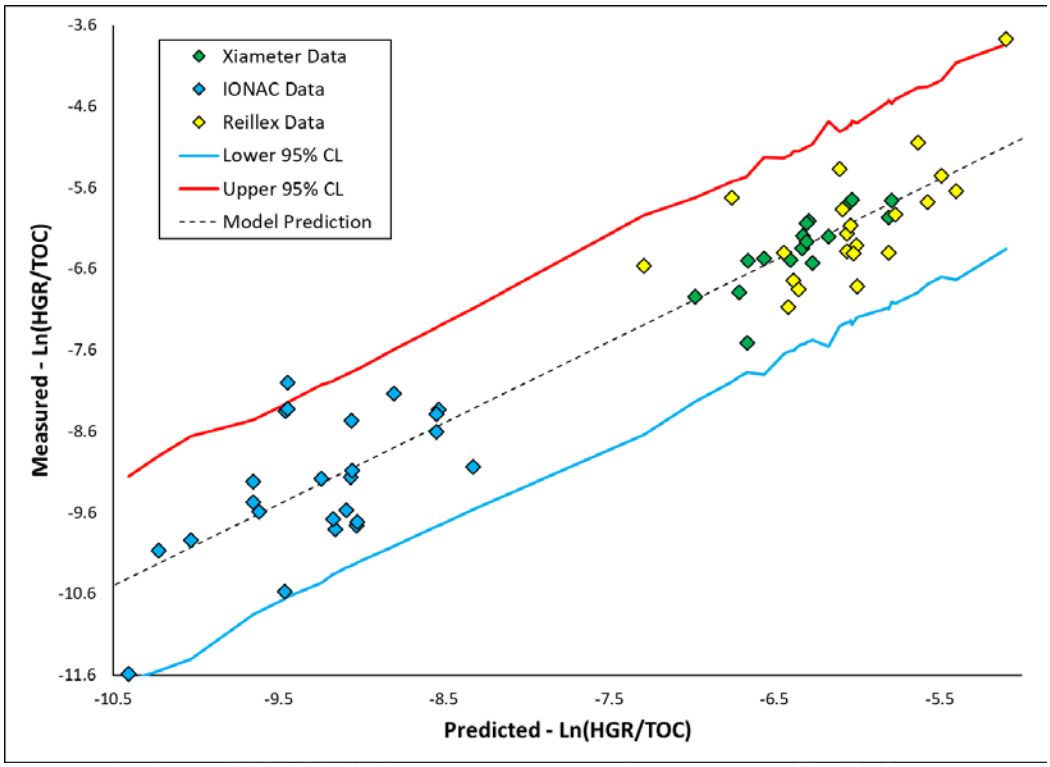

Figure 3-47. Plot of Measured HGRs from All Simulant Experiments vs. Predicted HGRs According to Global Model Regression Results Described in Equation [40] and Table 3-29.

The fit shown in Figure 3-47 suggests that the majority (89%) of variation seen in the data is well described with the model assumed in Equation [40]. Only a couple of the 62 data points used in this regression fall outside of the 95% confidence limit, which is consistent with the statistical uncertainty associated with the model.

The assumptions made earlier state that thermolytic production of hydrogen from organics in radioactive waste samples might be best described with the same mechanistic functionality as was observed during simulant testing. This suggests that the thermolytic HGR from real waste may be described according to the model expression given in Equation [41].

$$HGR_{real} = k_{real}[OH]^{0.925}[TOC]e^{-E_{real}/RT} \qquad [41]$$

Given that there is no expectation for the organic compounds distributed throughout the CSTF to be identical (that is, to have similar rates of reactivity as influenced by k_{real} and E_{real}), it is preferable to find values of k_{real} and E_{real} that may successfully *bound* thermolytic HGR in the CSTF. This may be accomplished by evaluating measured HGRs from tests performed with radioactive waste in terms of the Arrhenius-type expression given in Equation [42].

$$\ln\left(\frac{HGR_{real}}{[OH]^{0.925}[TOC]}\right) = \ln k_{real} - \frac{E_{real}}{RT} \qquad [42]$$

To date, several experiments have been performed to measure the HGR from samples taken from SRS HLW tanks at a wide range of temperatures and compositions. Because radioactive waste may produce hydrogen by several mechanisms, it is important to critically evaluate the results of these radioactive waste tests and eliminate those conditions that are not relevant to sustained organic thermolysis. Table 3-30 lists the results of all HGR experiments with radioactive waste performed to date, as well as the conditions (composition and temperature) of those tests and the designation of the hydrogen generating mechanism by which hydrogen gas was believed to be observed.

Table 3-30. Summary of HGR Experiments Performed Using SRS HLW Tank Samples.

Tank No.	Temp. (°C)	[OH] (M)	[TOC] (M)	HGR ($ft^3\ h^{-1}\ gal^{-1}$)	HGR Source	Reference Documentation
51	23	9.73E-01	5.40E-06	1.00E-06	Dissolved	SRNL-STI-2018-00179 Rev 0[30]
51	50	9.73E-01	5.40E-06	2.00E-07	Dissolved	SRNL-STI-2018-00179 Rev.0
51	75	9.73E-01	5.40E-06	8.30E-07	Dissolved	SRNL-STI-2018-00179 Rev 0
51	85	9.73E-01	5.40E-06	5.00E-07	Dissolved	SRNL-STI-2018-00179 Rev 0
51	50	4.70E+00	8.74E-03	1.10E-06	Dissolved	SRNL-STI-2018-00179 Rev 0
51	75	4.70E+00	8.74E-03	3.00E-07	Dissolved	SRNL-STI-2018-00179 Rev 0
51	85	4.70E+00	8.74E-03	1.00E-06	Dissolved	SRNL-STI-2018-00179 Rev 0
22	30	1.89E-01	3.46E-03	< 5.60E-08	BDL	SRNL-STI-2018-00385 Rev 0
22	60	1.89E-01	3.46E-03	< 5.60E-08	BDL	SRNL-STI-2018-00385 Rev 0
22	80	1.89E-01	3.46E-03	< 5.60E-08	BDL	SRNL-STI-2018-00385 Rev 0
22	101.4	1.89E-01	3.46E-03	< 5.80E-08	BDL	SRNL-STI-2018-00385 Rev 0
38	35	2.85	1.14E-02	6.43E-08	Short-Lived	SRNL-STI-2018-00559 Rev 0
38	60	2.85	1.14E-02	6.98E-08	Short-Lived	SRNL-STI-2018-00559 Rev 0
38	80	2.85	1.14E-02	7.87E-08	Short-Lived	SRNL-STI-2018-00559 Rev 0
38	95	2.85	1.14E-02	9.28E-08	Thermolytic	SRNL-STI-2018-00559 Rev 0
38	111.5	2.85	1.14E-02	4.03E-07	Thermolytic	SRNL-STI-2018-00559 Rev 0
38	27	2.85	1.14E-02	4.8E-08	Glass-Enhanced	SRNL-STI-2017-00611 Rev 1
38	80	2.85	1.14E-02	1.7E-07	Glass-Enhanced	SRNL-STI-2017-00611 Rev 1
38	90	2.85	1.14E-02	4.7E-07	Glass-Enhanced	SRNL-STI-2017-00611 Rev 1
38	100	2.85	1.14E-02	5.9E-07	Glass-Enhanced	SRNL-STI-2017-00611 Rev 1
38	110.5	2.85	1.14E-02	2.6E-06	Glass-Enhanced	SRNL-STI-2017-00611 Rev 1
50	73	1.98E+00	5.81E-03	1.76E-08	Thermolytic	SRNL-STI-2018-00559 Rev 0
50	31.7	1.98E+00	5.81E-03	1.73E-09	Radiolytic	SRNL-STI-2018-00238 Rev 0
50	32.3	1.98E+00	5.81E-03	1.87E-09	Radiolytic	SRNL-STI-2018-00238 Rev 0
50	32.3	1.98E+00	5.81E-03	7.66E-10	Radiolytic	SRNL-STI-2018-00238 Rev 0
50	72.4	1.98E+00	5.81E-03	2.21E-08	Thermolytic	SRNL-STI-2018-00238 Rev 0
50	71.6	1.98E+00	5.81E-03	4.48E-08	Thermolytic	SRNL-STI-2018-00238 Rev 0
50	71.5	1.98E+00	5.81E-03	4.86E-08	Thermolytic	SRNL-STI-2018-00238 Rev 0
50	95	1.98E+00	5.81E-03	2.86E-07	Thermolytic	SRNL-STI-2018-00238 Rev 0
50	113.2	1.98E+00	5.81E-03	1.42E-06	Thermolytic	SRNL-STI-2018-00238 Rev 0
50	114.9	1.98E+00	5.81E-03	1.36E-06	Thermolytic	SRNL-STI-2018-00238 Rev 0
28	40	8.23E+00	4.42E-02	< 5.9E-08	BDL	SRNL-STI-2019-00411 Rev 0
28	70	8.23E+00	4.42E-02	6.7E-07	Short-Lived	SRNL-STI-2019-00411 Rev 0
28	70	8.23E+00	4.42E-02	1.3E-07	Thermolytic	SRNL-STI-2019-00411 Rev 0
28	85	8.23E+00	4.42E-02	6.1E-07	Short-Lived	SRNL-STI-2019-00411 Rev 0
28	100	8.23E+00	4.42E-02	8.1E-07	Thermolytic	SRNL-STI-2019-00411 Rev 0
28	124.8	8.23E+00	4.42E-02	6.27E-06	Thermolytic	SRNL-STI-2019-00411 Rev 0
39	34.6	1.79E+00	1.96E-02	< 5.5E-08	BDL	SRNL-STI-2019-00411 Rev 0
39	70	1.79E+00	1.96E-02	7E-08	Short-Lived	SRNL-STI-2019-00411 Rev 0
39	85	1.79E+00	1.96E-02	7E-08	Short-Lived	SRNL-STI-2019-00411 Rev 0
39	100	1.79E+00	1.96E-02	8E-08	Short-Lived	SRNL-STI-2019-00411 Rev 0
39	105.3	1.79E+00	1.96E-02	1.4E-07	Thermolytic	SRNL-STI-2019-00411 Rev 0

The test results listed in Table 3-30 are classified according to the suspected source of hydrogen at the time of measurement. Results designated as "Dissolved" are tests that exhibited significant HGRs upon heating followed by rapid decrease, suggesting the presence of released hydrogen gas by decreased solubility at elevated temperatures. Results designated as "BDL" are tests that resulted in either an unobserved HGR or an observed HGR below detectable limits and can therefore not be accurately quantified. Results designated as "Radiolytic" are tests that yield measurable, constant generation rates of hydrogen that exhibit no clear

temperature dependence, suggesting that the driver for hydrogen formation is the action of radiation on water molecules, deemed radiolysis. Results designated as "Short-Lived" are tests that yielded measurable hydrogen exhibiting a continuous decrease (observed either at the time of testing or during cool-down) that appears to be inconsistent with the mechanics of the release of dissolved hydrogen. It is proposed that these rates, though measurable, are due to "short-lived" organic species that are not expected to endure at temperature and should not be considered a threat for hydrogen generation over the course of more than the duration of a single HGR test (typically <12 hours). Results designated as "Glass-Enhanced" apply only to testing performed in 2017 with Tank 38 material in a borosilicate glass vessel. Ashby *et al.*[10] has previously observed that the presence of borosilicate glass seems to exhibit an enhancing effect on organic thermolysis, often yielding hydrogen-generating reactivities an order of magnitude higher than those observed in the absence of glass. Given this observation and the fact that the waste tanks at SRS are composed of carbon steel and not borosilicate glass, it is proposed that these tests are inapplicable to waste conditions expected in the CSTF. Finally, results designated as "Thermolytic" are those tests which exhibited sustained production of hydrogen as a function of temperature. For waste tank samples, the "thermolytic" results tended to be the measurements at the highest temperatures studied.

The test results that were designated as "Thermolytic" are plotted in a modified Arrhenius-type plot in Figure 3-48.

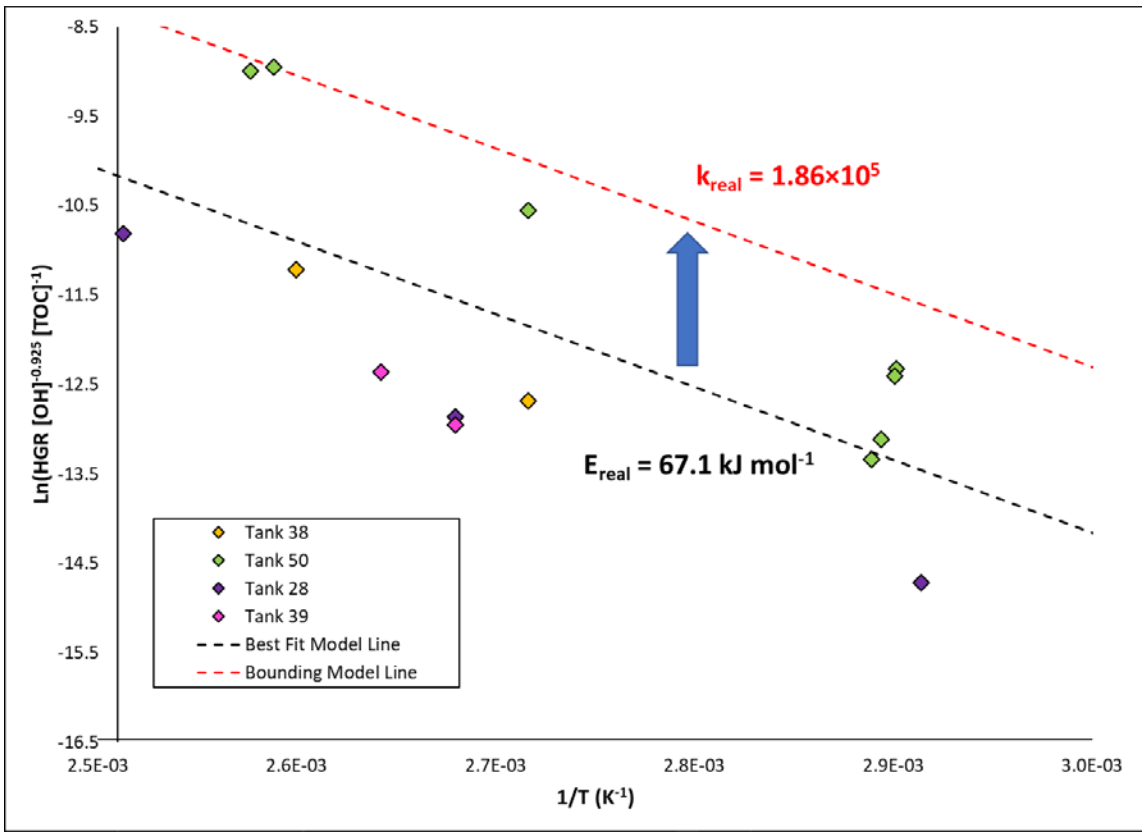

Figure 3-48. Modified Arrhenius Plot of Real Waste HGR Measurements Designated as Thermolytic Hydrogen Generation.

A "best-fit" line (black dashes) to the data presented in Figure 3-48 yields a slope corresponding to an apparent activation energy of 67.1 kJ mol^{-1}. This best-fit line, however, falls below the majority of data obtained from Tank 50 sample measurements using the SRNL sealed HGR measurement system, as

described by Duignan.[31] Therefore, a "bounding" model (red dashes) may be generated by artificially increasing the intercept of this line to pass through the data point with highest reactivity (relative to temperature). The new artificial intercept of the modified Arrhenius plot corresponds to a bounding pre-exponential factor of 1.86×10^5. The resulting model expression for bounding thermolytic HGR from radioactive waste is given in Equation [43].

$$HGR_{real} = 1.86\times10^5 [OH]^{0.925} [TOC] e^{-67{,}100/RT} \quad [43]$$

The model expression given in Equation [43] represents a global TOC model for thermolytic HGR in which the mechanistic understanding has been deduced by studying the reaction rates of the most reactive compounds expected in the CSTF. The reactivity of this model has further been reduced for the observed decrease in radioactive-waste organic thermolytic activity relative to that observed in simulant testing. For these reasons, it is expected that this model will suffice as a bounding approximation for hydrogen-producing organic thermolysis in SRS waste tanks.

It should be observed that among all the thermolytic data plotted in Figure 3-48, a notable difference exists between that of Tank 50 measurements and those of other tanks (i.e., 28, 38, and 39). The data suggests that Tank 50 samples measured in the sealed HGR system produce more hydrogen per carbon than those samples measured in the flow HGR system. It is currently unclear if this difference in reactivity is due to a systematic bias in sealed-system measurements or to differences in reactivity of organic species in Tank 50 (note that screening studies described earlier identified the CSSX/salt-waste processing organics present in Tank 50 as "unreactive" when compared to compounds like Xiameter AFE-1010). However, it may be noted that Tank 50 is currently operated under a separate flammability analysis (largely due to the increased presence of VOCs). Therefore, it is not necessary to include Tank 50 results in the development of a global TOC model for HGR (under the condition that the resulting model is not applied to Tank 50 controls). A separate modified Arrhenius plot excluding Tank 50 data is given in Figure 3-49.

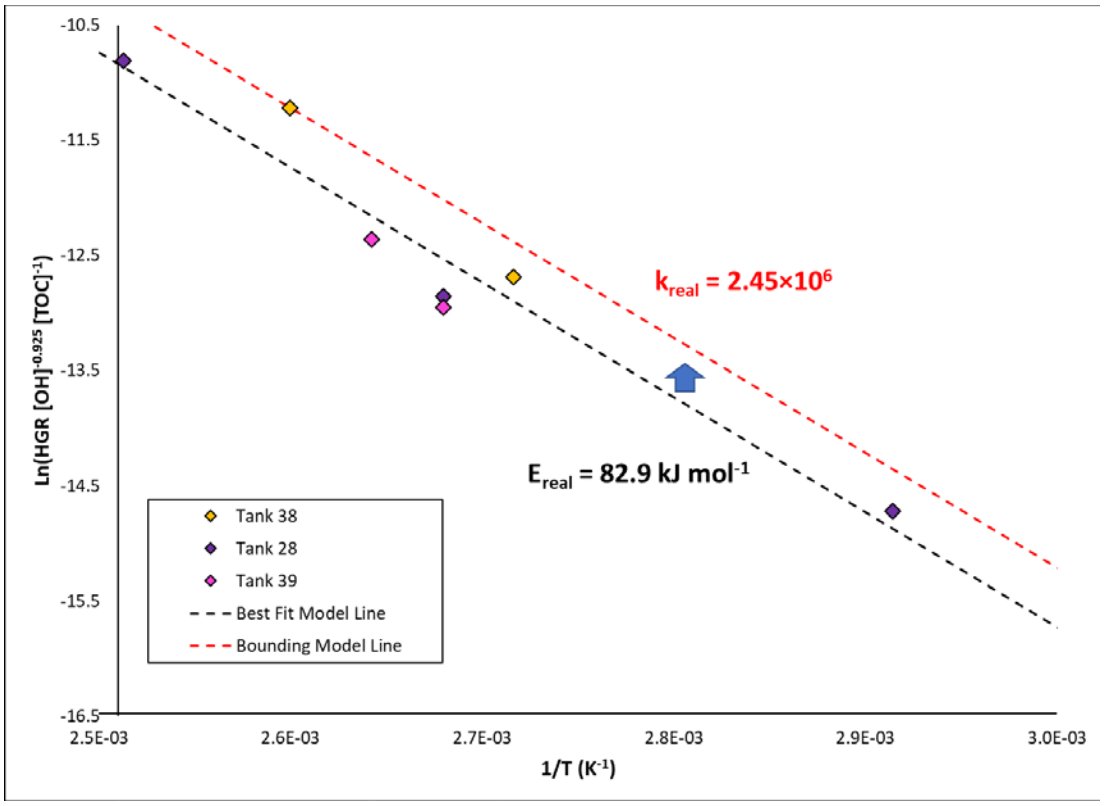

Figure 3-49. Modified Arrhenius Plot of Real Waste HGR Measurements Designated as Thermolytic Hydrogen Generation from Tanks Other Than Tank 50.

The resulting "best fit" line (black dashes) yields an apparent activation energy of 82.9 kJ mol^{-1}. It should also be noted that the best-fit line passes relatively close to all the data in the plot ($R^2 = 0.933$), suggesting that organic thermolysis in these tanks is well-described. An artificial increase in intercept (as described previously) generates a "bounding model" line (red dashes) and a bounding pre-exponential factor of 2.45×10^6. The resulting model from the exclusion of Tank 50 data is given in Equation [44].

$$HGR_{real} = 2.45\times10^{6}\left[OH\right]^{0.925}\left[TOC\right]e^{-82{,}900/RT} \qquad [44]$$

In Equation [44], the HGR_{real} refers to the thermolytic HGR from organics at standard conditions of 25 °C and 1 atm in ft^3 h^{-1} gal^{-1}, $\left[OH\right]$ is the concentration of hydroxide anion in mol L^{-1}, $\left[TOC\right]$ is the concentration of organic carbon in mol L^{-1}, R is the ideal gas constant (8.314 J mol^{-1} K^{-1}), and T is the supernatant phase temperature in K.

Given the quality of fit achieved by the model shown in Figure 3-49, it is recommended that thermolytic HGR due to non-glycolate TOC be estimated by the expression given in Equation [44] for waste tanks other than Tanks 48 and 50. It is recommended that Tank 50 be managed under a separate flammability evaluation using the data generated by Duignan using the sealed HGR system.[31] In cases where glycolate and other sources of organic carbon are present, it is recommended that Equations [17] and [44] be used separately to assess the HGRs from each mechanism. Appendix C contains an example CSTF flammability calculation using this non-glycolate thermolytic model in tandem with the glycolate thermolytic model and existing radiolytic calculations.

3.10 Extrapolation of the Global TOC HGR Model to Lower Temperatures

In October 2018, SRNL published results of HGR measurements obtained from simulant mixtures containing digested Reillex material in support of H-Canyon resin digestion.[29] The experiment with the lowest temperature measured (55 °C) was performed using a 60/40 blend of digestion material and Tank 39 simulant to predict the influence of the high TOC loadings expected in transfer pump tanks containing a hydroxide-bearing heel. This test (performed at estimated concentrations of 1.17 M hydroxide and 92 mg/L of organic carbon) yielded an HGR below the detection limit of 3×10^{-8} ft^3 h^{-1} gal^{-1}. This value is much lower than the HGR expected from the model generated from other Reillex testing data (2.6×10^{-6} ft^3 h^{-1} gal^{-1}), indicating that this low-temperature (i.e., <70 °C) HGR from Reillex is well-bounded by the Reillex model generated from data gathered at 70 °C and above (Equation [31]). Given the fact that the observed temperature dependence of organics in radioactive waste (82,900 J/mol, as indicated in Equation [44]) is more significant than that observed from Reillex material alone (27,900 J/mol, as indicated in Equation [31]), it is reasonable to assume that extrapolation of the Global TOC model to temperatures lower than 70 °C may be performed to estimate the HGRs of the organics expected in CSTF caustic media with minimal risk to conservatism. Additional testing is recommended to validate this extrapolation.

3.11 Applicable Ranges of Salt Species Concentrations and Temperature

To define the applicability of the models described above, the parameter ranges of experiments performed was assessed in combination with the D-optimal design space developed during experiment planning (as described in Section 2.4). Table 3-31 lists the maximum and minimum parameters evaluated during experimental design and experiment execution in support of the temperature-modified glycolate HGR model. Table 3-32 lists the maximum and minimum parameters evaluated during experimental design and experiment execution in support of the Global TOC model. For ease of identification, overall maximum and minimum parameter values are indicated in bold.

Table 3-31. Parameter Ranges for Experimental Design and Performance of Glycolate HGR Measurements.

Parameter	Experimental Design Space		Experiments Performed	
	Minimum	Maximum	Minimum	Maximum
Aluminum	1.29E-03 M	1.98E+00 M	**9.64E-04 M**	**2.49E+00 M**
Nitrite	**2.21E-01 M**	2.58E+00 M	2.24E-01 M	**2.78E+00 M**
Nitrate	6.75E-02 M	5.58E+00 M	**6.55E-02 M**	**6.34E+00 M**
Hydroxide	1.58E-01 M	1.18E+01 M	**4.66E-02 M**	**1.22E+01 M**
Sulfate	**4.94E-04 M**	2.05E-01 M	1.04E-03 M	**2.50E-01 M**
Carbonate	8.14E-03 M	5.79E-01 M	**2.38E-03 M**	**6.54E-01 M**
Temperature	60 °C	130 °C	**60 °C**	**134 °C**

Table 3-32. Parameter Ranges for Experimental Design and Performance of Non-Glycolate HGR Measurements.

Parameter	Experimental Design Space		Experiments Performed	
	Minimum	Maximum	Minimum	Maximum
Aluminum	**1.29E-03 M**	**1.98E+00 M**	3.93E-03 M	7.69E-01 M
Nitrite	**2.21E-01 M**	2.58E+00 M	2.37E-01 M	**2.74E+00 M**
Nitrate	**6.75E-02 M**	**5.58E+00 M**	8.61E-02 M	3.69E+00 M
Hydroxide	**1.58E-01 M**	1.18E+01 M	1.23E+00 M	**1.25E+01 M**
Sulfate	**4.94E-04 M**	**2.05E-01 M**	1.04E-03 M	2.01E-01 M
Carbonate	**8.14E-03 M**	5.79E-01 M	1.38E-02 M	**7.23E-01 M**
Temperature	**70 °C**	**130 °C**	73 °C	113 °C

From the data given in Table 3-31 and Table 3-32, a minimum and maximum sodium concentration can be calculated according to Equation [2]. Table 3-33 lists these calculated values along with the recommend ranges of applicability for the other parameters of interest to each HGR model expression.

Table 3-33. Recommended Parameter Applicability Ranges for HGR Models.

Parameter	Glycolate Thermolysis		Global TOC Thermolysis	
	Minimum	Maximum	Minimum	Maximum
Aluminum	9.64E-04 M	2.49E+00 M	1.29E-03 M	1.98E+00 M
Nitrite	2.21E-01 M	2.78E+00 M	2.21E-01 M	2.74E+00 M
Nitrate	6.55E-02 M	6.34E+00 M	6.75E-02 M	5.58E+00 M
Hydroxide	4.66E-02 M	1.22E+01 M	1.58E-01 M	1.25E+01 M
Sulfate	4.94E-04 M	2.50E-01 M	4.94E-04 M	2.05E-01 M
Carbonate	2.38E-03 M	6.54E-01 M	8.14E-03 M	7.23E-01 M
Sodium	3.40E-01 M	2.56E+01 M	4.65E-01 M	2.47E+01 M
Temperature	60 °C	134 °C	70 °C	130 °C

Given that the temperature-modified glycolate HGR model is a function of nitrate, hydroxide, sodium, and temperature, it is recommended that application of this model be made to solutions with:

- concentrations of nitrate greater than or equal to 6.55×10^{-2} M and less than or equal to 6.34 M,
- concentrations of hydroxide greater than or equal to 4.66×10^{-2} M and less than or equal to 12.2 M,
- concentrations of sodium greater than or equal to 3.40×10^{-1} M and less than or equal to 25.6 M, and
- solution-phase temperatures less than or equal to 134 °C (see earlier discussion on low temperature extrapolation in Section 3.3.4.6).

Extrapolation of the temperature-modified glycolate HGR model beyond these regions has not been investigated and should be evaluated if implementation is required beyond the specified ranges.

Given that the Global TOC model is a function of hydroxide and temperature, it is recommended that application of this model be made to solutions with:

- concentrations of hydroxide greater than or equal to 1.58×10^{-1} M and less than or equal to 12.5 M, and
- solution-phase temperatures less than or equal to 130 °C (see earlier discussion on low temperature Reillex measurements in Section 3.10).

Extrapolation of the Global TOC model beyond these regions has not been investigated and should be evaluated if implementation is required beyond the specified ranges.

4.0 Conclusions

The following are conclusions made because of the research detailed in this report.

- An experimental apparatus has been developed to study the time-dependent generation rate of hydrogen from liquids. A methodology to determine steady-state generation rates has been described.
- Screening tests using Tank 38 simulant material have been performed to identify the most reactive organic compounds introduced to the SRS tank farm. The following designations were assigned to each species.
    - Glycolate (not currently in CSTF waste), propanal, Xiameter AFE-1010 (formerly marketed as Dow Corning antifoam H-10), and some resin digestion products were identified as being significantly reactive toward the generation of hydrogen gas in caustic waste media.
    - Polyethylene oxide was identified as being marginally reactive, with HGRs similar to or just above those observed at baseline conditions without added organic material.
    - Sodium formate, CSSX solvent, dibutylphosphate, butanol, and trimethylsilanol were identified as not being significantly reactive compared to baseline conditions.
    - Marginal HGR was observed when oxalate was tested in the presence of formate and CSSX solvent. However, it is believed that this observation is due to the combination of multiple organic species and hydrogen observations near the limits of detection and should not be interpreted as propensity of oxalate to produce thermolytic hydrogen (oxalate has no hydrogen atoms available to form hydrogen gas).
- Thermolytic HGR from glycolate was shown to be independent of glycolate source (e.g., processing history of glycolate has no appreciable impact on generation rates).
- Statistically-designed matrices of test conditions were generated to evaluate the reactivity of glycolate, Xiameter AFE-1010, IONAC A-641 resin digestion products, and Reillex HPQ resin digestion products across the range of composition and temperature conditions expected in the SRS CSTF.
- The results from these statistically-designed test matrices were used to regress models to predict the thermolytic HGR at standard conditions of 25 °C and 1 atm from glycolate, Xiameter, IONAC, and Reillex-containing samples. The resulting models are given by the following expressions. Note that these expressions calculate the mean expected HGR and do not account for the uncertainty of the models' fit to the data.

$$HGR_{Glycolate} = 6.262\times10^{5}\left[Na\right]^{1.520}\left[NO_3\right]^{0.282}\left[OH\right]^{1.441}\left[C_{GLY}\right]e^{-82{,}300/RT}$$

$$HGR_{Xiameter} = 3.238\times10^{5}\left[OH\right]^{1.141}\left[C_{XIA}\right]e^{-62{,}300/RT}$$

$$HGR_{IONAC} = 1.361\times10^{6}\left[NO_3\right]^{0.542}\left[OH\right]^{1.065}\left[C_{IAC}\right]e^{-76{,}100/RT}$$

$$HGR_{Reillex} = 8.134\times\left[OH\right]^{0.891}\left[C_{RLX}\right]e^{-27{,}900/RT}$$

- The thermolytic HGR from glycolate was shown to be independent of added select Lewis acids (i.e., silicon and boron).
- The thermolytic HGR from glycolate was shown to be independent of the presence of select noble metals (i.e., silver, palladium, rhodium, and ruthenium).
- The thermolytic HGR from glycolate was shown to be somewhat dependent on the presence of sludge solids. It is believed that this dependence was observed due to the ability of sludge solids (notably MnO_2 solids) to oxidize glycolate and reduce the available concentration of hydrogen-producing reagent.
- The thermolytic HGR from glycolate was shown to be strongly dependent on the presence of added $Hg(NO_3)_2$, with near complete disappearance of all HGR in the presence of added $Hg(NO_3)_2$. Due to the apparent formation of an HgO phase, insolubility of the mercury used during this testing, and the introduction of suspended Hg-containing solids in the supernatant phase, it is not believed that this species is representative of conditions in radioactive SRS supernatant waste and is therefore not recommended as a credit to be used to decrease the amount of hydrogen expected during thermolysis.
- Testing at extreme conditions (of high aluminum and high temperature) in Tank 30 simulant has been performed with glycolate. These results fall within the 95% confidence limit predicted by the glycolate thermolytic model.
- The HGR profiles yielded from testing with glycolate suggest the presence of a reactive intermediate, implying that the destruction rate of glycolate may be markedly faster than the HGR in caustic waste media.
- Testing performed with IONAC A-641 digestion products revealed that HGRs from resin digestion products are not impacted by the presence of solids, suggesting that thermolysis should be considered a supernatant phenomenon.
- Testing performed with propanal suggests that while propanal exhibits a relatively high reactivity to produce hydrogen, its volatility and high reaction rate limits its ability to endure for longer than approximately 3 hours and is not expected to be present in measurable concentrations in tank farm waste at elevated temperatures.
- Propanal thermolysis was shown to be dependent primarily on hydroxide concentrations and temperatures, which is consistent with the Cannizzaro-type reaction mechanism put forward by Ashby[10] for the generation of hydrogen from aldehydes in caustic waste media.
- Testing with combined additions of glycolate, Xiameter, IONAC, and Reillex digestion products suggests that there is little to no risk of synergistic interactions between organic molecules. Further, test results suggest that antagonistic effects may be present, possibly due to the interaction of organic molecules with MnO_2 added with resin digestion products. This antagonistic effect is not universal, is believed to be scale- and process-dependent, and would not be expected in a settled tank's supernatant phase; therefore, it is not recommended as a credit to decrease expected HGRs from organic compounds.
- A global, source-independent model for organic thermolytic HGR at standard conditions of 25 °C and 1 atm in SRS waste media has been developed, taking the following form. Note that this equation is not applicable to HGRs from glycolate.

$$HGR_{real} = 2.45 \times 10^{6} [OH]^{0.925} [TOC] e^{-82,900/RT}$$

- The global model is expected to be applicable to all SRS waste tanks except for Tanks 48 and 50, which should be managed under separate flammability evaluations. Data applicable to Tank 50 has been previously generated by Duignan using a sealed HGR system.

5.0 Recommendations

The following are recommendations made considering the results from the tests described in this report.

- Additional investigations should be made into the generation rates of methane from organic molecules in the CSTF. The organic compounds of most importance are methylsilanes (such as those employed as antifoam agents throughout SRS processing) and methylmercury (a known toxin in the HLW flowsheet at SRS).
- Previous work predicting the impact of glycolate thermolysis on the composition of hydrogen in bubbles of trapped gas in SRS waste should be revised to account for the improved rate prediction models generated in this report.
- Further investigation should be made in the composition of total gas evolutions from organic thermolysis to better credit hydrogen retention in trapped gas bubbles.
- Further investigation should be made into the mechanism of mercury impact on glycolate and non-glycolate organic HGR to assess creditability in the CSTF.
- Further testing is recommended to validate the models proposed herein at extremes in hydroxide concentration and temperature ([OH] > 12.2 M and T > 134 °C for glycolate; [OH] > 12.5 M, T < 70 °C, and T > 130 °C for non-glycolate TOC).

6.0 References

1. Walker, D. D. "Organic Compounds in Savannah River Site High-Level Waste"; WSRC-TR-2002-00391, Rev. 0; Savannah River Technology Center: **2002**.

2. Brotherton, K. M. "Potentially Inadequate Recognition of the Effect of Organics on Hydrogen Generation Rates in DWPF Process Vessels"; PI-2017-0004; Savannah River Remediation: **2017**.

3. Condon, W. A. "Potentially Inadequate Recognition of the Effect of Organics on Hydrogen Generation Rates in CSTF"; PI-2017-0003; Savannah River Remediation: **2017**.

4. Staub, A. V. "Potentially Inadequate Recognition of the Effect of Organics on Hydrogen Generation Rates in Saltstone"; PI-2017-0002; Savannah River Remediation: **2017**.

5. Martino, C. J.; Woodham, W. H.; McCabe, D. J.; Nash, C. A. "Task Technical and Quality Assurance Plan for Simulant and Radioactive Testing of the Impacts of Glycolate on Hydrogen Generation in the Savannah River Site Liquid Waste System"; SRNL-RP-2017-00684, Rev. 2; Savannah River National Laboratory: **2019**.

6. Clark, M. C. "Simulant and Radioactive Testing - Impact of Glycolate on Tank Farm"; X-TTR-S-00067, Rev. 2; Savannah River Remediation: **2018**.

7. Bibler, N. E.; Pareizs, J. M.; Fellinger, T. L.; Bannochie, C. J. "Measurement and Prediction of Radiolytic Hydrogen Production in Defense Waste Processing Slurries at Savannah River Site"; WSRC-STI-2006-00114, Rev. 1; Savannah River National Laboratory: **2006**.

8. Crawford, C. L.; King, W. D. "Impacts of Glycolate and Formate Radiolysis and Thermolysis on Hydrogen Generation Rate Calculations for the Savannah River Site Tank Farm"; SRNL-STI-2017-00303, Rev. 0; Savannah River National Laboratory: **2017**.

9. Hu, T. A. "Empirical Rate Equation Model and Rate Calculations of Hydrogen Generation for Hanford Tank Waste"; HNF-3851, Rev. 1; **2004**.

10. Ashby, E. C.; Annis, A.; Barefield, E. K.; Boatright, D.; Doctorovich, F.; Liotta, C. L.; Neumann, H. M.; Konda, A.; Yao, C. F.; Zhang, K.; McDuffie, N. G. "Synthetic Waste Chemical Mechanism Studies"; WHC-EP-0823; Westinghouse Hanford Company: **1994**.

11. Martino, C. J.; Newell, J. D.; Woodham, W. H.; Pareizs, J. M.; Edwards, T. B.; Lambert, D. P.; Howe, A. M. "Investigation of Thermolytic Hydrogen Generation Rate of Tank Farm Simulated and Actual Waste"; SRNL-STI-2017-00611, Rev. 1; Savannah River National Laboratory: **2019**.

12. "Technical Reviews"; Manual E7, 2.60, Rev. 17; **2016**.

13. "Technical Report Design Checklist"; WSRC-IM-2002-00011, Rev. 2.

14. Baker, R. A.; Edwards, T. B.; Elizondo, A. D.; Harris, S. P.; Shine, E. P.; Watson, H. L. "Verification and Validation for Commercial Statistical Packages Utilized by SRNL Statisticians"; B-VVR-A-00002, Rev. 3; Savannah River National Laboratory: **2014**.

15. Woodham, W. H. "Run Plan for Testing to Screen and Assess the Hydrogen Generation Rates Evolved from the Thermolysis of Glycolate and Other Prominent Tank Farm Organics"; SRNL-L3300-2018-00004, Rev. 0; Savannah River National Laboratory: **2018**.

16. Lambert, D. P.; Zamecnik, J. R.; Newell, J. D.; Williams, M. S. "Antifoam Degradation Testing"; SRNL-STI-2015-00352, Rev. 0; Savannah River National Laboratory: **2015**.

17. Wu, C. F. J.; Hamada, M., *Experiments: Planning, Analysis, and Parameter Design Optimization*. Wiley: 2000.

18. Woodham, W. H.; Edwards, T. B. "Run Plan for Testing to Evaluate Importance of Major Salt Species on Thermolytic Production of Hydrogen from Glycolate"; SRNL-L3300-2018-00011, Rev. 1; Savannah River National Laboratory: **2018**.

19. Woodham, W. H.; Edwards, T. B. "Run Plan for Testing to Improve Interim Models for Thermolytic Production of Hydrogen from Glycolate and Other Prominent Tank Farm Organics"; SRNL-L3300-2019-00003, Rev. 0; Savannah River National Laboratory: **2019**.

20. Hay, M. S.; Coleman, C. J.; Diprete, D. P. "Analysis of Tank 30H (HTF-30-18-96, -97), Tank 32H (HTF-32-18-98, -99), and Tank 37H (HTF-37-18-100, -101) Samples for Support of the Evaporator Feed Qualification and Corrosion Control Programs for the 3H-Evaporator"; SRNL-STI-2019-00002, Rev. 0; Savannah River National Laboratory: **2019**.

21. Woodham, W. H. "Run Plan for Generation and Use of a High-Boiling Tank 30 Simulant for Glycolate Thermolysis Testing"; SRNL-L3300-2019-00012, Rev. 0; Savannah River National Laboratory: **2019**.

22. Woodham, W. H.; Zamecnik, J. R. "Evaluation of Simple Chemical Interactions in the Defense Waste Processing Facility (DWPF) Chemical Process Cell (CPC) Under the Glycolic Acid Flowsheet"; SRNL-STI-2017-00318, Rev. 0; Savannah River National Laboratory: **2018**.

23. Sudduth, C. B.; Chen, G. "Waste Tank Selection for Testing the Impact of Glycolate and Existing Tank Farm Organics on Thermolytic Hydrogen Generation Rate"; X-ESR-G-00066, Rev. 0; Savannah River Remediation: **2019**.

24. Martino, C. J.; Pareizs, J. M.; Newell, J. D. "Thermolytic Hydrogen Generation Testing of Tank 22 Material"; SRNL-STI-2018-00385, Rev. 0; Savannah River National Laboratory: **2018**.

25. Martino, C. J.; Newell, J. D.; Pareizs, J. M.; Duignan, M. R.; Restivo, M. L. "Investigation of Thermolysis Hydrogen Generation Rate in Tank 38 and Tank 50 Waste Samples with Sodium Glycolate"; SRNL-STI-2018-00559, Rev. 0; Savannah River National Laboratory: **2019**.

26. Martino, C. J.; Pareizs, J. M.; Woodham, W. H. "Investigation of Thermolytic Hydrogen Generation Rate in Tank 28 and Tank 39 Samples"; SRNL-STI-2019-00411, Rev. 0; Savannah River National Laboratory: **2019**.

27. Martino, C. J.; Pareizs, J. M. "Run Plan for Dissolved Tank 44 Saltcake Sample Thermolysis Tests Without and With Sodium Glycolate"; SRNL-L3300-2019-00014, Rev. 0; Savannah River National Laboratory: **2019**.

28. Woodham, W. H. "Run Plan for Testing to Evaluate Influence of Major Salt Species on Thermolytic Production of Hydrogen from Prominent Tank Farm Organics and Glycolate"; SRNL-L3300-2018-00056, Rev. 0; Savannah River National Laboratory: **2018**.

29. Woodham, W. H. "Measurement of Hydrogen Generation Rates during Digestion, Neutralization, Transfer, and Storage of Reillex HPQ Resin"; SRNL-STI-2018-00460, Rev. 0; Savannah River National Laboratory: **2018**.

30. Reboul, S. H.; Newell, J. D.; Pareizs, J. M.; Coleman, C. J. "Low Temperature Aluminum Dissolution (LTAD) Real Waste Testing of the November 2017 Tank 51 Slurry Sample"; SRNL-STI-2018-00179, Rev. 0; Savannah River National Laboratory: **2018**.

31. Duignan, M. R.; Nash, C. A.; Pareizs, J. M.; Restivo, M. L.; Crawford, C. L.; Edwards, T. B. "Hydrogen Generation Rates for Tank 50 and Saltstone Related Samples Using a Sealed Reactor System"; SRNL-STI-2018-00238, Rev. 0; Savannah River National Laboratory: **2018**.

Appendix A. Previous (August 2017) High Boiling Point (HBP) HGR Test with 10 g/L Glycolate

A previously reported HGR test used an evaporated Tank 42 simulant with a mixture of common SRS tank farm organics added at high levels relative to SRS waste.[11] That test consisted of subsequent HGR measurements at 140, 100, and 75 °C. See Sections 2.1.3, 2.2.1, and 3.2 of the report for details of that test. At the end of the previously reported testing, a set of HGR measurements with 10 g/L glycolate was conducted in the same evaporated simulant material. This appendix outlines the results of those HPB HGR measurements with 10 g/L of glycolate.

At the completion of the August 2017 thermolysis HGR experiment at three temperatures (140, 100, and 75 °C) with various CSTF organics, 10 g/L of glycolate was added to the HGR vessel (as sodium glycolate) and additional experiments were performed. Table A-1 contains a summary of the HGR result for the test with 10 g/L of glycolate. The testing was performed at a series of increasing temperatures, 75, 100, and 120 °C, and boiling at 135.8 °C. The 120 °C measurement was not originally planned, but a quick HGR measurement was made at 120 °C because based on the trends there was a risk that the HGR at boiling would be too high to measure safely given the purge rate limitations.

Figure A-1 contains a plot of the HGR measurements and temperatures for the set of August 2017 tests with 10 g/L glycolate. The circled regions are the data considered as the steady-state HGR measurement. The 75 °C HGR measurement trended upward and required considerable time for equilibration. Although the minimum purge rate of 3 sccm was used for that condition, the delay in equilibration appeared to be due to the glycolate reaction rate changing, possibly due to the buildup of a reactive intermediate compound. The HGR measurement at 100 °C used a higher purge rate and stabilized more quickly. The HGR measurement at 120 °C used the maximum possible purge rate and stabilized very quickly. The HGR measurement at 135.8 °C exhibited a constant decrease, likely due to the consumption of glycolate. The data from the onset of the measurements at 135.8 °C were used due to the decrease observed. Figure A-2 shows additional process data, namely the purge rate and the heating rod temperatures for this set of tests.

The Arrhenius plot of Figure A-3 shows a very consistent temperature dependence of the HGR reaction with 10 g/L glycolate with an activation energy of 104 kJ/mol.

The results of analysis of the samples immediately before the 75 °C test condition and after three of the four test conditions are contained in Table A-2. Glycolate remained stable during to 100 °C, remaining at 10 g/L within experimental uncertainty. After testing at 120 °C and at boiling for nearly 12 hours, the glycolate concentration dropped to approximately 4 g/L, only 40% of the original glycolate concentration. Likewise, oxalate was seen at elevated levels in the sample after the boiling measurement.

Table A-1. HGR measurements for August 2017 HBP test with 10 g/L glycolate

Temperature (°C)	Hydrogen Generation Rate ($ft^3\ h^{-1}\ gal^{-1}$)
75	2.63E-05
100	5.16E-04
120	4.08E-03
135.8 (boiling) initial	1.80E-02

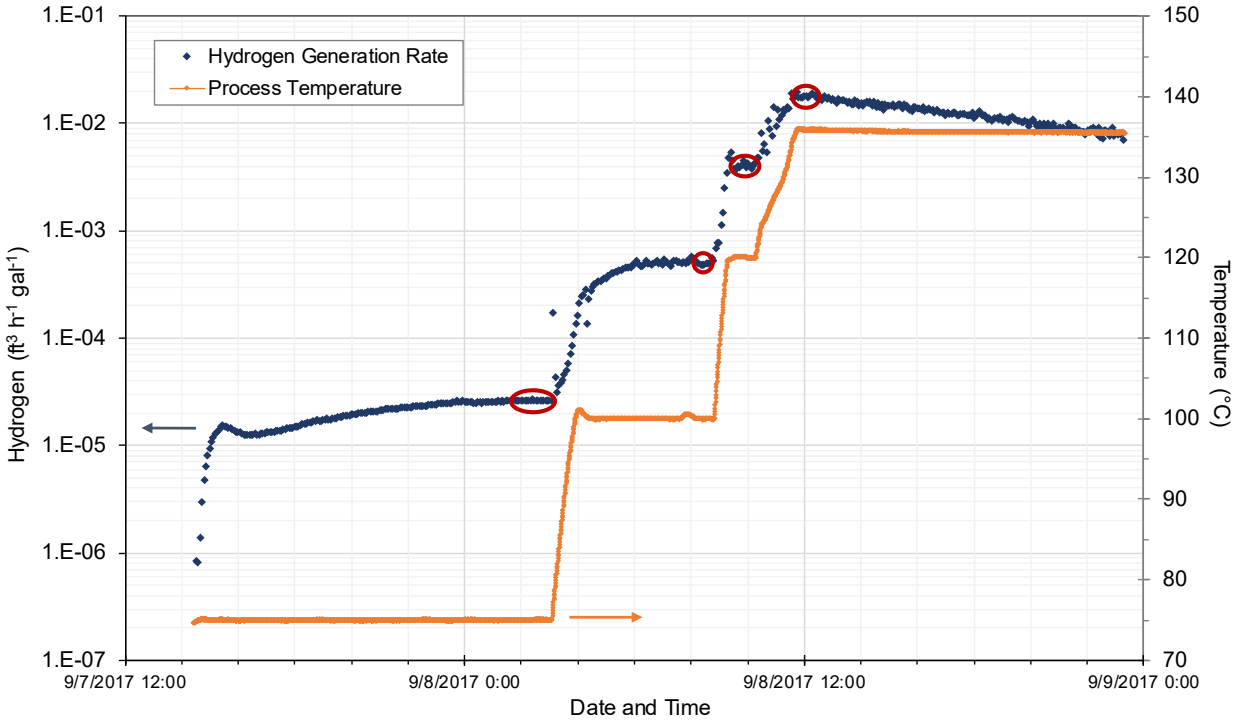

Figure A-1. HGR and temperature for HBP test with 10 g/L glycolate

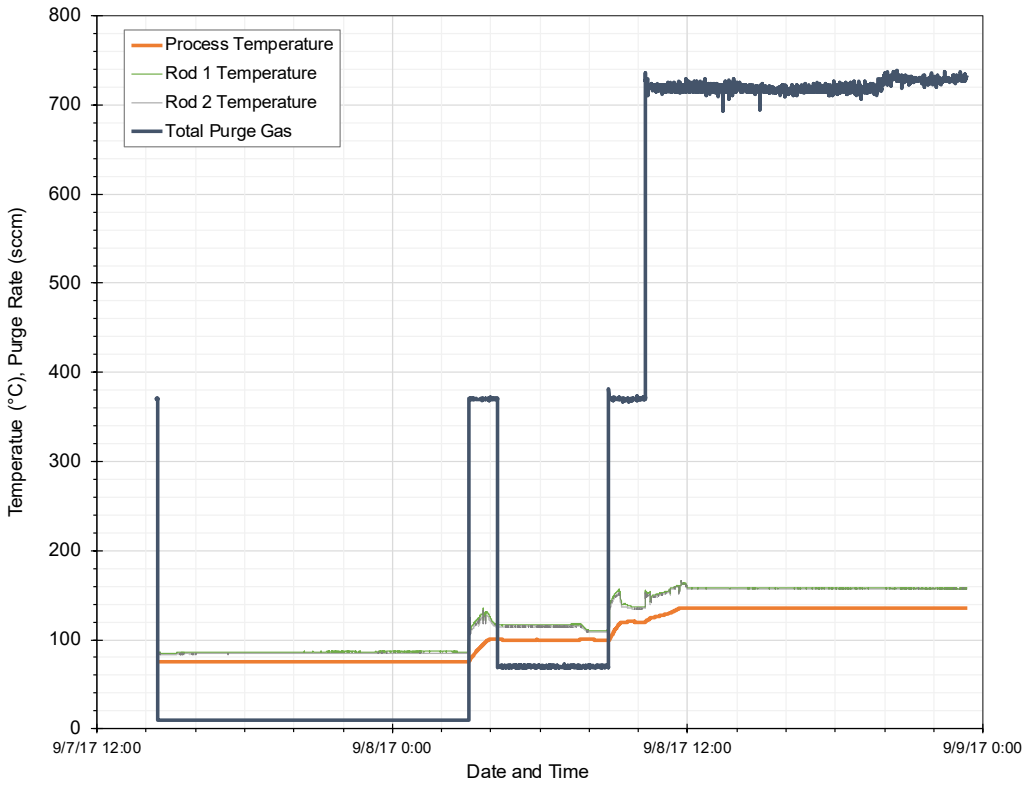

Figure A-2. Purge rate and rod temperatures for HBP HGR test with 10 mg/L glycolate

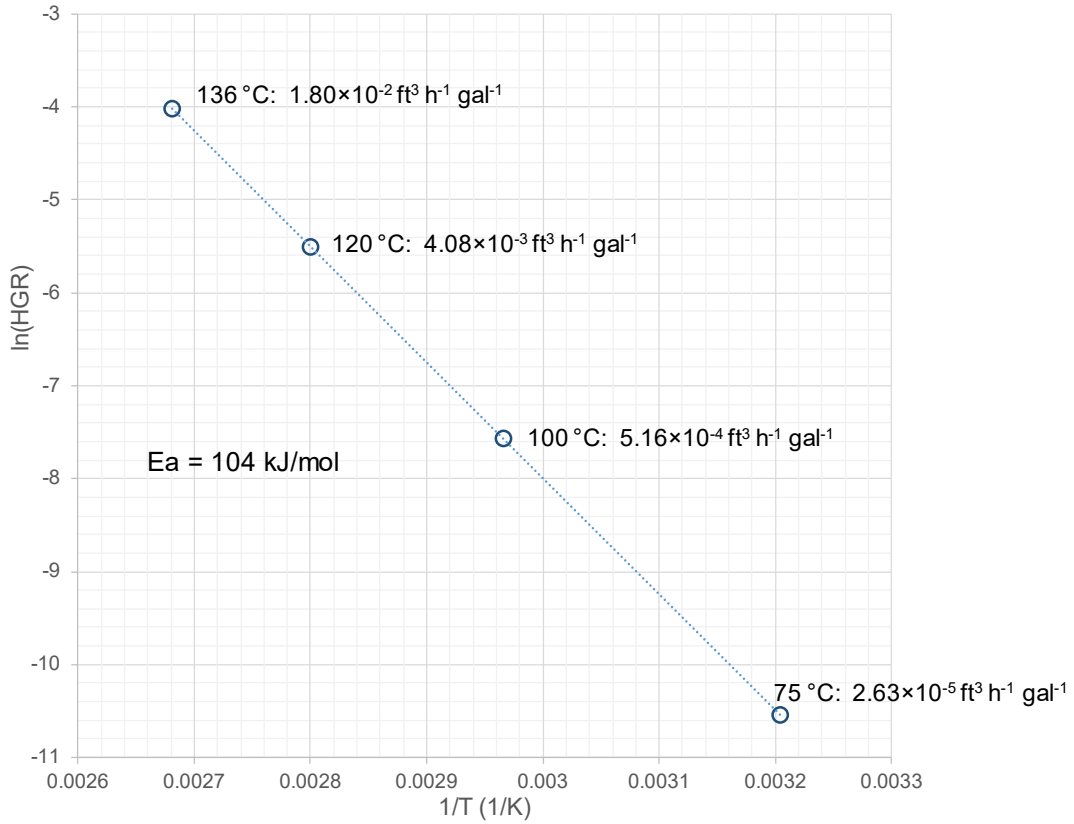

Figure A-3. Arrhenius plot for HBP HGR test with 10 g/L glycolate

Table A-2. Analytical results for HBP HGR test with 10 mg/L glycolate

analyte	method	units	1σ unc.	Glycolate Pre Test	Post 75 °C	Post 100 °C	Post 136 °C
Na^+	ICP-AES	M	10%	1.6E+01	1.7E+01	1.6E+01	1.6E+01
OH^-	TB/OH/OB	M	10%	9.1E+00	1.0E+01	9.6E+00	9.6E+00
NO_2^-	IC	M	10%	3.9E+00	3.9E+00	3.9E+00	4.0E+00
NO_3^-	IC	M	10%	3.1E+00	3.0E+00	3.0E+00	3.1E+00
$Al(OH)_4^-$	ICP-AES	M	10%	3.5E-01	3.4E-01	3.3E-01	1.2E-01
CO_3^{2-}	TIC/TOC	M	10%	2.7E-02	2.7E-02	3.0E-02	5.0E-02
		mg/L	10%	1.6E+03	1.6E+03	1.8E+03	3.0E+03
$C_2H_3O_3^{2-}$	IC	M	10%	1.3E-01	1.2E-01	1.2E-01	5.4E-02
		mg/L	10%	1.0E+04	9.2E+03	9.1E+03	4.0E+03
CHO_2^-	IC	M	10%	8.5E-02	8.3E-02	8.4E-02	9.7E-02
		mg/L	10%	3.8E+03	3.8E+03	3.8E+03	4.4E+03
$C_2O_4^{2-}$	IC	M	10%	3.2E-03	3.2E-03	4.1E-03	1.2E-02
		mg/L	10%	2.8E+02	2.8E+02	3.6E+02	1.0E+03
TOC	TIC/TOC	mg C/L	10%	5.0E+03	4.7E+03	4.7E+03	3.4E+03

Appendix B. Use of JMP 11.2.0 Statistical Mathematics Software Package to Evaluate HGR Data and Generate Empirical Reaction Rate Expressions.

During the performance of the research described in this report, it became necessary to employ a statistical tool for the evaluation of HGR data and the generation of empirical reaction rate expressions. The software package employed for this purpose was JMP 11.2.0. JMP is a statistical mathematics software package capable of comparing multiple data sets simultaneously for the regression of empirical models according to linear and non-linear methods. This appendix serves as an example to illustrate the use of JMP 11.2.0 in this capacity. The example given here is based on the generation of the final HGR model for Xiameter AFE-1010, previously described in Section 3.4.2.

Before JMP can be employed to regress a statistical model, a functional assumption of the model's form must first be made. Given that the interest of this research is to generate empirical models capable of bounding HGRs observed in radioactive waste, it is not necessary to assume a mechanistically-accurate model expression. Rather, experimental data may be fit to a simpler, Arrhenius-type model, such as the one shown in Equation [45].

$$HGR_{XIA} = k_{XIA}\left[Al\right]^{\alpha}\left[NO_2\right]^{\beta}\left[NO_3\right]^{\gamma}\left[OH\right]^{\delta}\left[SO_4\right]^{\varepsilon}\left[CO_3\right]^{\phi}\left[C_{XIA}\right]^{\mu} e^{-E_{XIA}/RT} \quad [45]$$

This model may be linearized to allow for linear regression of the test data recorded using the natural logarithm function. The linearized version of Equation [45] is given in Equation [46].

$$\ln\left(\frac{HGR_{XIA}}{\left[C_{XIA}\right]}\right) = \ln\left(k_{XIA}\right) + \alpha\ln\left[Al\right] + \beta\ln\left[NO_2\right] + \ldots + \varepsilon\ln\left[SO_4\right] + \phi\ln\left[CO_3\right] - \frac{E_{XIA}}{RT} \quad [46]$$

The format of Equation [46] suggests that an empirical model may be regressed by fitting dependent data (in the form of $\ln\left(\frac{HGR_{XIA}}{\left[C_{XIA}\right]}\right)$) with several possible independent parameters ($\ln\left[Al\right]$, $\ln\left[NO_2\right]$, $\ln\left[NO_3\right]$, $\ln\left[OH\right]$, $\ln\left[SO_4\right]$, $\ln\left[CO_3\right]$, and $1/T$). These dependent and independent values may be calculated from the raw data given in Table 3-14, Table 3-15, Table 3-16, and Table 3-17. These modified values are given in Table B-1.

Test Name	Ln(Al)	Ln(NO_2)	Ln(NO_3)	Ln(OH)	LN(SO_4)	Ln(CO_3)	T^{-1} (K^{-1})	Ln(HGR/[C_{XIA}])
XIA-1	-2.383	0.756	0.104	0.854	-2.974	-0.473	0.00268	-6.495
XIA-2	-1.474	0.908	0.140	0.975	-2.681	-0.387	0.00268	-6.011
XIA-3	-2.535	0.405	0.148	0.963	-2.652	-0.387	0.00268	-6.040
XIA-4	-2.328	0.863	-1.306	0.936	-2.861	-0.367	0.00268	-6.191
XIA-5	-2.343	0.916	0.470	0.519	<-6.869	-0.367	0.00268	-6.891
XIA-6	-2.351	0.824	0.113	0.932	-3.844	-0.406	0.00268	-6.351
XIA-7	-2.306	0.854	0.215	0.997	-2.807	-1.514	0.00268	-6.524
XIA-8	-2.463	0.815	0.148	0.959	-2.839	-0.448	0.00268	-6.265
XIA-9	-2.507	0.959	0.199	0.997	-2.609	-0.324	0.00279	-6.944
XIA-10	-2.317	0.854	0.131	1.022	-2.835	-0.457	0.00261	-5.967
P3-XIA-1	-5.539	0.148	0.948	1.766	-2.802	-1.630	0.00272	-5.761
P3-XIA-2	-3.480	-0.065	-1.845	2.526	-5.335	-3.568	0.00289	-6.203
P3-XIA-3	-2.996	-0.844	0.967	1.798	-2.163	-4.283	0.00276	-5.780
P3-XIA-4	-2.283	0.959	1.197	0.577	-3.854	-0.926	0.00268	-6.500
P3-XIA-5	-2.079	-0.921	0.652	0.820	-1.726	-1.802	0.00272	-7.509
P3-XIA-6	-0.934	-1.336	1.284	0.829	-1.609	-0.592	0.00262	-5.756
P3-XIA-7	-0.828	0.742	0.668	1.936	-4.123	-2.932	0.00286	-6.472

Table B-1. Linearized Xiameter AFE-1010 Experimental Data.

The data in Table B-1 may be uploaded to JMP 11.2.0 as a data table to be used for analysis and model fitting. This table is shown in Figure B-1, where "TOC" is equivalent to C_{XIA}.

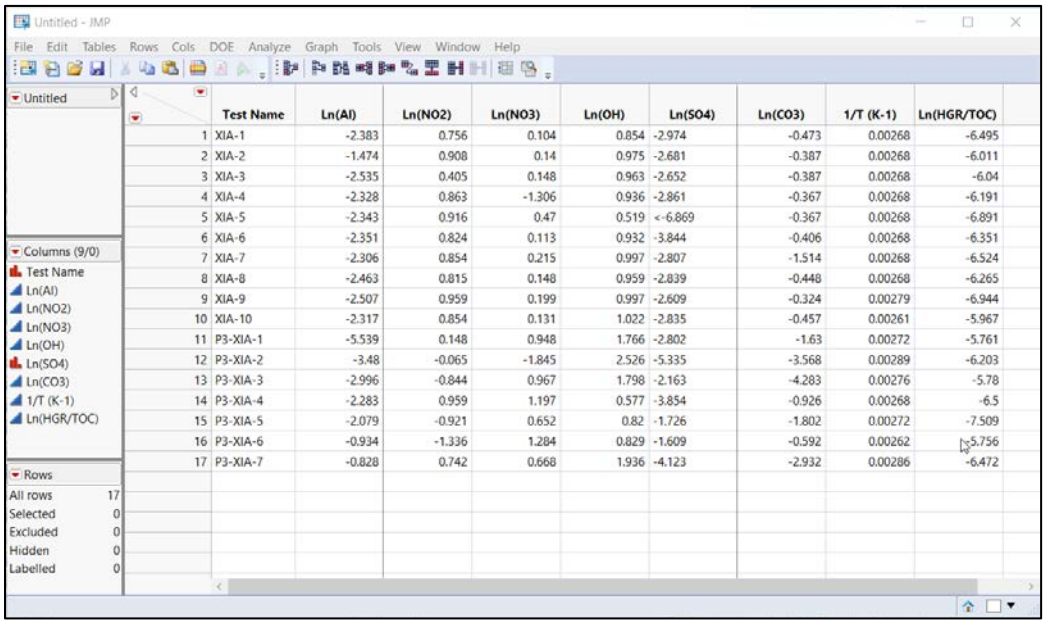

	Test Name	Ln(Al)	Ln(NO2)	Ln(NO3)	Ln(OH)	Ln(SO4)	Ln(CO3)	1/T (K-1)	Ln(HGR/TOC)
1	XIA-1	-2.383	0.756	0.104	0.854	-2.974	-0.473	0.00268	-6.495
2	XIA-2	-1.474	0.908	0.14	0.975	-2.681	-0.387	0.00268	-6.011
3	XIA-3	-2.535	0.405	0.148	0.963	-2.652	-0.387	0.00268	-6.04
4	XIA-4	-2.328	0.863	-1.306	0.936	-2.861	-0.367	0.00268	-6.191
5	XIA-5	-2.343	0.916	0.47	0.519	<-6.869	-0.367	0.00268	-6.891
6	XIA-6	-2.351	0.824	0.113	0.932	-3.844	-0.406	0.00268	-6.351
7	XIA-7	-2.306	0.854	0.215	0.997	-2.807	-1.514	0.00268	-6.524
8	XIA-8	-2.463	0.815	0.148	0.959	-2.839	-0.448	0.00268	-6.265
9	XIA-9	-2.507	0.959	0.199	0.997	-2.609	-0.324	0.00279	-6.944
10	XIA-10	-2.317	0.854	0.131	1.022	-2.835	-0.457	0.00261	-5.967
11	P3-XIA-1	-5.539	0.148	0.948	1.766	-2.802	-1.63	0.00272	-5.761
12	P3-XIA-2	-3.48	-0.065	-1.845	2.526	-5.335	-3.568	0.00289	-6.203
13	P3-XIA-3	-2.996	-0.844	0.967	1.798	-2.163	-4.283	0.00276	-5.78
14	P3-XIA-4	-2.283	0.959	1.197	0.577	-3.854	-0.926	0.00268	-6.5
15	P3-XIA-5	-2.079	-0.921	0.652	0.82	-1.726	-1.802	0.00272	-7.509
16	P3-XIA-6	-0.934	-1.336	1.284	0.829	-1.609	-0.592	0.00262	-5.756
17	P3-XIA-7	-0.828	0.742	0.668	1.936	-4.123	-2.932	0.00286	-6.472

Figure B-1. JMP Data Table with Linearized Xiameter AFE-1010 Data.

Once the data set has been uploaded into a JMP Data Table, it may be regressed using JMPs Fit Model tool, depicted in Figure B-2.

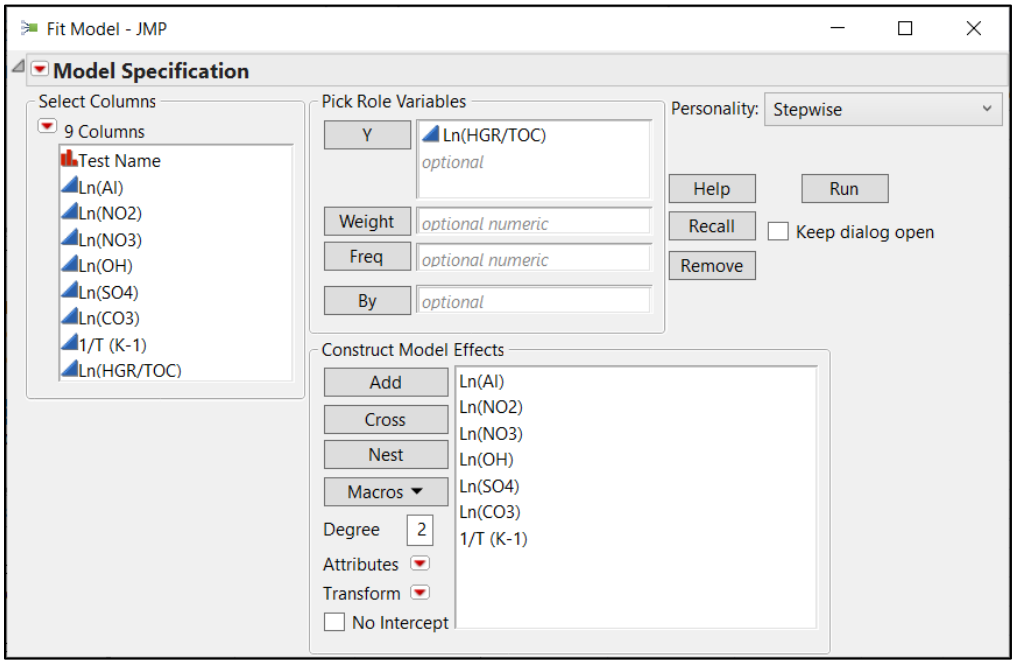

Figure B-2. Model Fitting Tool Available in JMP 11.2.0.

JMP is then used to perform a step-wise regression in which the use of each parameter is evaluated before a final solution is generated based on an optimized statistical parameter. In the case of the models prepared in this report, the Bayesian Information Criterion (BIC) was minimized to generate an optimal HGR model. The results of this process are shown in Figure B-3.

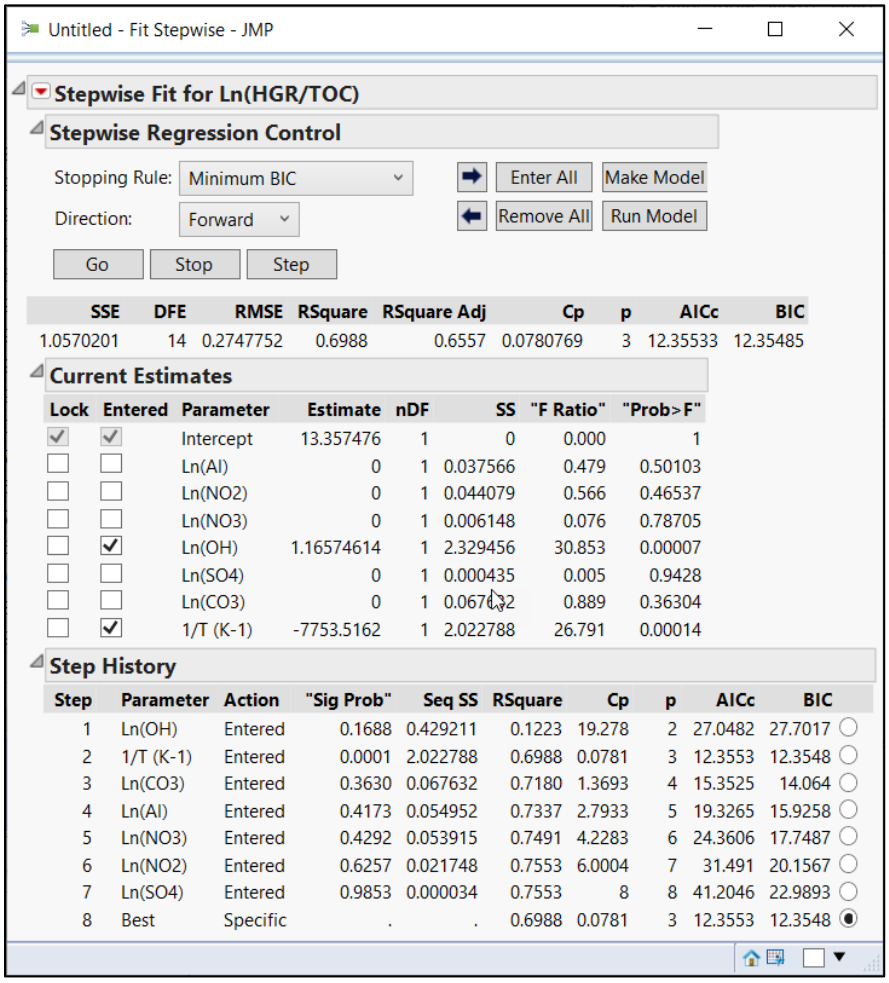

Figure B-3. Results of Step-wise Linear Model Regression on Xiameter AFE-1010 Data.

Once an optimum model has been generated, a full report may be produced that both graphically displays the quality of fit achieved by the model as well as statistical parameters related to the model fit (e.g., proposed values for linear equation coefficients). An example of this report is given in Figure B-4.

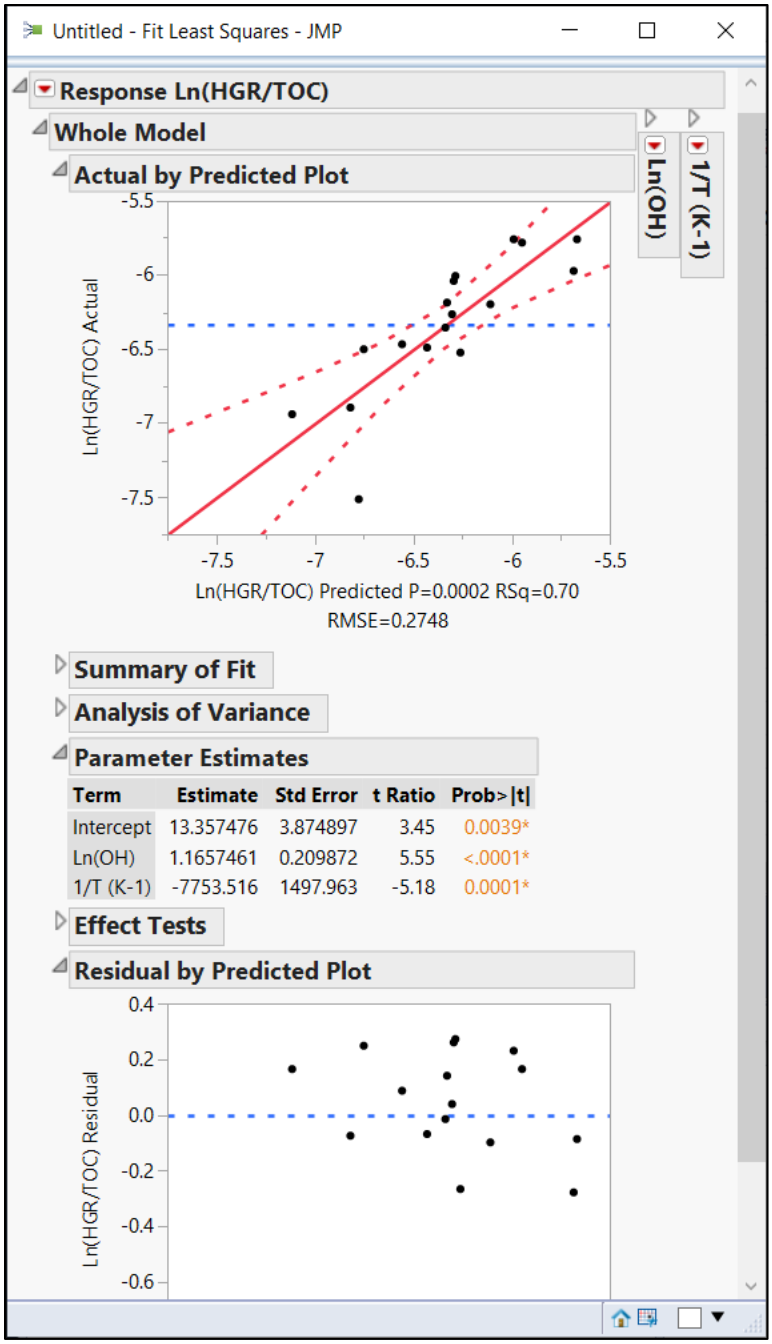

Figure B-4. Model Report for Fitted Xiameter AFE-1010 Data.

The report shown in Figure B-4 has several uses. First, it may be seen in the "Actual by Predicted plot" section of the report that good agreement is seen between the model prediction and measured values, with the vast majority of data points falling well within the 95% confidence limit of the model's mean prediction. It may also be observed in this section of the report that an R^2 value of 0.7 is achieved by this model, suggesting that about 70% of the variation in the data can be described by the model proposed. Second, the residual errors about the mean prediction from the model can be seen in the "Residual by Predicted plot" section of the report. The fact that the data are scattered evenly around a residual value of 0.0 suggests that there is no apparent bias in the model. Finally, the "Parameter Estimates" section of the report may be used

to assess the significance of each term of the fit achieved by the model by noting the "Prob > |t|" value for each parameter estimate. This value roughly relates to the "risk" associated with the specified parameter being unnecessary for a quality fit (e.g., there is a 0.01% chance that temperature is not necessary to adequately describe the Xiameter AFE-1010 HGR behavior).

The provided parameter estimates may then be used to specify the optimal linear model for the data being fit (in this case, Xiameter AFE-1010). The "intercept" value of 13.357 is a constant according to the optimal model. The "Ln(OH)" term is expected to have a value of 1.166, corresponding to the constant to be multiplied to the experiment-dependent logarithmic concentration of hydroxide. The "1/T" term refers to the constant associated with the effect of temperature (expressed as inverse temperature, or T^{-1}). The linear model resulting from these parameter estimates is given in Equation [47].

$$\ln\left(\frac{HGR_{XIA}}{[C_{XIA}]}\right) = 13.357 + 1.166\ln[OH] - \frac{7754}{T} \qquad [47]$$

By comparing Equation [46] and Equation [47], it can be observed that the intercept value of 13.357 corresponds to the constant $\ln(k_{XIA})$, the 1.166 coefficient for the Ln(OH) term corresponds to the δ coefficient (the reaction dependence on hydroxide), and the -7754 coefficient for the 1/T term corresponds to the value of $-E_{XIA}/R$, which is the ratio of the apparent activation energy of Xiameter AFE-1010 thermolysis to the ideal gas constant, R.

The linear model expression in Equation [47] can be easily transformed to a more useful form capable of calculating HGR in units of $ft^3\ h^{-1}\ gal^{-1}$. The product of this transformation is shown in Equation [48].

$$HGR_{XIA} = 6.322\times10^{5}[OH]^{1.166}[C_{XIA}]e^{-64{,}500/RT} \qquad [48]$$

The process described in this appendix can be modified to include multiple sets of data (as was done for the generation of a global TOC model described in Section 3.9), non-fitting analysis of validation data (as was performed for each organic species in Section 3.0), or analysis of a specified functional behavior (as was employed during the evaluation of non-glycolate HGRs from radioactive waste in Section 3.9). These statistical methods and variations were employed to generate the models presented within this report and represent a defensible strategy for establishing bounding models for the prediction of flammable gases.

Appendix C. Use of Global TOC and Glycolate HGR Models in CSTF Waste Tank Flammability Calculations.

To assess the impact of thermolysis on CSTF operations, it is necessary to evaluate the expected changes to hydrogen generation rates when organic thermolysis is considered at applicable waste conditions (i.e., salt concentrations, temperatures, liquid volumes, etc.). Table C-1 lists the relevant conditions of each active waste tank in the CSTF as they were reported on January 30th, 2019. Listed conditions include:

- Volume of supernatant phase (in gal),
- Volume of the vapor space (in ft^3),),
- Radiolytic HGR, as predicted using current CSTF methodology (in $ft^3\ h^{-1}$),
- Initial hydrogen concentration, y_0 (in volume fraction),
- Sodium concentration (in mol L^{-1}),
- Hydroxide concentration (in mol L^{-1}), and
- Nitrate concentration (in mol L^{-1}).

Tank No.	Supernatant Volume (gal)	Headspace Volume (ft^3)	Radiolytic HGR ($ft^3\ h^{-1}$)	y_0 (vol. frac.)	Na (M)	OH (M)	NO_3 (M)
1	148914.5	26389.51	2.02E-01	0.01	1.48E+01	9.30E+00	2.00E+00
2	163656.9	26954.66	7.49E-02	0.01	1.35E+01	7.18E+00	2.25E+00
3	163656.9	18669.42	1.06E-01	0.01	1.10E+01	6.76E+00	1.71E+00
4	118156	30657.12	1.02E-01	0.024	1.25E+00	4.58E-01	3.40E-01
7	209645.6	29899.96	1.90E-01	0.024	2.99E-01	8.22E-02	3.59E-02
8	319400.6	18307.15	3.99E-01	0.01	5.98E+00	3.83E+00	8.75E-01
9	166529.5	26864.09	4.45E-02	0.01	1.05E+01	3.80E+00	1.90E+00
10	95706.5	55936.70	1.18E-02	0.024	5.48E+00	2.05E+00	2.87E+00
11	124307.7	50593.14	2.90E-01	0.012	2.69E+00	1.35E+00	7.47E-01
13	546838.425	64851.33	5.35E-01	0.024	2.99E+00	1.02E+00	1.13E+00
14	58450	99984.70	4.86E-02	0.01	1.14E+01	4.10E+00	3.70E+00
15	213195.5	76548.41	4.37E-01	0.024	3.28E+00	1.15E+00	1.34E+00
21	1242193.08	45127.95	4.17E-01	0.024	5.46E+00	2.79E+00	1.65E+00
22	645306.6	111119.98	1.02E+00	0.024	5.83E-01	1.93E-01	8.22E-02
23	736670.46	45525.47	3.22E-02	0.01	2.58E+00	5.36E-01	1.61E+00
24	1173687	45080.63	5.10E-01	0.01	1.22E+01	7.93E+00	1.81E+00
25	784871.1	9432.45	1.12E-01	0.01	6.63E+00	2.95E+00	2.29E+00
26	949174.2	9211.92	2.32E-01	0.01	5.27E+00	2.58E+00	1.70E+00
27	423376.2	11642.48	1.48E-01	0.01	1.15E+01	7.54E+00	1.99E+00
28	496384.2	9179.07	1.73E-01	0.01	1.23E+01	8.16E+00	1.76E+00
29	377149.5	9469.99	1.14E-01	0.01	3.65E+00	1.15E+00	1.44E+00
30	1041136.2	9455.91	3.95E-01	0.01	1.25E+01	8.54E+00	1.66E+00
31	379080	9399.61	1.69E-01	0.01	9.81E+00	4.00E+00	2.48E+00
32	838574.1	39983.39	1.98E+00	0.01	7.81E+00	3.97E+00	1.90E+00
33	1000946.7	11712.86	1.48E+00	0.01	5.58E+00	3.20E+00	1.25E+00
34	1009019.7	14176.27	1.46E+00	0.01	7.72E+00	4.76E+00	1.51E+00
35	851455.8	18347.64	1.91E+00	0.01	4.83E+00	1.48E+00	2.01E+00
36	461284.2	9150.92	4.94E-01	0.01	1.17E+01	8.29E+00	1.44E+00
37	655738.2	9432.45	1.55E-01	0.01	8.57E+00	4.29E+00	2.08E+00
38	718005.6	9179.07	1.73E-01	0.01	3.52E+00	1.58E+00	6.77E-01
39	435766.5	44328.37	4.19E+00	0.01	4.01E+00	1.64E+00	2.02E+00
40	480238.2	100930.41	2.06E+00	0.024	5.98E-01	1.74E-01	1.01E-01
41	168104.43	39462.55	5.01E-02	0.024	2.58E+00	5.34E-01	1.61E+00
42	1231659	11778.55	4.75E-01	0.01	1.19E+01	7.60E+00	2.01E+00
43	1158254.37	13857.20	6.90E-01	0.01	4.16E+00	1.88E+00	8.13E-01
44	527377.5	9165.00	2.08E-01	0.01	1.05E+01	7.71E+00	1.27E+00
45	371182.5	9197.84	2.51E-01	0.01	1.58E+01	1.22E+01	1.17E+00
46	379009.8	9197.84	2.70E-01	0.01	1.24E+01	9.32E+00	1.13E+00
47	641663.1	9197.84	2.20E-01	0.01	1.32E+01	8.93E+00	2.09E+00
49	1249560	9549.76	8.20E-02	0.012	5.25E+00	2.62E+00	1.63E+00
51	768970.8	63392.79	7.62E-01	0.024	5.26E+00	3.65E+00	7.72E-01

Table C-1. Tank Conditions Relevant to Flammability Calculations (as Reported on 2019-01-30).

The data in Table C-1 may be used to predict the total HGR in each tank as a function of organic concentration and temperature. For the purpose of this comparison, organic loadings of 50 and 250 mg/L (glycolate) and 500 mg/L (non-glycolate TOC) are evaluated at 70 °C, 85 °C, and 100 °C using the model expressions given in Equation [17] and [44], respectively. 50 mg/L glycolate is examined as a possible limit of glycolate concentration in Tank 22 after the alternate reductant flowsheet is introduced. 250 mg/L glycolate is examined under an assumption of 5x concentration during CSTF evaporator operations. (Note

that this value is not applicable to CSTF flowsheets that do not actively concentrate glycolate-containing waste.) 500 mg/L TOC is chosen as a nominal TOC loading similar to values that have been previously observed. Cumulative HGRs for these temperatures are displayed in Figure C-1, Figure C-3, and Figure C-5, respectively. Blue bars are used to represent the total HGR predicted according to the currently-employed CSTF methodology (radiolysis only). Yellow bars are used to represent the HGR predicted from 500 mg/L of TOC using the global TOC HGR model. Green bars are used to represent the HGR expected from 50 mg/L of glycolate (according to the temperature-modified glycolate HGR model). Red bars represent the impact of an additional 200 mg/L of glycolate (for a total of 250 mg/L of glycolate). Those predicted HGRs are normalized by the amount of supernatant liquid at the same temperatures in Figure C-2, Figure C-4, and Figure C-6, respectively.

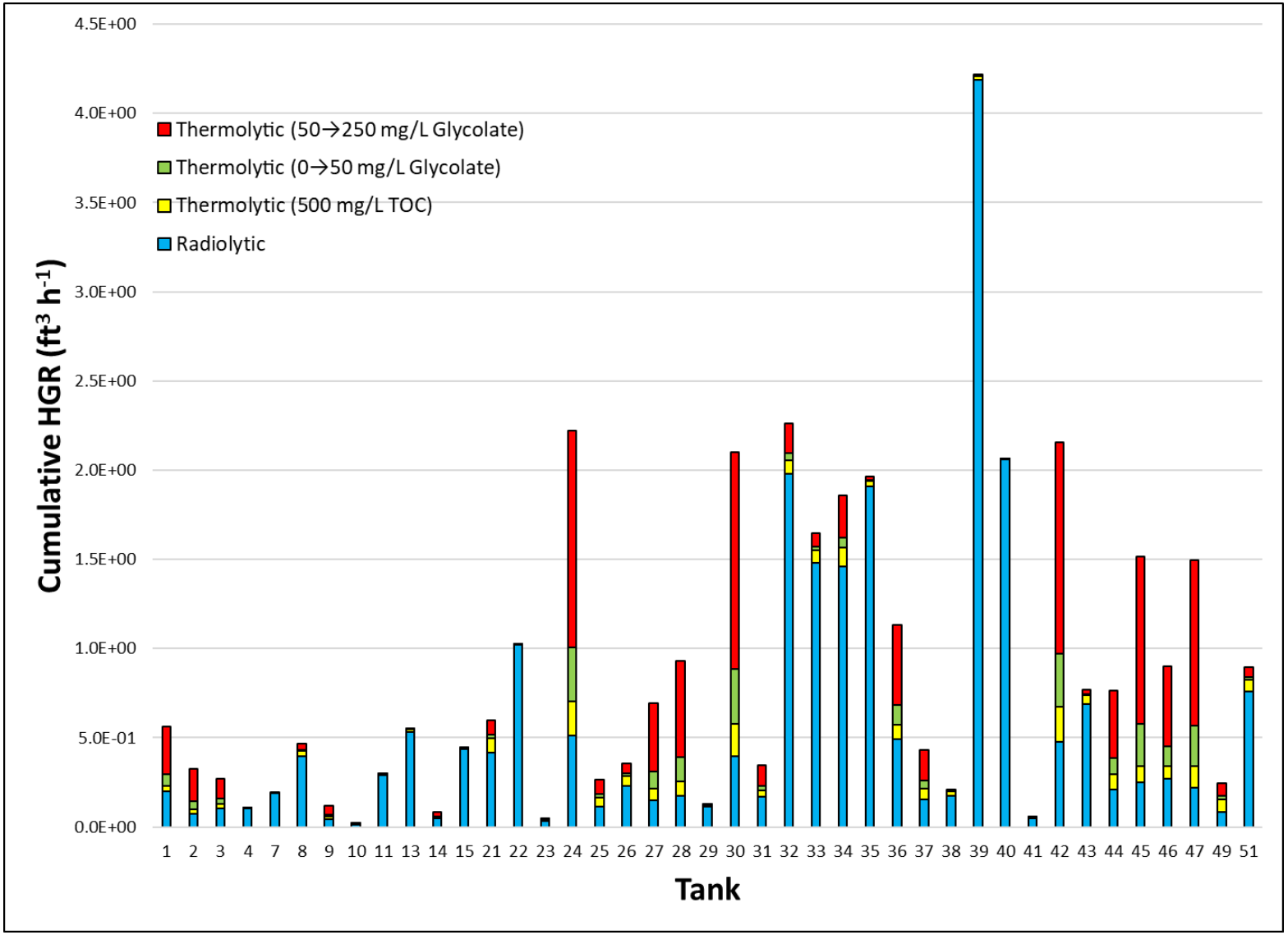

Figure C-1. Cumulative HGRs in CSTF Tanks With and Without Thermolysis at 70 °C.

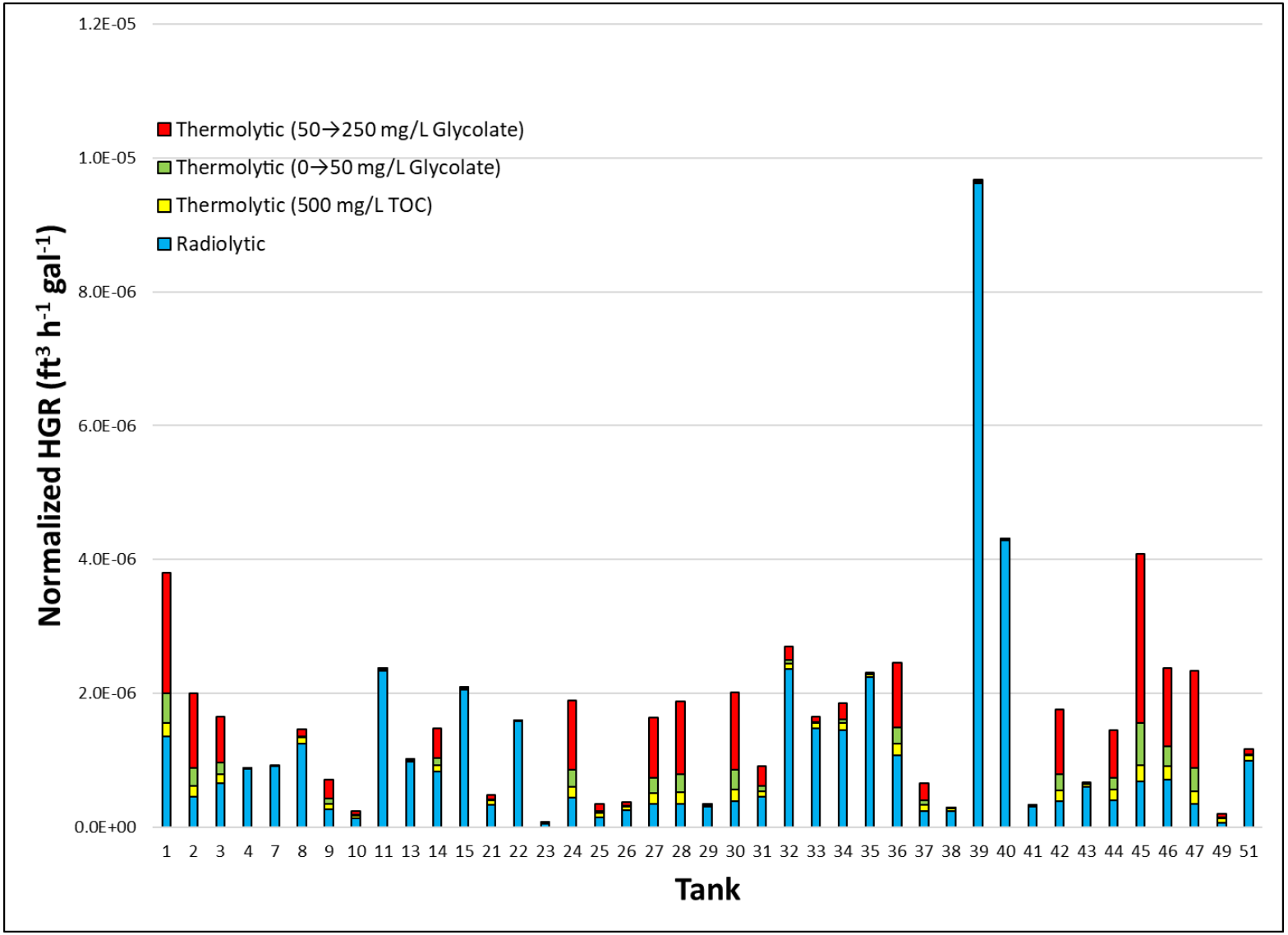

Figure C-2. Supernatant-Normalized HGRs in CSTF Tanks With and Without Thermolysis at 70 °C.

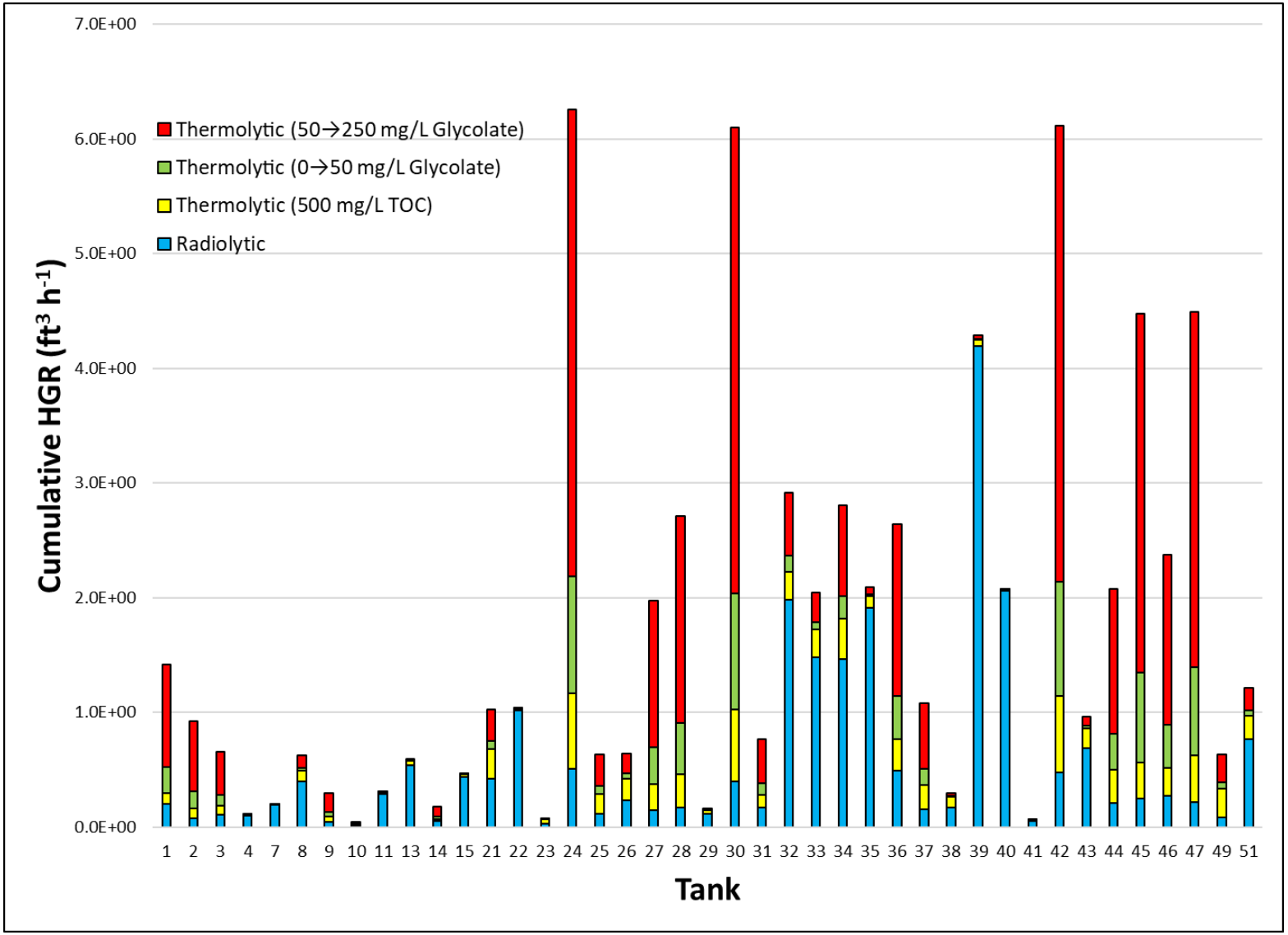

Figure C-3. Cumulative HGRs in CSTF Tanks With and Without Thermolysis at 85 °C.

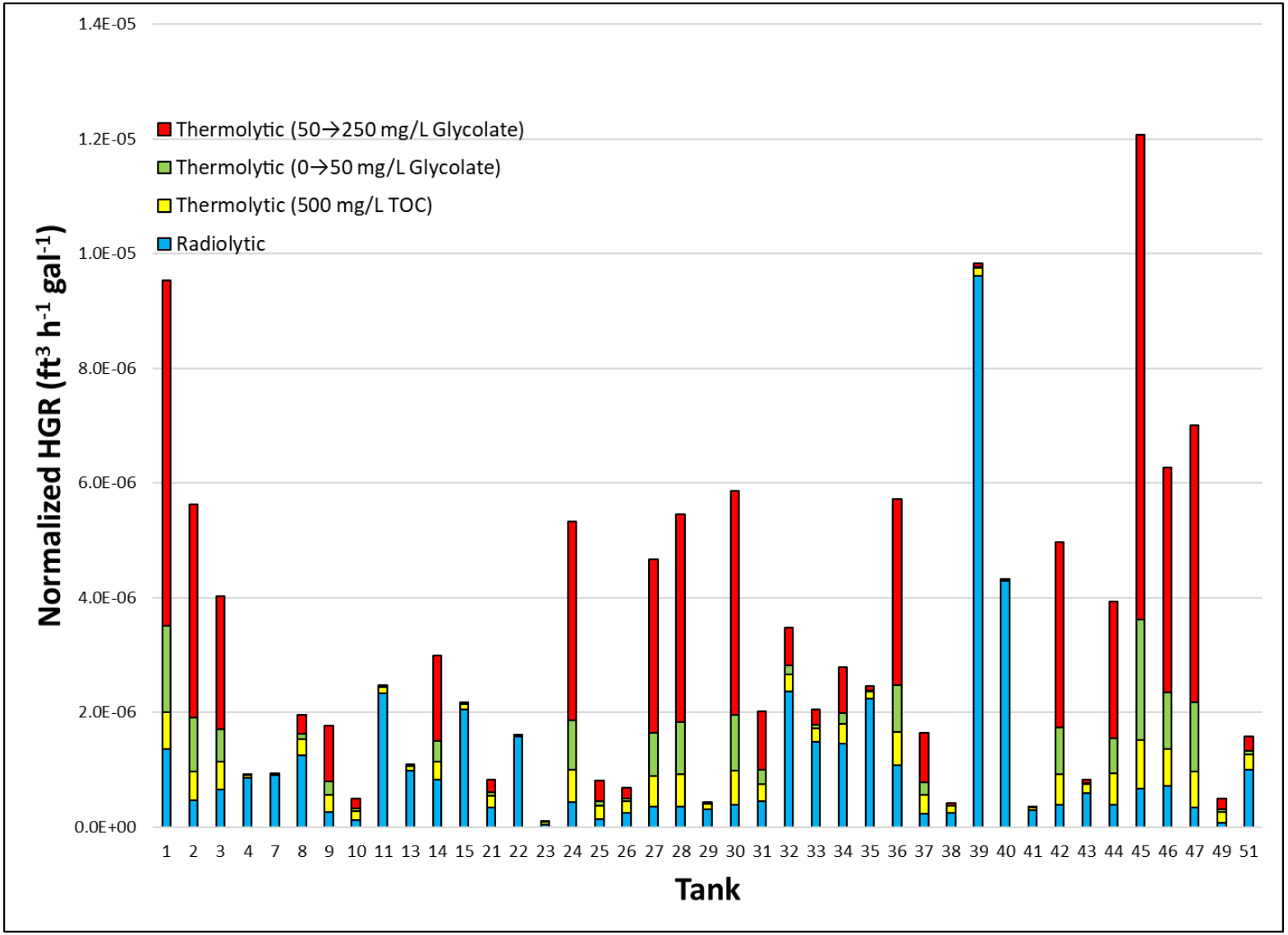

Figure C-4. Supernatant-Normalized HGRs in CSTF Tanks With and Without Thermolysis at 85 °C.

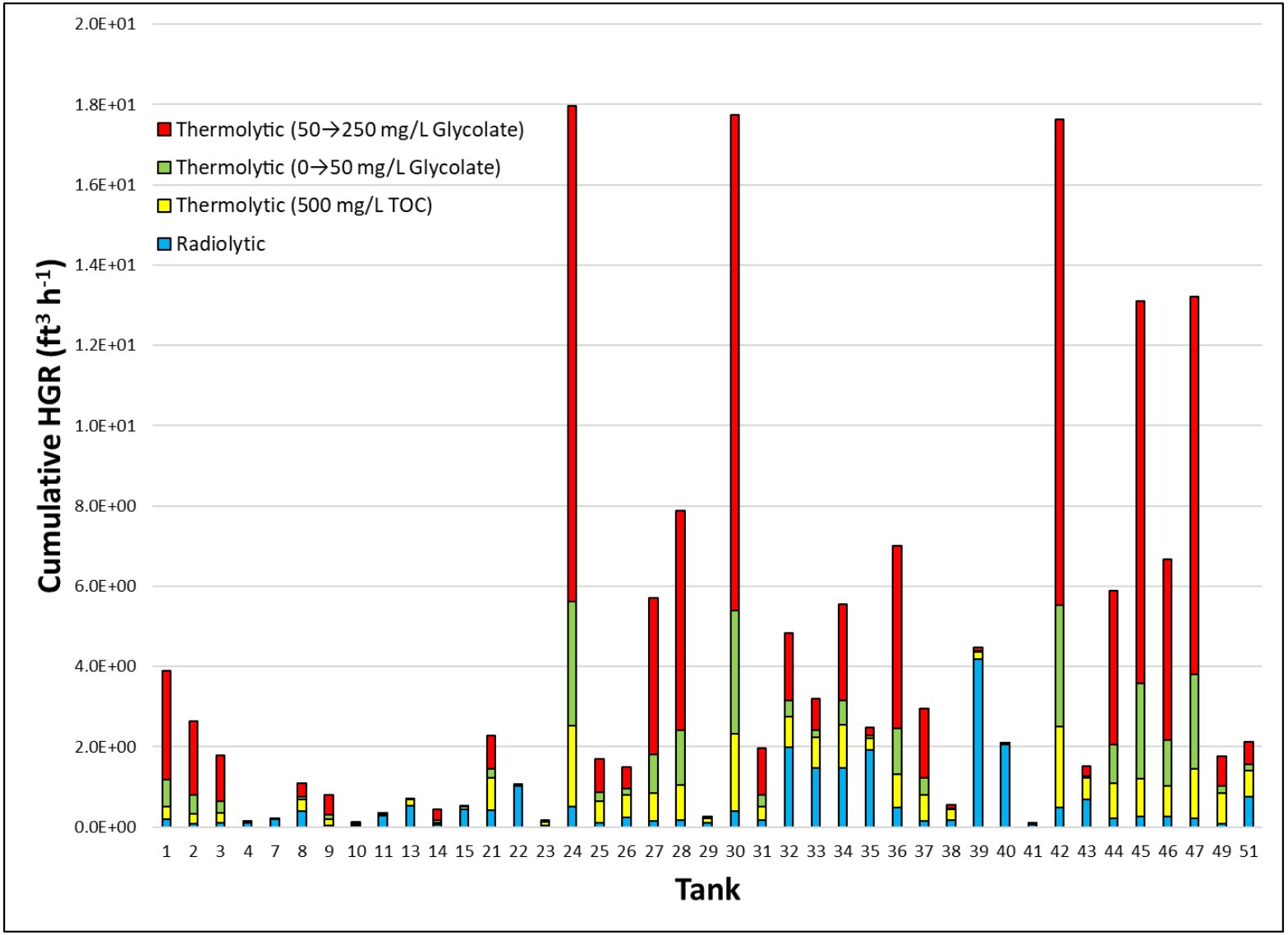

Figure C-5. Cumulative HGRs in CSTF Tanks With and Without Thermolysis at 100 °C.

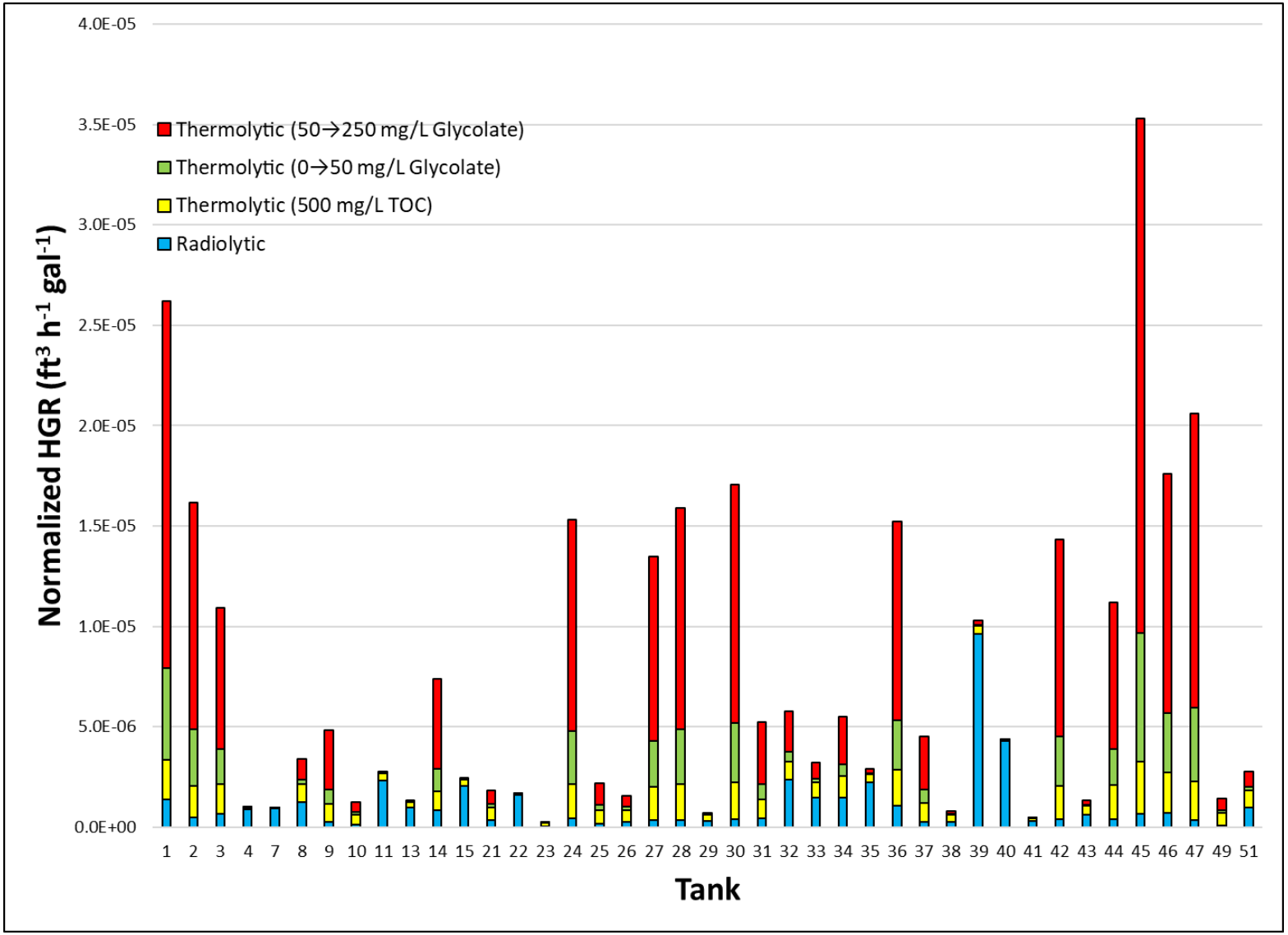

Figure C-6. Supernatant-Normalized HGRs in CSTF Tanks With and Without Thermolysis at 100 °C.

Review of the data in Figure C-1 through Figure C-6 show that, generally speaking, radiolysis is the largest contributor to HGR in CSTF waste tanks at temperatures of 70 °C and below, with only a few tanks exhibiting significant increases in HGR when glycolate and non-glycolate thermolysis is included. However, at 85 °C the relative contribution of organic thermolysis appears to be comparable to that expected from radiolysis, and generally dwarfs the radiolytic contribution at 100 °C. It should be noted that these HGRs are linearly dependent on organic concentration and would be expected to diminish as organic carbon concentrations decrease.

Distribution:

john.occhipinti@srs.gov
alex.cozzi@srnl.doe.gov
david.crowley@srnl.doe.gov
a.fellinger@srnl.doe.gov
samuel.fink@srnl.doe.gov
brady.lee@srnl.doe.gov
connie.herman@srnl.doe.gov
Joseph.Manna@srnl.doe.gov
Anna.Murphy@srs.gov
john.mayer@srnl.doe.gov
daniel.mccabe@srnl.doe.gov
frank.pennebaker@srnl.doe.gov
William.Ramsey@SRNL.DOE.gov
Jocelyn.Lampert@srnl.doe.gov
arthur.wiggins@srs.gov
michael.stone@srnl.doe.gov
Boyd.Wiedenman@srnl.doe.gov
Records Administration (EDWS)
jeffrey.crenshaw@srs.gov
james.folk@srs.gov
Azikiwe.hooker@srs.gov
celia.aponte@srs.gov
Christine.Ridgeway@srs.gov
tony.polk@srs.gov
patricia.suggs@srs.gov
Kevin.Brotherton@srs.gov
Richard.Edwards@srs.gov
terri.fellinger@srs.gov
Anthony.Robinson@srs.gov
bill.clark@srs.gov
jeffrey.gillam@srs.gov
barbara.hamm@srs.gov
bill.holtzscheiter@srs.gov
john.iaukea@srs.gov
Vijay.Jain@srs.gov
earl.brass@srs.gov
Gregg.Morgan@srnl.doe.gov
Jeremiah.Ledbetter@srs.gov
MARIA.RIOS-ARMSTRONG@SRS.GOV
jonathan.duffey@srnl.doe.gov
phillip.norris@srs.gov
chris.martino@srnl.doe.gov
jeff.ray@srs.gov
Brenda.Garcia-Diaz@srnl.doe.gov
cj.bannochie@srnl.doe.gov
Curtis.Gardner@srs.gov
Pauline.hang@srs.gov
Azadeh.Samadi-Dezfouli@srs.gov
hasmukh.shah@srs.gov
dennis.jackson@srnl.doe.gov
eric.skidmore@srnl.doe.gov
Grace.Chen@srs.gov
lauryn.jamison@srs.gov
mark-a.smith@srs.gov
robert.hoeppel@srs.gov
thomas.temple@srs.gov
Amy.Ramsey@srnl.doe.gov
Thomas.Huff@srs.gov
ryan.mcnew@srs.gov
Spencer.Isom@srs.gov
thomas.colleran@srs.gov
timothy.baughman@srs.gov
hilary.bui@srs.gov
tommy.edwards@srnl.doe.gov
charles.crawford@srnl.doe.gov
Wesley.Woodham@srnl.doe.gov
aaron.staub@srs.gov